UNIVERSITY OF OKLAHOMA

GRADUATE COLLEGE

REDOX FUNCTIONAL GROUPS OF HUMIC SUBSTANCES

A Dissertation

SUBMITTED TO THE GRADUATE FACULTY

In partial fulfillment of the requirements for the

Degree of

Doctor of Philosophy

By

NOPAWAN RATASUK
Norman, Oklahoma
2004

UMI Number: 3150965

UMI Microform 3150965

ProQuest Information and Learning Company
300 North Zeeb Road
P.O. Box 1346
Ann Arbor, MI 48106-1346

REDOX FUNCTIONAL GROUPS OF HUMIC SUBSTANCES

A dissertation APPROVED FOR THE
SCHOOL OF CIVIL ENGINEERING AND ENVIRONMENTAL SCIENCE

BY

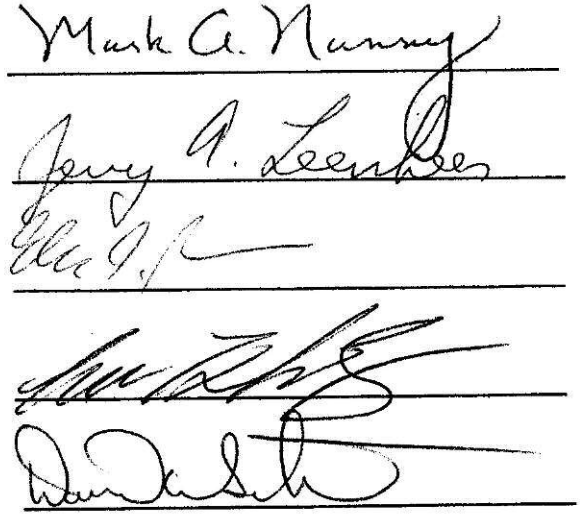

DEDICATION

This dissertation is dedicated to my mother Chamnong and my sisters Nan da, Chalatip and Phanit.

ACKNOWLEDGEMENTS

I must first thank Budda. This dissertation would not have been possible without his teachings that keep my spirit in check and ready for everything unimaginable.

I also would like to thank the following individuals for being so supportive particularly during the last six months before my graduation. I wish to thank Lixia Chen for her friendship and understanding whenever I needed; Drs. Kulwadee and John Pigott for their encouragement; Sebastian, Sabrina, Snowbell and Socrates Pigott for the joyful and companions they shared with me. I also would like to extend my special thanks to Aimee and Roy Guha, Crystal K. Stearn, Jesus P. Maza, Lucinda Brothers, Praveen Gadad, Dr. Hongxia Lei, Lee Acer, Hongbo Shao, Wu Junjie, Xingdong Zhu, Ngoc Hoang, and Liu Yun for their friendship and immeasurable support.

In addition, I would like to acknowledge my committee members Dr. Butler for the opportunity to use the anaerobic chamber and for her valuable comments for this dissertation; Dr. Krumholz for his kind and constructive advice; Dr. Nanny, Dr. Leenheer and Dr. Sabatini for their time serving throughout my course of study. I am particularly grateful to Dr. Strevett for his helps that led to my dissertation defense. I would also like to thank the office staff of the School of Civil Engineering and Environmental Science; Molly Smith, Brenda Finch, Susan Williams, Audre Carter and Ron Conlon. Without their assistance my graduate experience would not be have been enjoyable.

Finally I would like to thank my entire family for their constant support throughout my life.

TABLE OF CONTENTS

LIST OF TABLES

LIST OF FIGURES

PREFACE

Humic substances, ubiquitous compounds in the environment, can facilitate redox processes by acting as electron mediators. Since electron mediators eliminate the necessity for direct contact between an electron donor and acceptor during redox processes, electron transfer via humic substances can enhance the reductive transformation of many organic contaminants as well as reductive detoxification of several toxic metals. Despite the extensive evidence of this capability, little is known about the redox functional groups of humic substances which directly involve electron transfer processes.

This dissertation described experiments that were carried out in order to identify and quantify the redox function groups of humic substances. It consists of four chapters. The first three chapters are written according to the guideline established for Environmental Science and Technology to which all of these manuscripts will be submitted. The last chapter contains the overall conclusions and recommendations derived from the results of each chapter. The following discussion will briefly highlight each chapter.

The discussion in Chapter 1 focuses on the methodology developed to characterize and identify redox functional groups in fourteen humic substances. The analytic technique was based on three catalytic reduction methods. Results from these three methods reveal that not all humic substances are electron mediators. Landfill leachate humic substances apparently lack redox functional groups and thus can not act as electron mediators. For other humic substances, redox sites include functional groups both with and without a quinone structure. The identity of redox sites with nonquinone

structure could not be identified by the developed technique. These nonquinone sites are responsible for 21%-56% of electron carrying capacity of humic substances samples. There is evidence of the possibility that different types of microorganisms in a natural system might activate individual redox functional group of humic substances.

Chapter 2 presents the attempt to identify redox functional groups in the nonquinone category. Two candidates for the redox sites, iron and sulfur, in humic substances were selected for detailed analysis. Both candidates were chosen because they are well-known redox centers of several proteins and enzymes in biological systems and both of them occur in humic substances. The role of iron in humic substances was investigated using cation exchange techniques whereas the significance of sulfur redox centers was evaluated by X-ray photoelectron spectroscopy. Results with Aldrich humic acid (the sample with the highest iron content) demonstrated that iron in this sample is not the redox site in the nonquinone category. Sulfur functional groups, on the other hand, are members of this category. They are responsible for 18%-120% of the electron carrying capacity of nonquinone redox sites.

Although results in Chapter 1 indicate the lack of redox functional groups of landfill leachate humic substances, it was unclear whether this deficit was permanent or temporary. Decomposition of municipal solid waste (MSW) in landfills occurs in several steps. Each step produces leachate of a different chemical composition. Current chemical characteristic of landfill leachate humic materials are distinct with the substantial enrichment of aliphatic carbon components. This characteristic does not occur in those humic substances that contain redox functional groups. It is possible that future degradation of refuse may change the chemical characteristic and produce redox

functional groups of leachate humic substances. To evaluate this possibility, detailed investigation of variation in organic carbon OC component of MSW was investigated and described in Chapter 3. MSW core samples that had been degraded to different extents were excavated from the Norman landfill and characterized for their OC composition. The observed ^{13}C NMR spectra of the OC of MSW samples suggested the preferential preservation of an aliphatic carbon component during the refuse degradation processes in the landfill. This result suggests the continuing enrichment of the aliphatic carbon component of humic substances in the leachate, thus further implying that it is less likely that the redox functional groups of humic substances will be developed over time. Therefore, it is rather confirmed that landfill leachate humic substances are not electron mediators. In addition to this result, the sources of OC, as well as an interaction between degraded MSW and hydrophobic contaminants in the landfill, are discussed in this chapter. In the final chapter, the overall conclusions are made based on the data from the preceding chapters. Recommendations for future research are also discussed in Chapter 4.

In summary, it has been demonstrated that redox functional groups of humic substances include more than one redox species. At least two redox sites, quinone and sulfur functional groups, have been identified. This knowledge advances our understanding of the basic elements of the electron mediating function of humic substances and can help direct us towards a better understanding of the redox processes that are facilitated by the humic substances in a natural system.

CHAPTER 1

QUANTITATIVE CHARACTERIZATION OF THE REVERSIBLE ELECTRON CARRYING CAPACITY OF HUMIC SUBSTANCES

ABSTRACT

A new analytical technique based on palladium (Pd) and H_2 catalytic system showed significant potential as a useful method for reliably assessing redox sites in humic substances. The technique identifies redox sites as a function of their resistance to the hydrogenolysis process. The test system consists of catalytic reduction process, the measurement of electron carrying capacity, and simple air oxidation. The extent of hydrogenolysis, which occurs during the catalytic reduction, can be controlled by pH and the type of catalyst used in the system. Verification of the reversibility of the redox sites is also permitted due to the use of a removable catalyst that allows the test to be repeated. Eight quinone compounds and fourteen humic substance samples were examined using this technique. The tests with quinone compounds demonstrated that hydrogenolysis occurring in the pH 6.5-Pd/Al_2O_3 (Pd supported on Al_2O_3) redox system effectively removed quinone moieties in all model compounds. When the system's pH was increased to 8, the extent of hydrogenolysis became less intense. Quinones with an electron withdrawing substituent were left intact. As hydrogenolysis was further compromised by removing Al_2O_3 from the system, quinones without substituents and quinones with adjacent electron donating functional groups also remained intact. At that point, only

quinones with an electron donating substituent located far away in a separate conjugated system suffered hydrogenolysis. The humic substance samples' tests showed that six landfill leachate humic substances, which were highly aliphatic, did not have redox sites. Therefore, they were not electron mediators. Eight other humic substance samples were capable of shuttling electrons, even in the pH 6.5-Pd/Al_2O_3 redox system, which, according to FT-IR data, had removed their quinone redox sites. Thus, the technique revealed that electrons could be transferred by multiple redox species in humic substances and not just by quinone moieties as is widely understood. The technique showed that redox sites in humic substance samples include both nonquinone (NQ) and quinone groups. Redox sites in the NQ group were responsible for 21%-56 % of the electron carrying capacity (ECC) of the samples. The technique further divided redox sites in the quinone group into two subgroups. The first subgroup includes redox sites with a neighboring electron withdrawing substituent (Q1), which was liable for 13%-58 % of the ECC. The second subgroup contains redox sites characterized by having an adjacent electron donating substituent (Q2). Redox sites in the Q2 category were accountable for 8%-50% of ECC. The relative abundance of Q1 and Q2 redox sites is moderately related to the amount of carboxylic carbon, which is one of electron withdrawing functional groups in humic substances. The Q1 sites are relatively prevalent in humic substances with high carboxyl carbon content, such as fulvic acid samples. Q2 sites, on the other hand, are relatively more abundant in humic acid samples, which generally have a lower carboxyl carbon content.

INTRODUCTION

Natural attenuation of many pollutants relies on oxidation-reduction processes. For chlorinated compounds, such as hexachloroethane, and toxic metals, such as chromium VI, reductive transformation is the major mechanism to reduce their toxicity (*1*,*2*). The rate of the reduction process can be significantly increased in the presence of electron mediators. For example, when humic acids and quinone compounds were added as electron mediators, reductive transformation of carbon tetrachloride by anaerobic granular sludge was enhanced by a factor of six (*1*). In the natural environment, common electron mediators are humic substances, which are ubiquitous compounds of diverse origins. Many studies during the past decade have shown that humic substances may participate in a wide range of redox processes involving organic contaminants and metal ions in natural systems (*3*-*7*). The capability of humic substances to perform this function is measured as the number of mole equivalents of electrons transferred from a donor to an acceptor, which is termed electron carrying capacity (ECC). The ECC of humic substances varies from sample to sample (*8*-*10*).

The differences in humic substances' ECC are not surprising because the contents of their functional groups vary among samples. However, for the same sample, the inconsistency found in a humic substance's ECC when measured by different analytical techniques is rather unexpected. ECC estimated using the I_2 oxidation method for soil and Suwanee river humic acids (*11*) are one order of magnitude higher than reported in microbial reduction studies of the same samples (*8*-*10*). The difference could not be clearly explained because of the ambiguity of the redox functional group that governs the

ECC of humic substances. Currently, quinone moieties have been hypothesized as the primary redox functional group in humic substances (*8*-*9*). This hypothesis has been widely adopted. However, there are some issues that are not consistent with this hypothesis. Struyk and Sposito (*11*) pointed out that the content of quinone moieties calculated from the amount of free radicals (recognized as semiquinone radicals) in soil and Suwanee River humic acids were almost 1-3 orders of magnitude lower than the actual number of electrons transferred to an acceptor. In a separate case, free radical content, which was measured by Electron Paramagnetic Resonance spectroscopy (EPR), was accountable for only 10 % of the vanadium reduced by a soil fulvic acid. Moreover, the participation of free radicals was doubted because there was no loss in the intensity of these radicals after reduction occurred (*12*). In addition, an electrochemical study (*13*), which examined redox properties of humic substances and several quinone compounds, showed that the two groups of compounds had different electrochemical properties.

The ambiguity in the basic element of humic substances' electron shuttling function has limited the understanding of the thermodynamic (i.e., reduction potentials) and kinetic (i.e., rate constants) aspects of the redox processes in which these materials are involved. To resolve this issue, an analytical method is necessary to clarify the redox functional groups in humic substances. In this study, an analytical technique based on a redox system using Palladium (Pd) catalytic reduction has been developed to evaluate redox sites in humic substances. Unlike other techniques, use of a removable reducing agent provides an opportunity to test the redox reversibility of electron transfer sites in humic substances. This capability is essential because the ability to repeatedly cycle electrons is the most crucial character of electron mediators. The primary objectives of

the development were *i*) to characterize redox functional groups in humic substances and *ii*) to quantify the ECC of these functional groups. Since quinone moieties are widely understood as the primary redox sites in humic substances, this functional group was used as a starting point in this study. The hypothesis of the study is that humic substances can act as electron mediator due to the presence of quinone redox sites.

MATERIALS AND METHODS

Samples

Eight humic substance samples were purchased from the International Humic Substance Societies (IHSS). They included Suwanee river fulvic acid (SRFA) and humic acid (SRHA), Elliot soil humic acid (SHA), Summit Hill soil humic acid (SHHA), Leonardite humic acid (LHA), peat humic acid (PFA) and fulvic acid (PFA). One sample, Aldrich humic acid (AHA), was purchased from Aldrich. Six additional samples were humic substances that were isolated from leachate collected from three municipal landfills. Details of the isolation procedures used and the chemical characteristics of these materials can be found elsewhere (*14*). These samples include Norman landfill humic acid (NHA) and fulvic acid (NFA), South East Landfill humic acid (SEHA) and fulvic acid (SEFA), East Oak landfill humic acid (EOHA) and fulvic acid (EOFA).

The following model quinone compounds were obtained from Sigma or Aldrich and were used as received: anthraquinone-2-carboxylate (AQC), 2,6-dihydroxyanthraquinone (AQOH), anthraquinone-2,6-disulfonate (AQDS), 5-hydroxy-

1,4-naphthoquinone (juglone), 2-hydroxy-1,4-naphthoquinone (lawsone), 2-methyl-5-hydroxy-1,4-naphthoquinone (plumbagin), 1,4-naphthoquinone (NTQ), and 1,4-naphthoquinone-2-sulfonate (NQS). The structure of these quinone compounds are given in Figure 1.1.

Redox Cycling Experiments

Experimental Procedures

Since redox reversibility is the most crucial property of an electron mediator, the redox experiment was designed to validate this aspect of an electron transfer site. In this experiment, a series of four tests was conducted in a cyclic manner. These four tests, which were finished in one cycle, included *i*) the catalytic reduction of the sample, *ii*) the ECC measurement of the reduced sample, *iii*) the reoxidation of the reduced sample, and *iv*) the ECC measurement of the oxidized sample. For each experiment, these four tests were repeated five times (five cycles). The details of each test are given in the following paragraphs.

Experimental Conditions

For each sample, the redox cycling experiment was carried out in three different conditions. Each condition was different in terms of the system's pH and/or the type of catalyst used in the reduction step. In the first condition, the experiment was conducted at

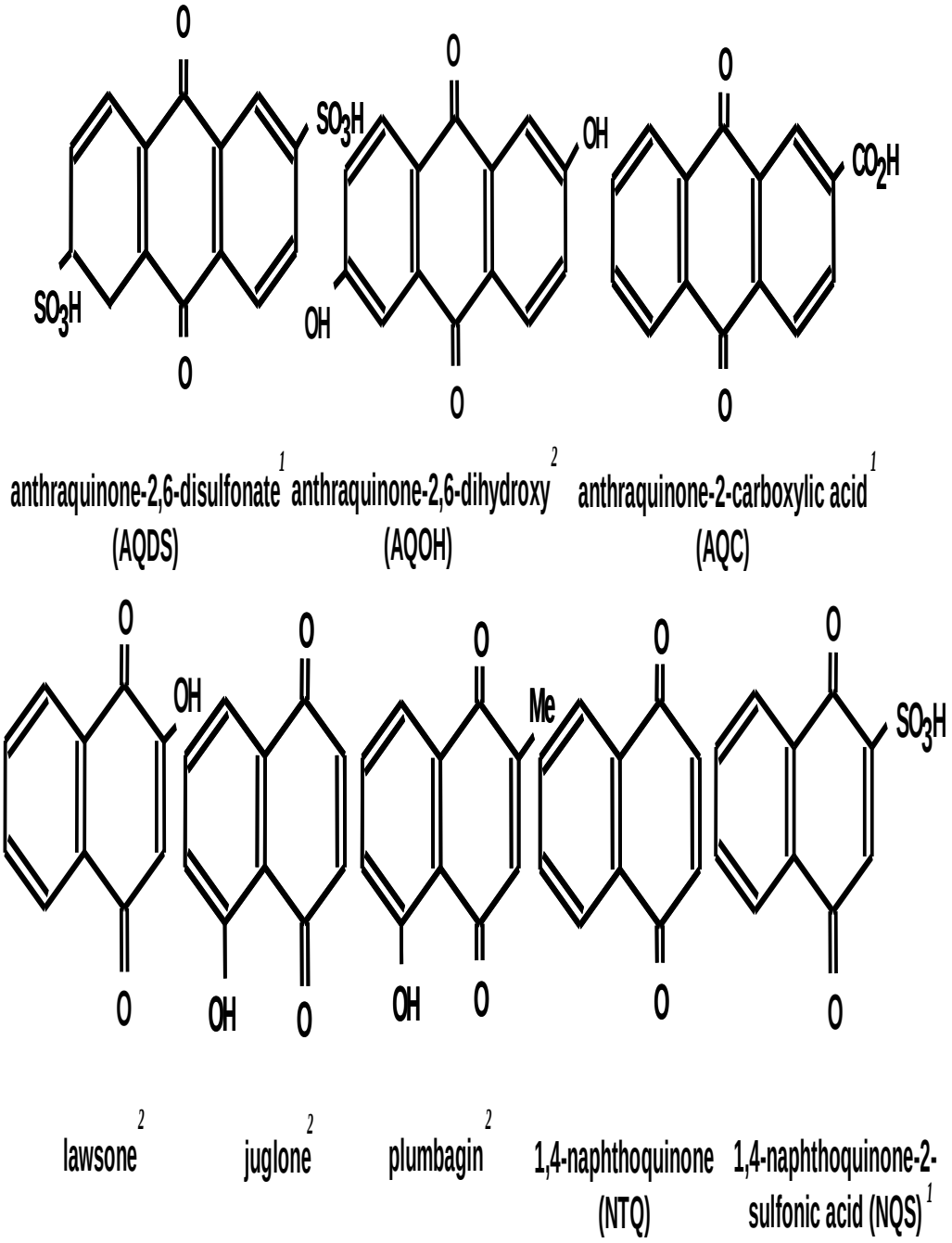

FIGURE 1.1 Chemical structures of quinone compounds used in the study.[1] quinone with an electron withdrawing substituent, [2] quinone with an electron donating substituent

pH 8 using Pd powder (Aldrich) as a catalyst in the reduction step. In the second condition, the experiment was also performed at pH 8 but used Pd support on Al_2O_3 (Pd/Al_2O_3; Aldrich) as the catalyst. For the third condition, the experiment was run at pH 6.5 using Pd/Al_2O_3 as the catalyst. The two pHs (6.5 and 8) were selected as optimum conditions closest to the pH of the electron acceptor, iron (III) citrate (pH 6.8). The catalyst selection was based on the extent of hydrogenolysis, which is discussed in detail in the results and discussion section.

Experimental Details

In the first experimental condition, humic substance samples and quinone compounds were dissolved in a 10 ml buffer (0.3 M phosphate buffer prepared anaerobically with Nanopure water that was boiled for 15 min and cooled with N_2) in an anaerobic chamber (Coy Instrument) filled with N_2-H_2 (95:5). The sample concentration was 0.5 mg/ml for each humic substance, but it varied among quinone compounds due to their differing solubilities. Pd powder was added to the solution, and the bottle was sealed and removed from the chamber. The mixture of N_2-H_2 gas in the sample bottle was evacuated and replaced with H_2. The sample was shaken for 24 hrs and then returned to the anaerobic chamber. After removing the seal, 0.1 ml of sample was filtered with a 0.2 μm cellulose acetate membrane (Whatman), and then its ECC was measured using the procedure described below. The remaining sample was removed from the chamber, and the catalyst was filtered from the solution. The sample solution was bubbled with air for 30 min. Later, the dissolved oxygen was later removed by warming the sample solution

to 40°C in a water bath, bubbling with N_2 for another 30 min, and then returning it to the anaerobic chamber. Now oxidized, this oxidized sample was measured for ECC in the same way as the reduced sample. After the ECC measurement, a new catalyst was added, and the process was repeated.

In the second and third experimental conditions, clean Pd/Al_2O_3 pellets (Pd supported on Al_2O_3; Aldrich; catalyst was washed with Nanopure water twice, dried at 50°C, and cooled to room temperature before use) were added to each sample solution (3 pellets/ml) instead of Pd powder. After the sample was sealed and removed from the anaerobic chamber, catalytic reduction was initiated by introducing H_2 into the sample solution via a needle inserted through the stopper. The reduction was maintained for 90 min with constant shaking. Except for these changes, the procedure was identical to the first experiment. Each sample was tested under all three redox conditions, and each test was run in triplicate. Additionally, a blank solution, which contained no humic substance, was run. The times specified for the reduction period in each set-up was chosen to allow a steady-state ECC to be reached for both AQDS and AHA (*9*). All redox experiments were conducted at room temperature and ambient pressure.

Dextrose Experiment

The concept of this experiment was adopted from the Blue Bottle Experiment described by Shakhashiri (*15*). In the anaerobic chamber, the dextrose solution was prepared by mixing dextrose (0.5g/ml) with 0.3 M anaerobically prepared phosphate buffer pH 8. This solution was then used to dissolve the humic substance (0.5 mg/ml),

AQDS (0.5 mM), juglone (0.05 mM) and NQS (1 mM). After 24 hrs of continuous stirring, triplicate measurements of ECC for each sample solution were determined using the procedure described below. The dextrose solution was also tested as a blank. The sugar reduction experiment was conducted only once, since the sample could not be reoxidized due to the inability to remove the reductant (*i.e.*, dextrose) from the system.

Electron Carrying Capacity (ECC) Measurement

For each sample, this procedure was conducted in anaerobic chamber following the protocol described by Lovley et al. (*8*). Briefly, 0.01 ml of iron (III) citrate (50 mM, pH 6.8) was mixed with 0.1 ml of filtered sample and allowed to incubate for 15 min. Then 0.05 ml of the mixture was added to 2.5 ml ferrozine solution (1 mg/ml of 0.025 M HEPES buffer (N-[2-Hydroxyethyl]piperazine-N'-[2-ethanesulfonic acid]). This mixture was removed from the anaerobic chamber, and its absorbance was measured at 562 nm (A_{562}). The concentration of iron (II) was determined based on a standard curve prepared using a series of standard solutions of iron (II). In all catalytic redox experiments, the difference in the amount of iron (II) between the reduced and oxidized samples was considered to be the ECC of the sample. For the sugar experiment, the iron (II) produced by the sample was determined by subtracting the A_{562} of blank sugar solution and A_{562} of the blank sample solution (in phosphate buffer, no sugar added) from the A_{562} of the reduced sample solution.

Examination of Quinone Moieties

This part of the study was conducted differently for quinone compounds and humic substance samples. For quinone compounds, before starting the experiment and after finishing each redox cycle, the status of quinone moieties was examined using UV-Vis spectroscopy (a single beam HP 8452 Diode Array Spectrophotometer, fixed grating with 512 detectors integrated on a photodiode array, deuterium discharge lamp for the full UV and visible range, scan range 190-820 nm). An additional experiment using FT-IR spectroscopy (Bruker Equinox 55 FTIR, liquid nitrogen cooled MCT detector, Globar source; the experiments were run in transmission mode at $4cm^{-1}$ resolution, 120 scans were averaged for each sample examined) was performed with AQDS to supplement the results from the UV-Vis examination. The solution of AQDS after the 5^{th} redox cycle was dialyzed (cellulose acetate membrane, MWCO 100; Spectrum; Spectra/Por) and freeze dried before subjecting it to the test. For humic substances, samples before starting the experiment were dissolved in Nanopure water and titrated with tetrabutylammonium hydroxide (TBA) to pH 10 (*16*), freeze-dried, and then examined by FT-IR spectroscopy (Bruker Equinox 55 FTIR). Identical procedures were performed on samples from the 5^{th} redox cycle (these samples were dialyzed (cellulose acetate membrane, MWCO 100; Spectrum; Spectra/Por) and freeze dried prior to the TBA titration).

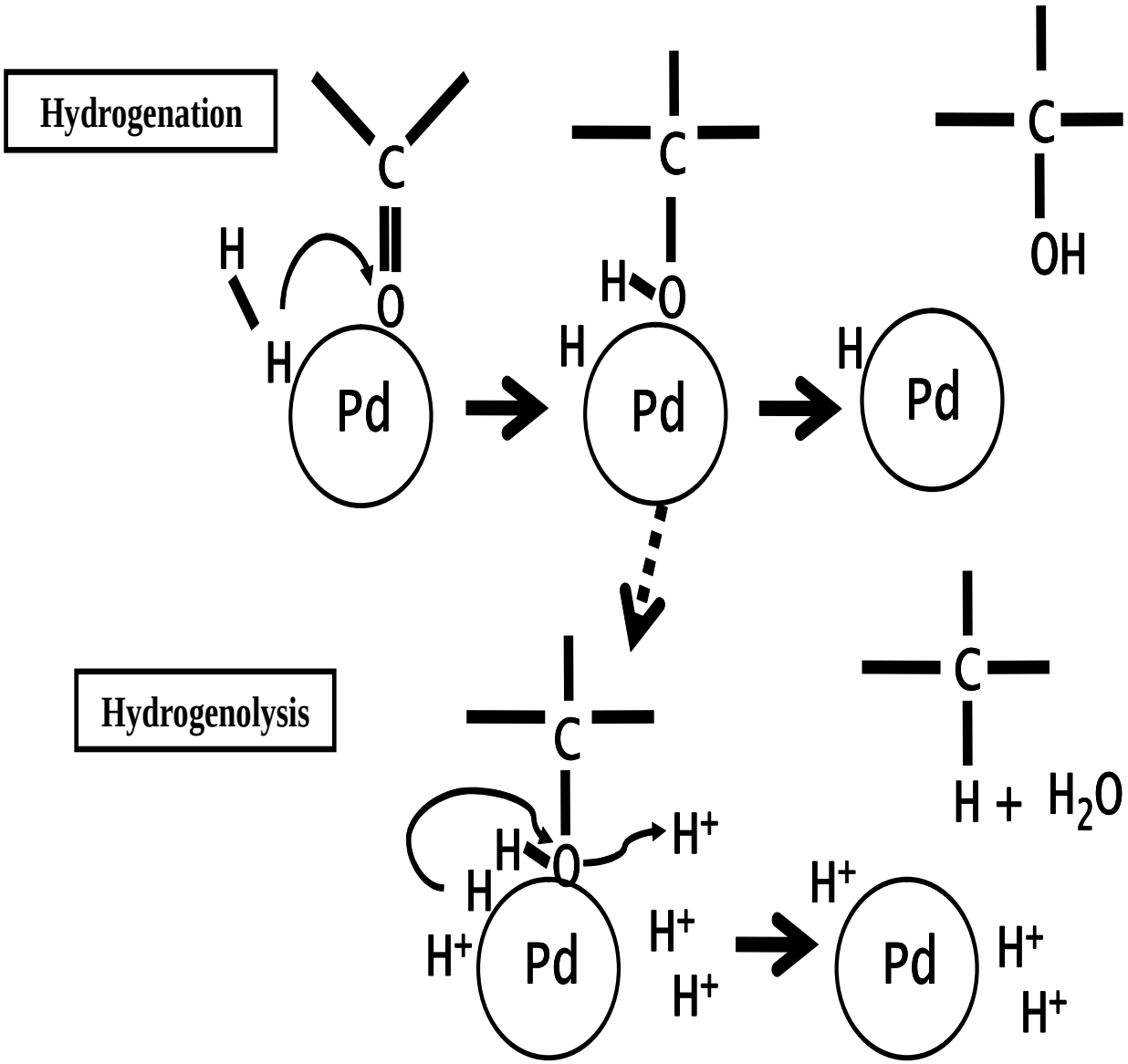

FIGURE 1.2 Mechanisms of hydrogenation and hydrogenolysis.

RESULTS AND DISCUSSION

Basic Concepts

The essence of the redox system in this study is catalytic reduction. This reaction occurs in two steps. The first step is hydrogenation, which is the addition of H across π bonds (Figure 1.2). The second step is hydrogenolysis, which is the insertion of H across σ bonds (Figure 1.2). These two steps do not occur simultaneously. Advancing from the first to the second step depends on the pH of the medium. An acidic medium promotes hydrogenolysis, while a basic solution inhibits the process (*17-18*). A good leaving group attached to the target carbon center is also required for hydrogenolytic cleavage. Better leaving groups undergo faster hydrogenolytic cleavage. For quinones, reductive hydrogenation, the first step, is the process that reduces quinone to hydroquinone. In an acidic medium, the reaction proceeds to the second step, in which H^+ protonates the hydroxyl group of hydroquinone, and makes water the leaving group. Since water is a good leaving group, the hydrogenolysis of hydroquinone is favorable in an acidic medium (*17*). Pd was chosen for this study because it is the most widely used catalyst for the catalytic cleavage of benzylic C-O bonds (*17*), such as those found in hydroquinone. In addition, its catalytic effect toward quinones is sufficient even under mild conditions. At room temperature and ambient pressure, Pd/H_2 assisted hydrogenation has been shown to successfully reduce benzoquinone to hydroquinone, and upon the addition of 5% HCl, the reaction proceeded to hydrogenolysis with cyclohexanol as a final product (*19*).

Besides the pH of the medium, a catalyst support also shares a pivotal role in determining the rate of hydrogenolysis. γ-Al_2O_3, one of many materials used as a support for Pd is also a common catalyst by itself for hydrogenolysis of alcohol (dehydration). In an aqueous system, the surface of γ-Al_2O_3 is occupied by OH groups attached to Al atoms. The attraction between the O atoms in OH groups and Al atoms turns the OH groups into Brønsted acid sites (*20*). Coordination of an OH group of alcohol to this acid site leads to the cleavage of the C-O (*21*). The C-O bond breaking process is crucial because, when undergoing this reaction, hydroquinone loses its ability to be oxidized back to quinone. This results in the ending of the quinone-hydroquinone cycle. Since the cycling capability is the principal mechanism defining an electron mediator, losing it means the termination of the electron transfer function of the quinone.

Tests with Quinone Model Compounds

The effects of the pH and catalyst support, which are the controlling factors of hydrogenolysis, were first tested with quinone compounds. Redox experiments using three reduction methods with differing pHs and catalyst types (i.e., *a*) pH 6.5-Pd/Al_2O_3, *b*) pH 8-Pd/Al_2O_3, and *c*) pH 8-Pd) were tested with eight quinone model compounds (structures given in Figure 1.1). The test assumed that, if hydrogenolysis occurs during the reduction process, OH functional groups of the reduced quinone would be cleaved, and the compound would not be able to change back to its original form. If this happened, quinone moieties will not be detected after the reduced compound was reoxidized. The examination of quinone moieties was done by verifying their characteristic UV

absorbance in the 290-nm region (A_{290}; quinonoid electron-transfer absorption band (*22*)). UV-Vis spectra of quinone compounds before and after undergoing each redox experiment (Figure 1.3 and Figure 1.4a, respectively) were used to determine the stabilities of quinone moieties. As shown in Table 1.1, all of the tested compounds lost their quinone moieties in the pH 6.5-Pd/Al_2O_3 reduction. Therefore hydrogenolysis had occurred. Loss of quinone moieties in AQDS was confirmed by results from FT-IR analysis (performed only with AQDS). In the FT-IR spectra of AQDS (Figure 1.4b), the well defined characteristic absorption band of quinone moieties, which was present at 1650 cm^{-1} before the reduction (Figure 1.4b: B), disappeared after the sample was subjected to the pH 6.5-Pd/Al_2O_3 redox system (Figure 1.4b: A1). Therefore, the influence of Al_2O_3 and the available H^+ at this pH were sufficient to remove quinone moieties in eight different configurations.

Table 1.1 also shows that, when pH of the testing system was increased to 8 with Pd/Al_2O_3 as a catalyst, three compounds, AQDS, AQC, and NQS, were able to keep their quinone moieties intact (Figure 1.3). FT-IR analysis of AQDS confirmed that, unlike the result from the reduction at pH 6.5, the quinone moieties were not removed (Figure 1.4b: A2), and AQDS was able to function as an electron mediator for five redox cycles (Figure 1.4c). This outcome was not the same for other five quinones. AQOH, lawsone, juglone, plumbagin and NTQ lost their quinone moieties as indicated by the loss of A_{290} in Figure 1.3. This result indicates that hydrogenation still occurred at pH 8, but it was effective only on certain types of quinone compounds. Examinations of the structures of AQDS, AQC, and NQS revealed one common feature that may have been crucial to the compounds' survival. As shown in Figure 1.1, quinone moieties in AQDS,

TABLE 1.1 The Stability of Quinone Moieties in Model Compounds Tested in Three Different Reduction Systems

Quinones	Stability of quinone moieties		
	$Pd(H_2O)_4Cl_2$	$Pd(H_2O)_4(OTf)_2$	$Pt(H_2O)_4(OTf)_2$
AQDS	no	yes	yes
AQOH	no	no	no
AQC	no	yes	yes
anthrone	no	no	yes
xanthone	no	no	no
phenanthrenequinone	no	no	yes
NTQ	no	no	yes
NQS	no	yes	yes

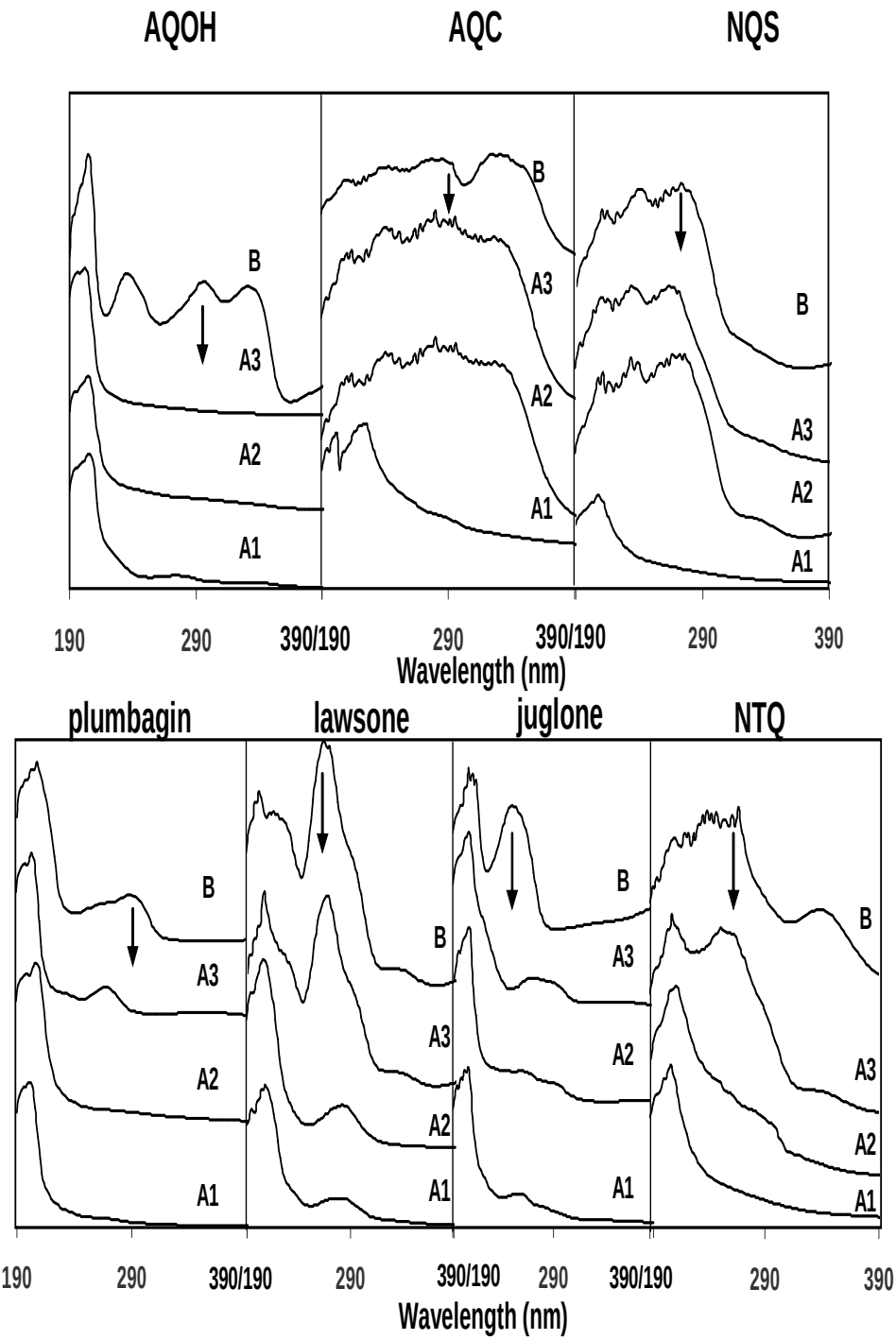

FIGURE 1.3 UV-Vis spectra verifying the stability of quinone moieties in model compounds before the reduction (B); after pH 6.5-Pd/Al2O3 reduction system (A1); after pH 8-Pd/Al2O3 reduction (A2); after pH 8-Pd reduction (A3). The arrow indicates the signal from quinone moieties.

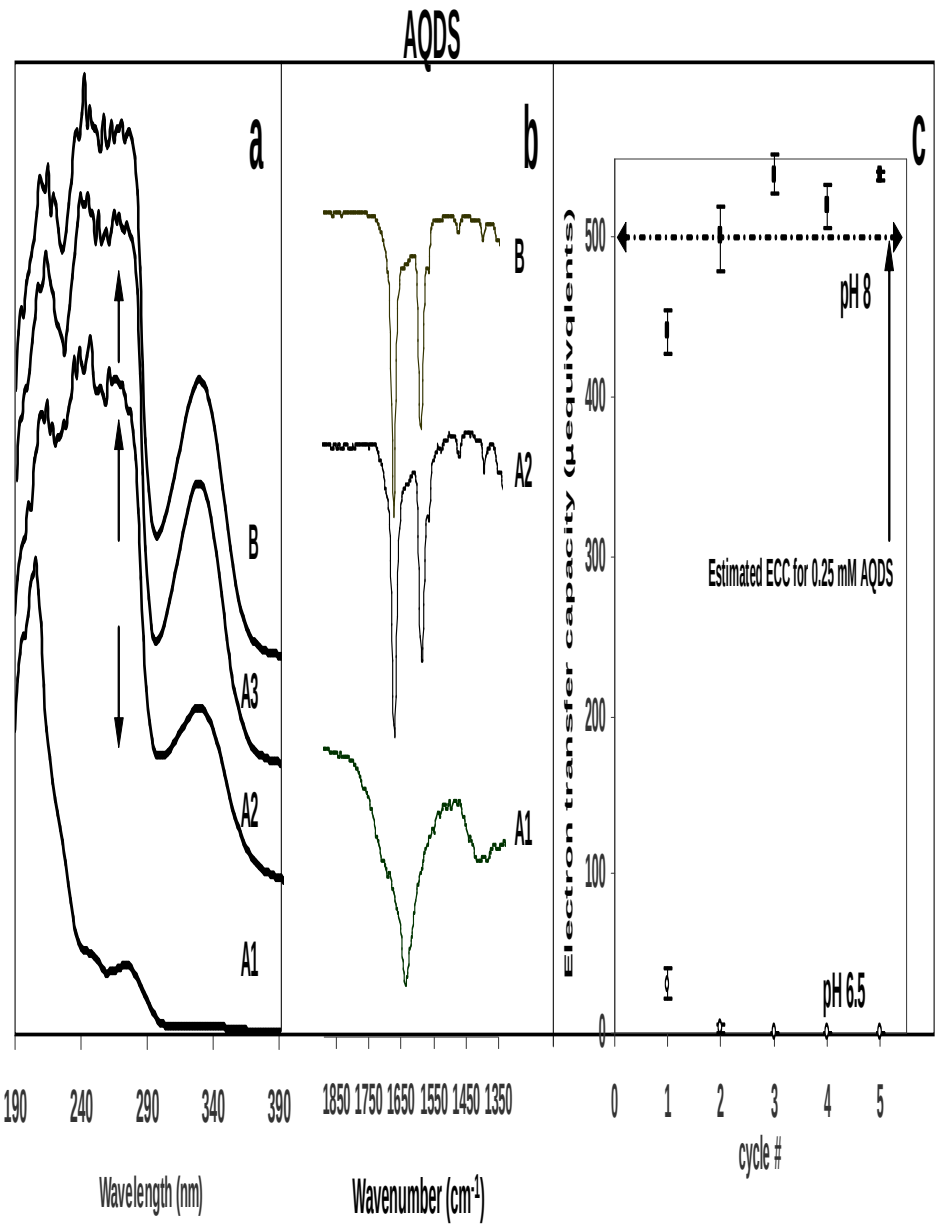

FIGURE 1.4 Analysis of AQDS samples : a) UV-VIS spectra; b) FI-IR spectra. The samples include AQDS before the reduction (B); after the redox experiment using the pH 6.5-Pd/Al_2O_3 reduction system (A1); after the redox experiment using the pH 8-Pd/Al_2O_3 reduction (A2); after the redox experiment using the pH 8-Pd reduction (A3). c) electron carrying capacity of 0.25 mM measured in redox experiments pH 6.5 and pH 8 both using Pd/Al_2O_3 as a catalyst.

AQC, and NQS all have a neighboring electron withdrawing group (EWG; SO_3^- and COO^-). The other five compounds, which lost their A_{290}, either have no functional group (e.g. NTQ) or have an electron donating group (EDG; CH_3, O^-) nearby their quinone moieties. This suggests that the electronic property of any nearby substituent plays a crucial role in protecting quinone moieties in the pH 8-Pd/Al_2O_3 redox system. Substituent effects can be explained in a similar fashion as for a S_N2-type reaction, which is the mechanism of the hydrogenolytic cleavage catalyzed by Pd (*17*). EWG, such as SO_3^- and COO^-, decrease the electron density of quinones moieties, which makes them less nucleophilic and consequently less attractive to electrophilic sites on the catalyst surface.

Some of the active sites for hydrogenolytic cleavage are on the Al_3O_2 surface. Therefore, after Al_2O_3 was removed from the redox system (i.e., Pd powder with no Al_3O_2 support was used as the catalyst), the outcome was changed significantly. As shown in Table 1.1, the number of compounds surviving pH 8-Pd reduction was six compared to only three surviving pH-8-Pd/Al_2O_3 reduction. The three additional compounds that were able to keep their quinone moieties intact were lawsone, plumbagin and NTQ. Hydrogenolysis still occurred but affected only two compounds, juglone and AQOH. When looking at the structure of NTQ, one of the additional three survivors (Figure 1.1), it is apparent that the quinone functional group by itself is not susceptible to catalytic cleavage in the pH 8-Pd test. The vulnerability of the quinone moieties in juglone and AQOH, therefore, might be due to the addition of EDG. However, since lawsone and plumbagin, which also have EDG located adjacent to quinone moieties were intact, the position of the EDG relative to the quinone moieties must be critical.

In S_N2 reactions, rates are slow when the carbon atom undergoing substitution is surrounded by large substituents (*23*). Although OH and CH_3 in lawsone and plumbagin are both small molecules, their close proximity might obstruct the coordination of quinone moieties to the reaction sites on the catalyst surface. This event would impede hydrogenolysis of the quinone moieties. In addition, substituent effects from the EDG of lawsone and plumbagin should be less intense than those in juglone and AQOH. Compared to O^- (deprotonated form of OH), CH_3 is a weaker EDG. In lawsone and juglone, the O^- substituent exerts different effects due to its position relative to quinone moieties. The inductive effect from the adjacent quinone moieties decreases the negative charge density of the O^- of lawsone. Therefore, compared to juglone, the O^- of lawsone is less nucleophilic and less attractive to the reaction site on catalyst surface. One result of this electronic effect from quinone moieties is the much lower p*Ka* of 4.0 of lawsone as compared to juglone's p*Ka* of 6.9 (*24*).

It appears that the three redox systems tested can alter quinone moieties to different extents. The first system, pH 6.5-Pd/Al_2O_3, creates hydrogenolysis to the extent that all quinone moieties are eliminated. The second system, pH 8-Pd/Al_2O_3, generates hydrogenolysis that does not affect quinone moieties with EWG. The third system, pH 8-Pd, produces hydrogenolytic conditions that remove only quinone moieties that have EDG in a separate conjugated system. These results have established analytical approaches to evaluate the contribution of quinone moieties, to characterize their chemical structures, and to quantify their ECC simultaneously.

Tests with Humic Substance Samples

Fourteen humic substance samples were subjected to the three redox systems. The hypotheses of the tests included; *i*) the ECC of HS samples measured by the pH 6.5-Pd/Al_2O_3 method is zero, if quinone moieties are the only redox functional group of humic substances, *ii*) the ECC measured by the pH 8-Pd/Al_2O_3 and pH 8-Pd methods are equal, if quinone moieties exist in one configuration. According to the average ECC value of each humic substance sample (from five test cycles; Figure 1.5) in Table 1.2, both hypotheses were rejected. As shown in Table 1.2, eight out of fourteen samples had measurable ECC values in all three test systems. The ECC of each sample increased as a function of the reduction system used, from pH 6.5-Pd/Al_2O_3 to pH 8-Pd/Al_2O_3 to pH 8-Pd. This observation is consistent with previous findings with quinone compounds.

None of the six landfill leachate humic substance samples showed a measurable ECC in any of the three systems, which indicated that they had no redox sites (at least not sites that could be detected using these test methods). Therefore, the landfill leachate samples are probably not electron mediators. This finding suggests that electron mediating function is limited to certain types of humic substances. Landfill leachate humic substances have a distinct chemical characteristics compared to the other eight samples. They are highly aliphatic (51%-70% aliphaticity) and have a low aromatic carbon content (10%-14% aromaticity (*14*); Table 1.2). The lack of electron transfer abilities in highly aliphatic samples suggests that redox sites in humic substances are unlikely to associate with aliphatic carbon functional groups.

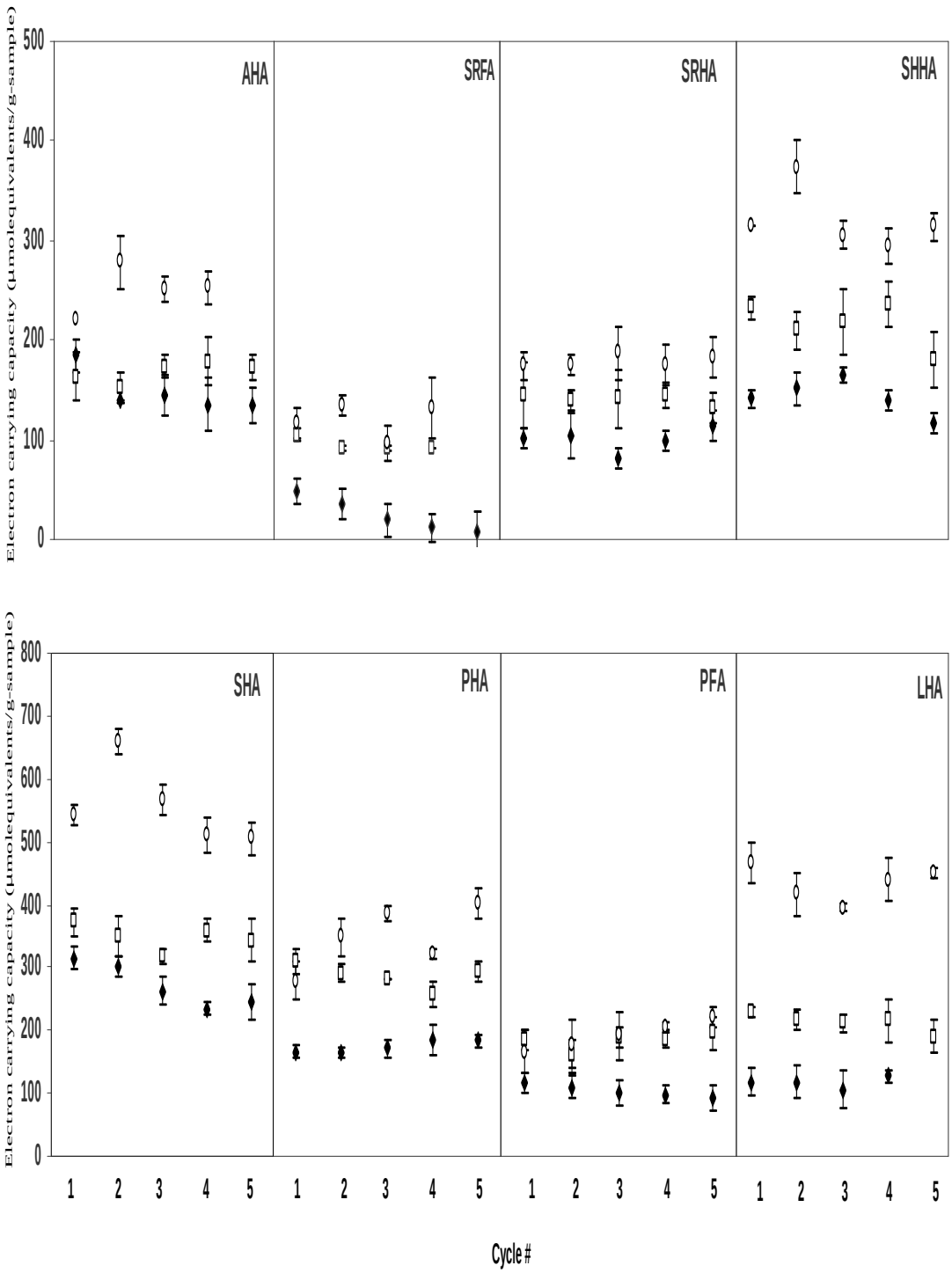

FIGURE 1.5 Electron carrying capacity of humic substance samples measured with three reduction systems. Key:♦, pH 6.5-Pd/Al_2O_3; □,pH 8-Pd/Al_2O_3;○, pH 8-Pd. Each data point represents the value in each redox cycle. Suwanee River fulvic acid (SRFA): Suwanee River humic acid (SRHA): soil HA (SHA): peat humic acid (PHA): peat fulvic acid (PFA): Leonardite humic acid (LHA): Summit Hill humic acid (SHHA): Aldrich humic acid (AHA)

TABLE 1.2 Aromatic, Carboxyl Carbon Contents and Electron Carrying Capacity of Humic Substance Samples.

Sample	Aromatic C(%)	Carboxyl C(%)	Electron carrying capacity (μmolequivalents/g-sample)			
			pH 6.5-Pd/Al_2O_3[3]	pH 8-Pd/Al_2O_3[3]	pH 8-Pd[3]	Calculated values[4]
AHA	45[1]	15[1]	132±8	167±12	260±13	na
SRFA	24[1]	20[1]	25±17	95±7	120±17	0.090
SRHA	37[1]	19[1]	100±12	140±18	179±15	0.106
SHHA	30[1]	19[1]	143±18	216±22	320±31	0.894
SHA	50[1]	18[1]	262±35	349±21	538±31	2.144
PHA	47[1]	20[1]	174±10	287±19	385±26	0.881
PFA	34[1]	28[1]	103±10	183±13	199±19	0.042
LHA	58[1]	15[1]	117± 9	213±15	429±28	3.323
NHA	14[2]	10[2]	0	0	0	*na*
NFA	10[2]	11[2]	0	0	0	*na*
SEHA	14[2]	8[2]	0	0	0	*na*
SEFA	13[2]	11[2]	0	0	0	*na*
EOHA	12[2]	8[2]	0	0	0	*na*
EAFA	11[2]	12[2]	0	0	0	*na*

[1] from the International Humic Substances Societies (IHSS)

[2] from ref 22

[3] average values of five redox cycles

[4] calculated from the free radical content available from IHSS and data reported by Struyk and Sposito (*11*)

na = data not available

Suwanee River fulvic acid (SRFA): Suwanee River humic acid (SRHA): soil humic acid (SHA): peat humic acid (PHA): peat fulvic acid (PFA): Leonardite humic acid (LHA): Summit Hill humic acid (SHHA): Aldrich humic acid (AHA)

The most interesting data in Table 1.2 is the ECC measured in the pH 6.5-Pd/Al_2O_3 redox system. Except for landfill leachate samples, humic substances showed measurable ECC values in this test. Due to the detrimental effects of hydrogenolysis in this system to all eight quinone compounds, the detected ECC should not relate to presence of quinone functional groups. To confirm this conclusion, samples taken before and after the redox test were esterified with TBA and analyzed by FT-IR. This method determined the status of the quinone moieties by comprehensively checking them with all aromatic ketones (*16*). As shown in Figure 1.6, the disappearance of an aromatic ketone peak (resolved at 1630 cm^{-1}) in FT-IR spectra of samples after the pH 6.5-Pd/Al_2O_3 redox process verified the loss of quinone moieties in the humic substance samples. This evidence shows that redox sites responsible for ECC in the pH6.5-Pd/Al_2O_3-redox system are not quinone moieties.

Similar to the increased number of quinone compounds that survived the test, the ECC of each humic substance sample (except the landfill leachate humic substances) improved when the pH of the test system was increased to 8 (pH8-Pd/Al_2O_3 redox system). Based on results from model compounds (AQDS, AQC, and NQS), the quinone moieties with EWG (now called Q1) should survive and be responsible for the increased fraction of ECC in this test system (Figure 1.7). Likewise, when Al_2O_3 was removed, quinone moieties with structures similar to lawsone, plumbagin, and NTQ (now called Q2) should account for the increased fraction of ECC in the pH8–Pd redox system. These two descriptions of quinone moieties are in contrast to the general concept that depicts quinone moieties in humic substances as only in AQDS format.

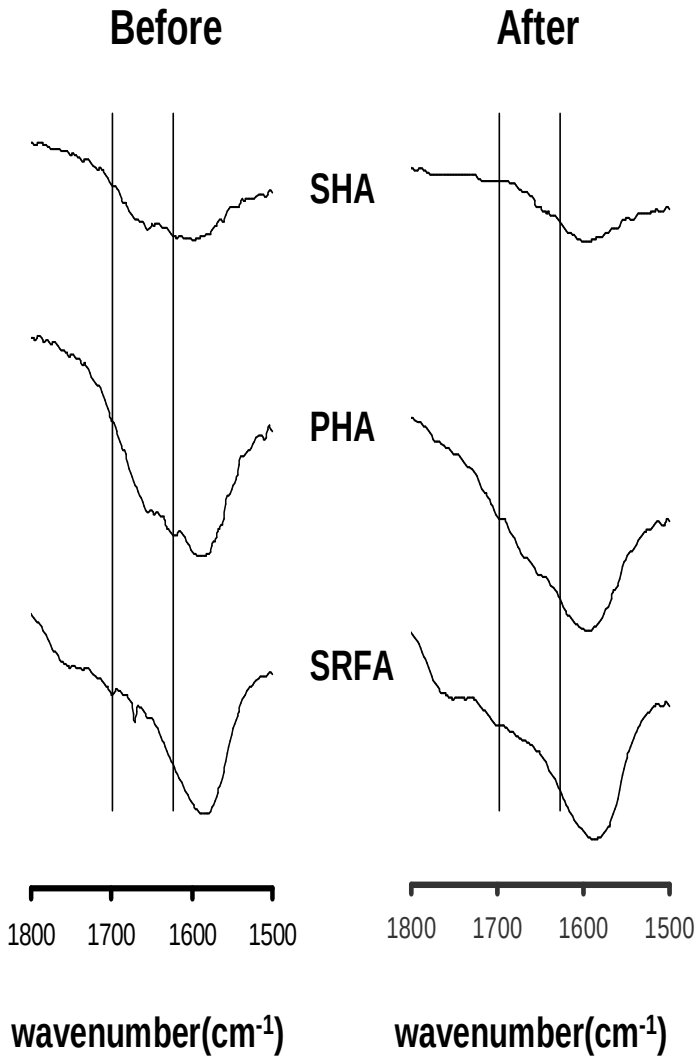

FIGURE 1.6 Examples of FT-IR spectra of humic substance samples before and after the redox experiment conducted at pH 6.5 using Pd/Al_2O_3 as a catalyst. Samples were esterified with tetrabutylammonium hydroxide. The response from aromatic ketones, which include quinone moieties, is in the area between the two vertical lines.

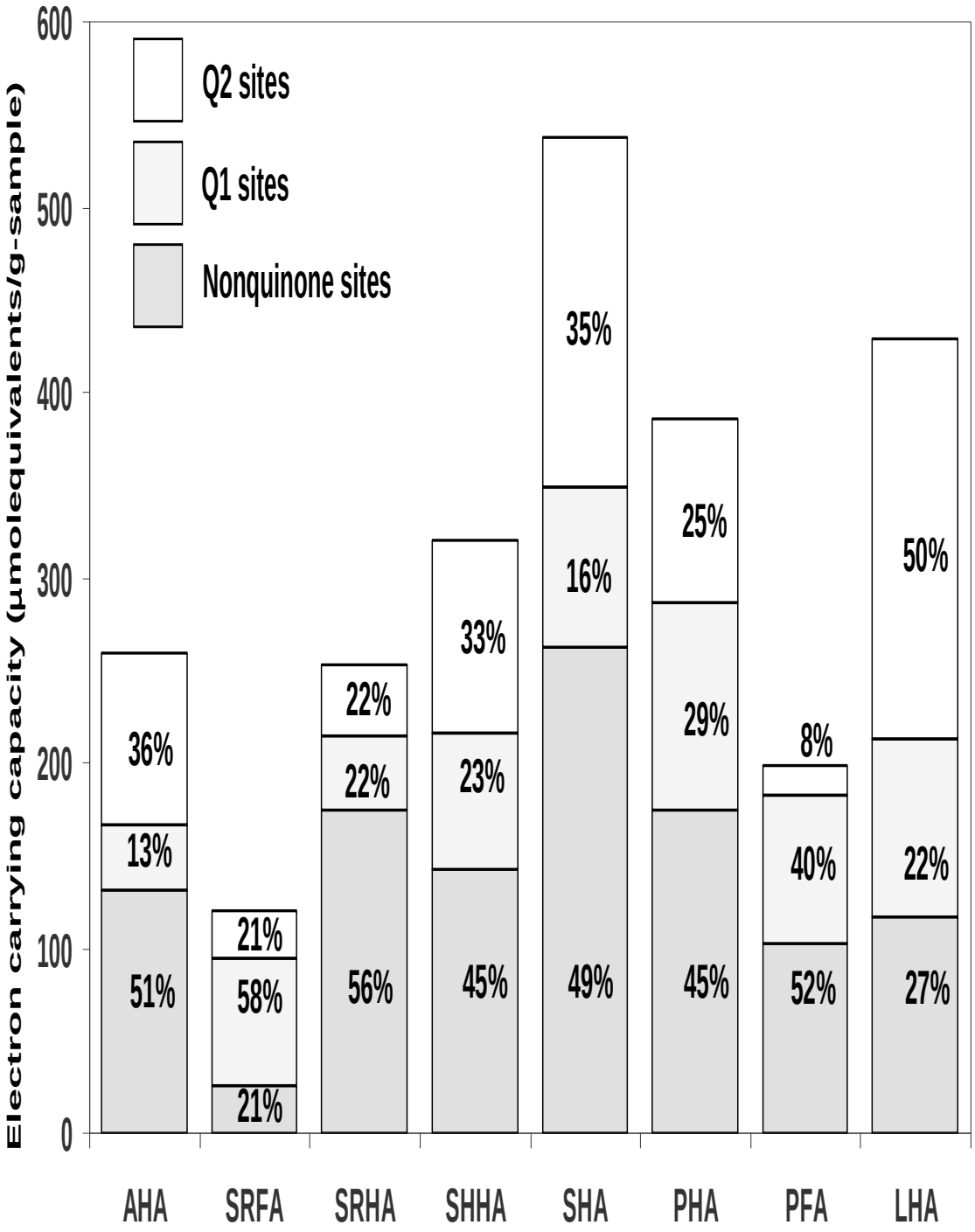

FIGURE 1.7 Contribution of each redox functional group to the electron carrying capacity of humic substance samples. In each case, the electron carrying capacity was an average of the values measured in 5 redox cycles.

It was observed that the ECC values of SRHA, PHA and SHA in this study are one to two orders of magnitude lower than their oxidation capacities measured by I_2 titration at pH 7 (11,500, 4,600, 3300 μmolequivalents/g-sample, respectively; (*11*)). Since the I_2 titration method could not verify the reversibility of the functional groups that were oxidized by I_2, it is still inconclusive whether these oxidized functional groups were the actual redox centers. The strong oxidizing power of I_2 might react with electron rich functional groups that were not involved in the electron transfer processes of these three humic substances.

Since reversibility is the key requirement for every electron mediator, the fact that nonquinone redox sites (abbreviated as NQ) demonstrated the fundamental act of adding and/or removing electrons through at least 5 redox cycles (pH 6.5-Pd/Al_2O_3 system; Figure 1.5) firmly proved that the NQ redox species are electron transfer sites. An interesting aspect regarding the NQ sites is that they survive hydrogenolytic cleavage that is intolerable for sites with quinone structures. Due to this property, they are considered more robust than sites with quinone structure. Natural attenuation of several organic contaminants, such as chlorinated compounds, occurs through hydrogenolysis processes (*x*). Under environmental conditions that promote hydrogenolysis, it is possible that electrons might be transferred by humic substances at the NQ sites, since they are robust in this situation. Q1 and Q2 sites might no longer be active because they are vulnerable to hydrogenolysis. The contribution of NQ sites to the total ECC (values reported from the pH8- Pd redox system) is substantial, ranging between 21%-56 %. Particularly in humic acid samples (except LHA), approximately 50 % of the total ECC can be attributed to NQ sites (Figure 1.7). The identities of these sites are unknown. The observed lack of ECC in

highly aliphatic samples, such as landfill leachate humic substances, makes aliphatic carbon functional groups unlikely NQ redox sites. However, as shown in Figure 1.8a, the correlation between aromatic carbon content and ECC attributed to NQ sites is not good either. An R^2 of 0.75 suggests that NQ sites might not entirely relate to aromatic functional groups. The addition of the ECC of Q1 and Q2 sites to those of NQ improves the correlation between the total ECC and aromatic carbon (R^2 increasing from 0.75 to 0.89: Figure 1.8 b). This correlates well with the fact that quinone moieties are included in Q1 and Q2 sites. The combination of Q1 and Q2 sites is responsible for 44%-79% of the total ECC (Figure 1.7). Since quinone moieties form semiquinone radicals when undergoing one electron reduction (*25*), Scott *et al.* (*9*) related radical content to ECC and found a strong relation between these two parameters of humic substances (R^2 = 0.91). However, Struyk and Sposito (*11*) calculated the ECC of SHA and SRHA based on the samples' radical contents and obtained numbers two to four orders of magnitude lower than the ECC directly measured with I_2 (reported as oxidation capacity) and the ECC reported from a microbial reduction study (*9*). This finding led them to conclude that quinone sites are not the only redox centers in humic substances. Since there are no details on their calculation procedure, it is not possible to evaluate their calculated results. In this study, a good correlation between the ECC of Q1 plus Q2 and the radical content is also found (R^2= 0.91; Figure 1.9), which further substantiates that quinone sites are included in Q1 and Q2 categories. However, the ECC values are still two to three orders of magnitude higher than numbers calculated from radical contents (Table 1.2; the calculation was performed based on results presented by Struyk and Sposito (*11*)).

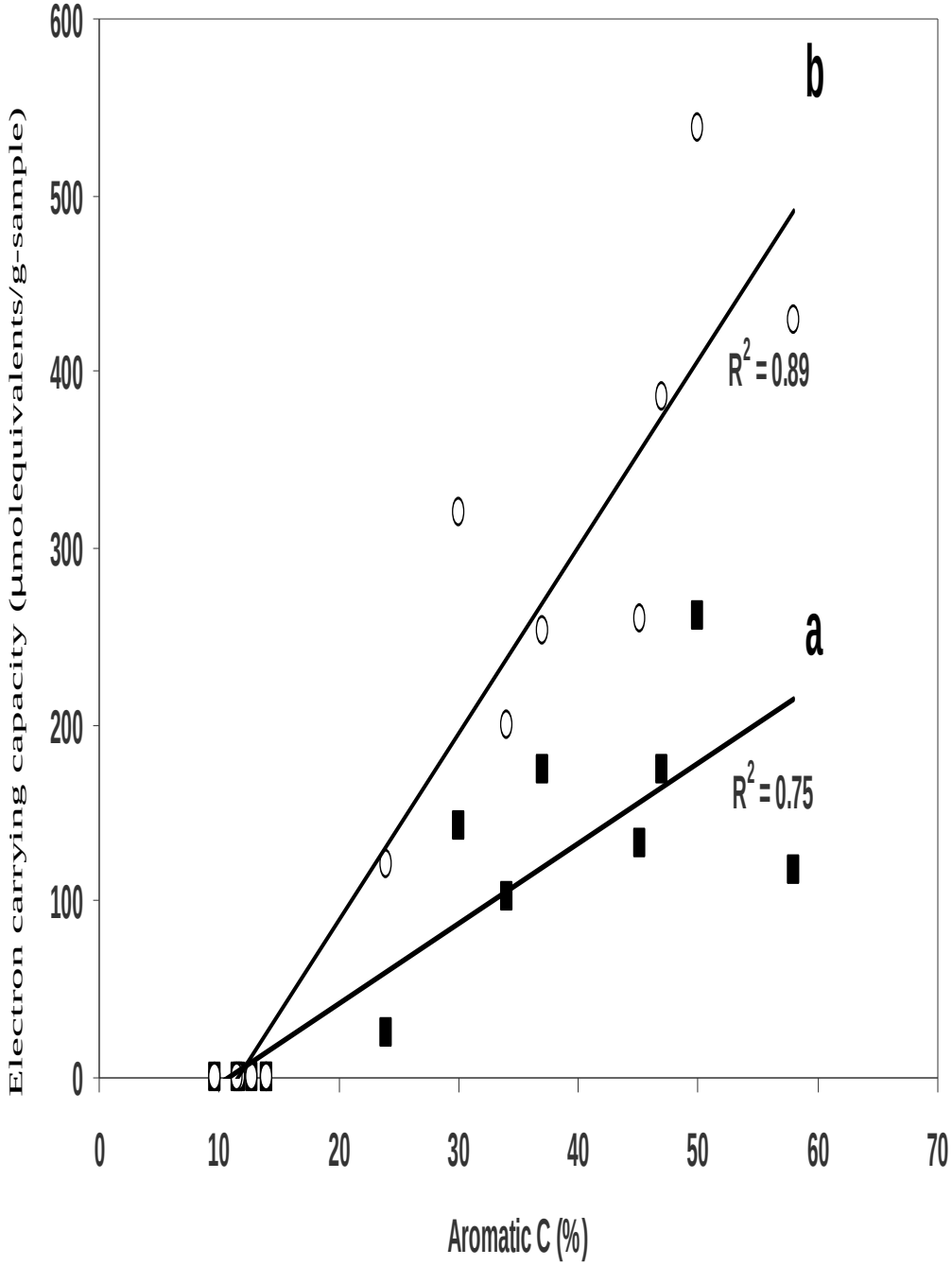

FIGURE 1.8 Correlation between aromatic carbon and electron carrying capacity of a)■, nonquinone sites, b)○, all sites (NQ+Q1+ Q2).

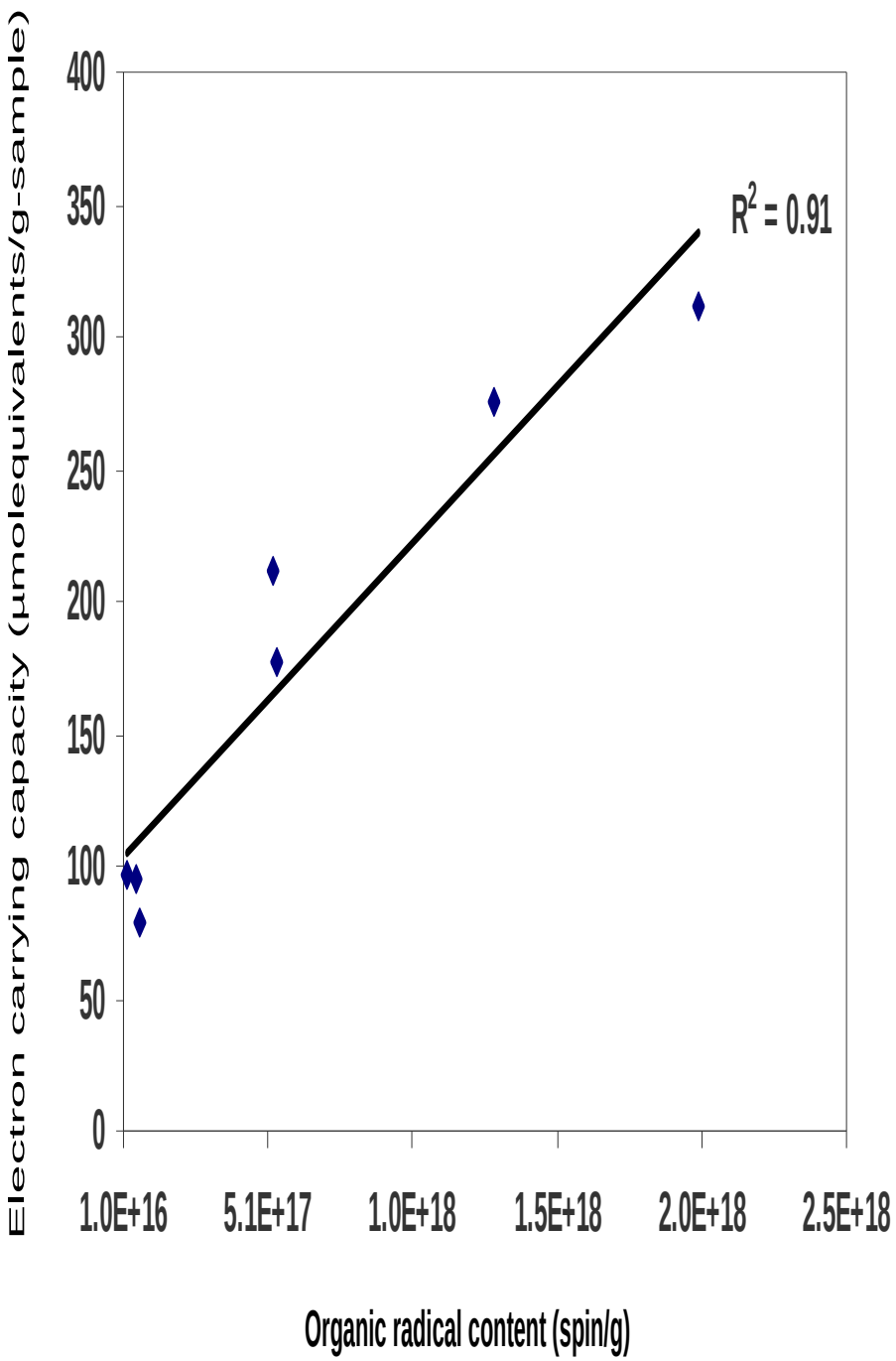

FIGURE 1.9 Correlation between organic radical content and electron carrying capacity.

Since hydrogenolysis still occurred in the pH 8-Pd redox system at a level that was harmful to quinone functional groups in juglone and AQOH, it is uncertain whether all sites with quinone structures were counted. In order to address this issue, an additional experiment, which used dextrose as a reducing agent, was tested with all humic substance samples. Prior to humic substances tests, AQDS, NQS (quinones with EWG) and juglone were subjected to the sugar experiment. All three quinones were fully reduced with their quinone moieties intact (Figure 1.10). As shown in Figure 1.11, the ECC of humic substance samples measured by the dextrose reduction method are comparable to the sum of the ECC from Q1 and Q2 sites. Note that the six landfill humic substances still did not have ECC in this experiment. Based on the results from quinone compounds and humic substance samples, quinone sites with structures similar to those in juglone and AQOH (with EDG in a separated conjugated system) are a minimal part of the quinone functional group in humic substance samples.

Between Q1 and Q2 redox sites, the contribution from Q1 redox sites is relatively higher in two fulvic acid samples (PFA and SRFA; Figure 1.7). As demonstrated with AQDS, AQC, and NQS, EWG are a crucial factor in defending the destructive effects of hydrogenolytic cleavage in the pH 8-Pd/Al_2O_3 redox system. Carboxylic functional groups for instance, have shown to be an effective shield for quinone moieties in AQC during the hydrogenolysis in this system. Generally, fulvic acids are considered more acidic than humic acids due to their greater number of carboxyl functional groups (Table 1.2), so redox sites with quinone structures in fulvic acid samples should have more opportunities to locate close to a carboxyl substituent. Among humic substances that are electron mediators, a plot of carboxyl carbon content versus ECC_{Q1}/ECC_{tot} (Figure 1.12a)

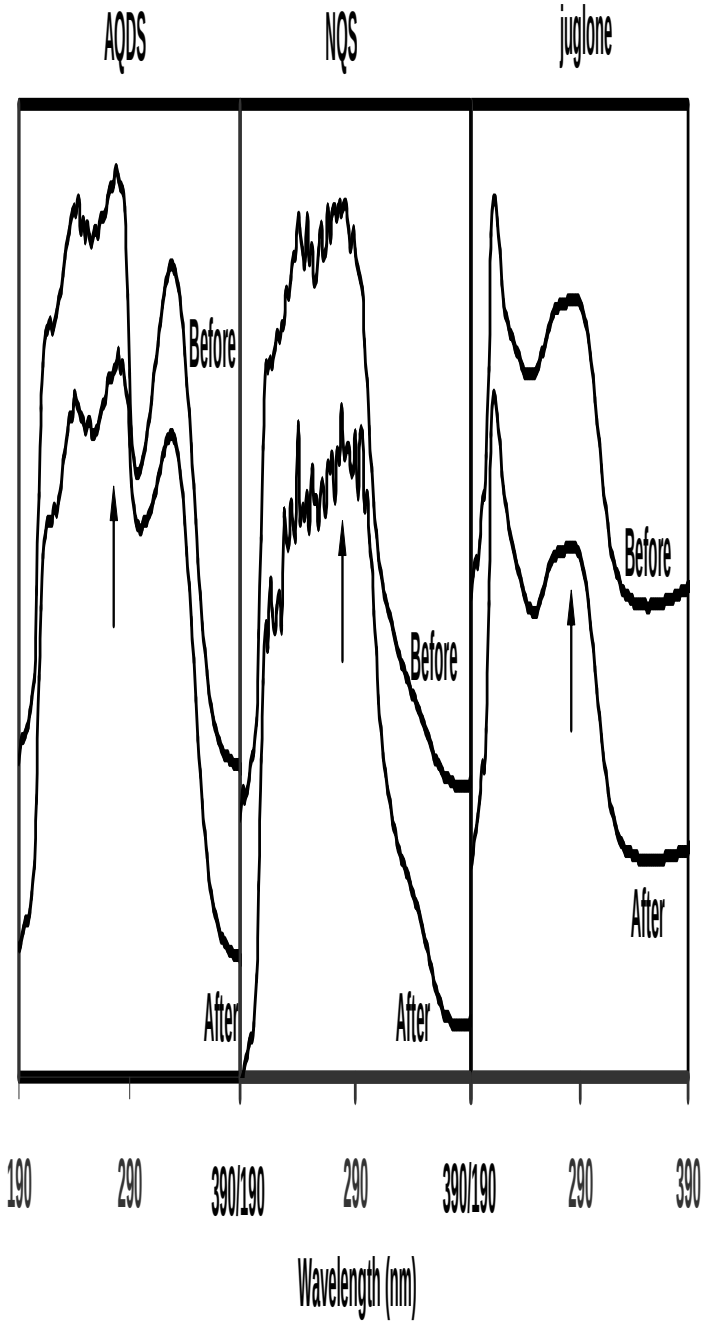

FIGURE 1.10 UV-Vis spectra verifying the stability of the quinone moieties in AQDS, NQS and juglone before and after the dextrose reduction experiment. The arrow indicates signal from the quinone moieties.

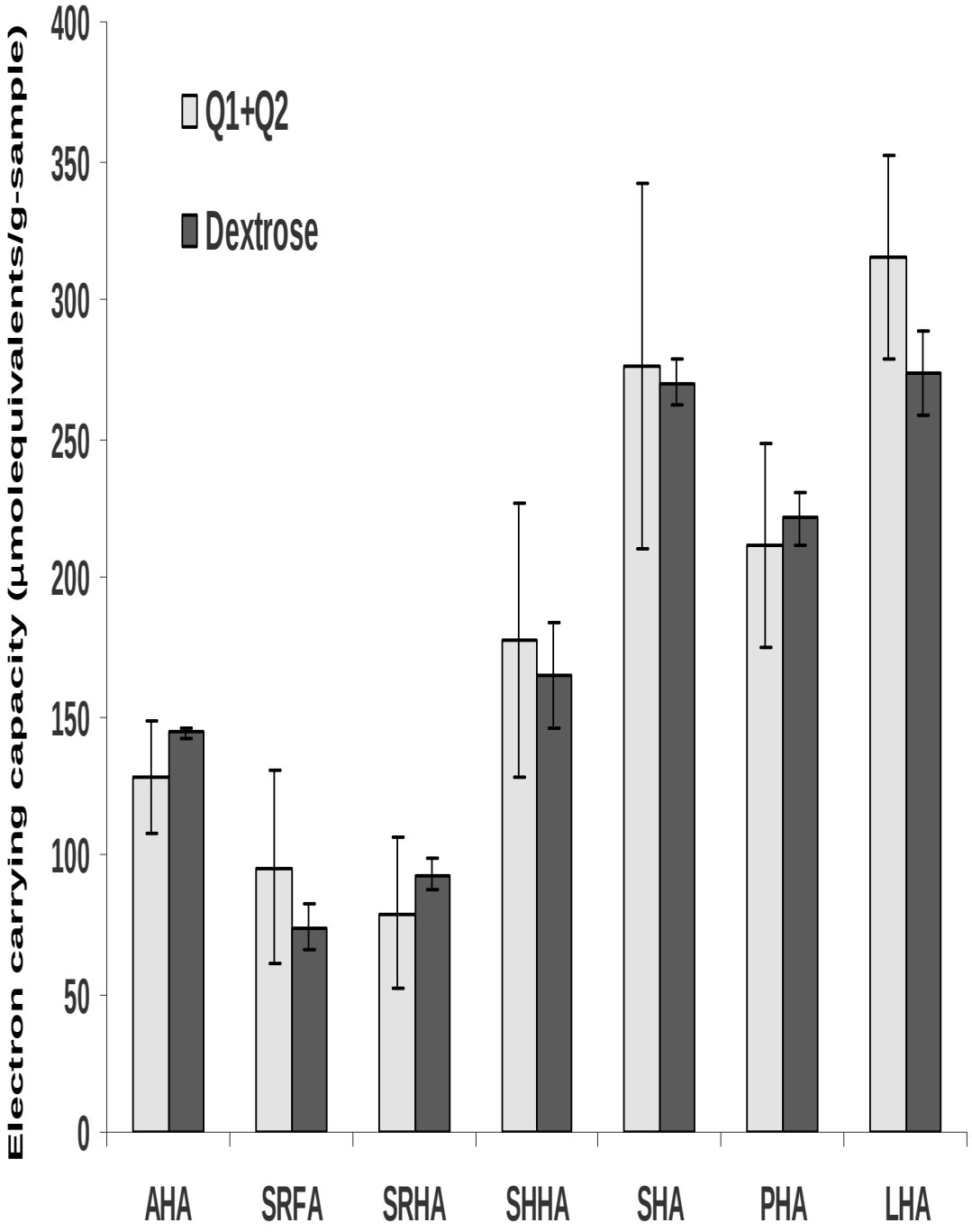

FIGURE 1.11 Combined electron carrying capacity of Q1 and Q2 sites and the value measured using the dextrose reduction method.

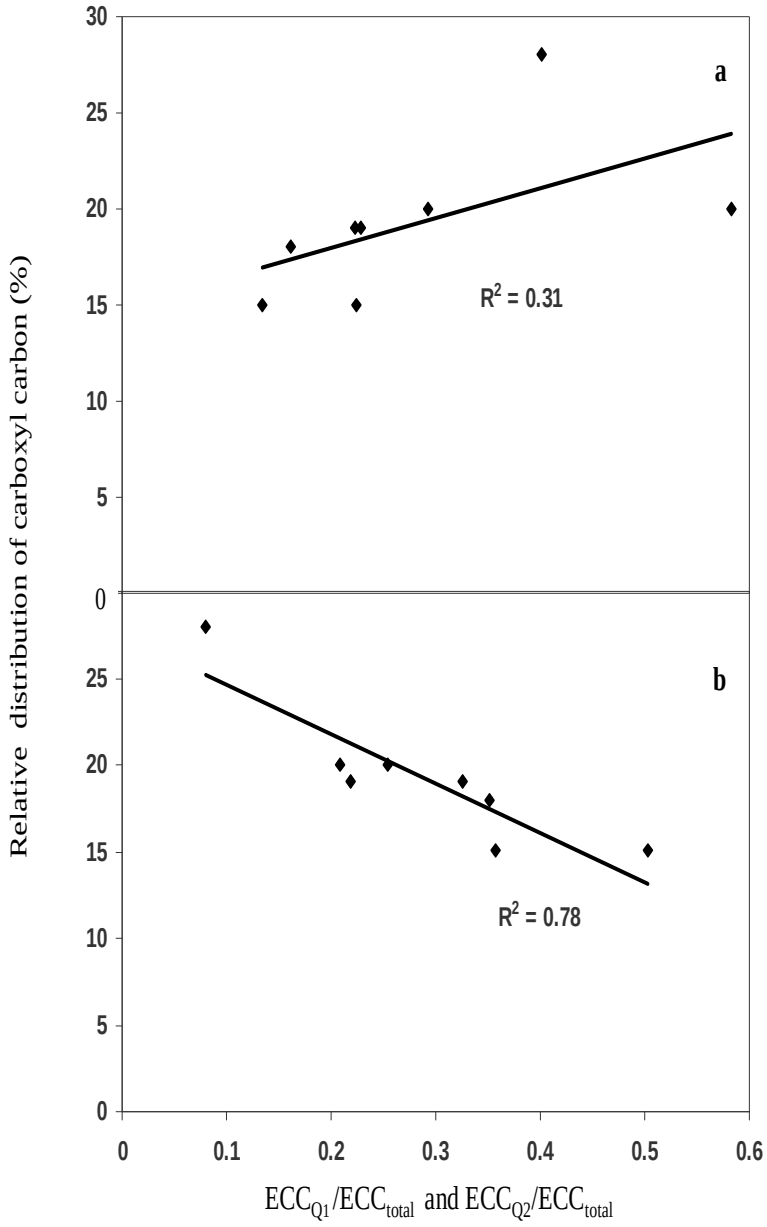

FIGURE 1.12 Correlation between carboxyl carbon and ratio of a) electron carrying capacity of Q1 sites to total ECC (ECC_{Q1}/ECC_{total}) /, b) electron carrying capacity of Q2 sites to total ECC (ECC_{Q2}/ECC_{total})

shows a tendency for Q1 sites to be more abundant in samples with higher carboxylic carbon content. However, the opposite trend occurs for the prevalence of Q2 sites in a plot between carboxyl carbon content and ECC_{Q2}/ECC_{tot} (Figure 1.12 b). The weak correlation between a carboxyl carbon content and ECC_{Q1}/ECC_{tot} ($R^2 = 0.31$) is probably due to the fact that carboxylic functional groups are just one of many EWG that can associate with quinone moieties.

Microbial Accessibility of Redox Sites

It was observed that, although the total electron carrying capacity (ECC) reported in this study was in good agreement with the values measured with the microbial reduction method (*18,9,26*) (Figure 1.13, line a), based on the slope of line b in Figure 1.13, the latter data set, was practically a 1:1 ratio with the ECC of all the quinone sites (Q1 plus Q2). Due to this observation, it would appear that the microorganism, *Geobacter metallireducens,* transfers electrons only via quinone sites in humic substance samples. The possibility that the nonquinone (NQ) redox sites might not be activated by the microbe could be due to many factors. One is the difference in redox potential of test systems. Redox potential for Pd-catalyzed reduction was -480 mV, which is significantly higher than -390 mV measured in the reduction of hydrous ferric oxide by *Geobacter metallireducens* (*27*). If this assumption is valid, the NQ redox sites would be activated at a redox potential that lower than quinone's. However, thiol, such as cysteine/cystine redox couple has a redox potential of approximately -340 mvV (*28*), which is still within

the range reported for *Geobacter metallireducens*. Thus, it seems that the redox potential should be irrelevant.

The next plausible factor is type of bacteria. Different microorganisms might use different redox centers in humic substances. In the case of *G. metallireducens*, the microbe might not be able to use sulfur redox sites in humic substance because it is not a good sulfur reducer. During the microbial reduction of iron (III) oxides using elemental sulfur and cysteine as electron mediators, *G. metallireducens* was replaced by *G. sulfurreducens* because it was considered to be a less effective sulfur reducer (*29).* A previous study (*26*) showed that *G. metallireducens* transferred approximately 152 μmolequivalents of electrons per gram of Aldrich humic acid (AHA). Meanwhile, *Propionibacterium freudenreichii*, fermenting bacteria reportedly transferred 191 μmol equivalents of electrons per gram of AHA (*30*) (data not available for other humic substance samples). *P. freudenreichii* contains the enzyme ferrochelatase, which has cysteinyl ligands for a [2Fe-2S] cluster (*31*).This microbe is one of microorganisms typically used in the production of cheese. *P. freudenreichii* produces several volatile sulfur compounds, which are the sources of cheese flavor, by utilizing sulfur-containing amino acids in milk (*32*). Due to this background, it is possible that *P. freudenreichii* could use sulfur redox sites in humic substances.

The other factor could be chemical structures of the redox sites. Some of sulfur reducing bacteria such as *G. sulfurreducens* can use cysteine as an electron mediator transferring electrons to *Wolinella succinogenes* (*33*). However, anthraquinone disulfonate (AQDS), a model quinone redox site in humic substances, could not be used for the same purpose (*33*). This finding is rather surprising because both *Geobacter*

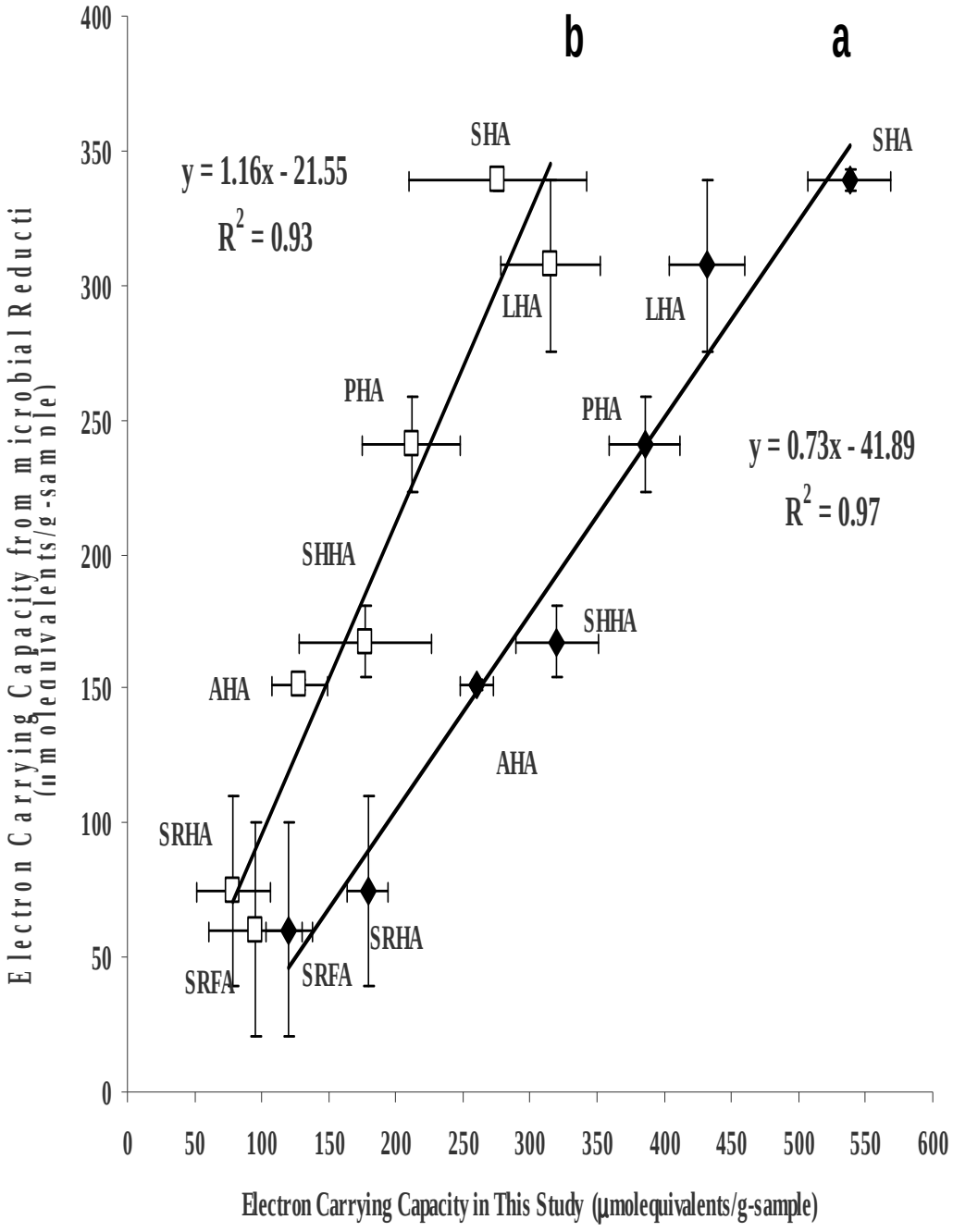

FIGURE 1.13. Correlation between electron carrying capacity measuring by the catalytic reduction method and by the microbial reduction method (ref. *1-3*): a) total electron carrying capacity, b) electron carrying capacity of quinone sites (Q1 plus Q2)

sulfurreducens and *W. succinogenes* can reduce iron (III), AQDS and humic substances (*34*). Even more interesting than that, it is appeared that not every thiol compound can shuttle electrons between these two bacteria. Among several thiols and disulfides, which include L-cysteine, D-cysteine, L-homocysteine, cysteamine, glutathione, and 2,2'-dithiodiethanesulfonic acid (Coenzyme M; Figure 1.14), only L-cysteine was reported to be the effective electron carrier (*33*).

The performance of an electron mediator might depend on its molecular size. Air oxidation of the self-assembled monolayer of alkanethiols on silver and gold surfaces occurs at a different rate depending on the chain length of the thiols. Short chain thiols oxidize faster than the long chain ones (*35*). However, this is not the case for L-cysteine and D-cysteine. Both compounds are identical, different only the orientation of the amine group (Figure 1.14). Given these complications, it is clear that more studies on factors controlling the accessibility of the redox sites in humic substances are inevitably essential.

ENVIRONMENTAL SIGNIFICANCE

This new analytical technique proves to be a valuable tool in providing insightful information about redox sites in humic substances. This technique revealed that electron transfer functions of humic substances are carried out by redox functional groups that can be divided into nonquinone and quinone redox sites. Since redox sites with a nonquinone structure are more resistant to hydrogenolysis than quinone moieties, these redox sites might be able to function in more varied environments than do the quinone redox centers.

For example, in a remediation process using zero valent iron, one of three reductive transformation pathways of pollutants included catalyzed hydrogenolysis by the H_2 that is formed by the reduction of H_2O during anaerobic corrosion of the iron (*36*). In such condition, if humic substances are involved, quinone redox sites would be disabling. Only nonquinone sites supposedly remain operable. For quinone redox sites, the finding that they exist with various neighboring substituents implies that this group has diverse redox activity abilities. As demonstrated by the microbial reduction of an azo dye (*37*), quinone compounds with different substituents facilitated the reaction with different relative activities. Therefore, even among quinone functional groups, redox activities could be different. Thus it is plausible that redox sites in humic substances might not work together simultaneously. It may depend on the environmental conditions that switch on some sites but not others.

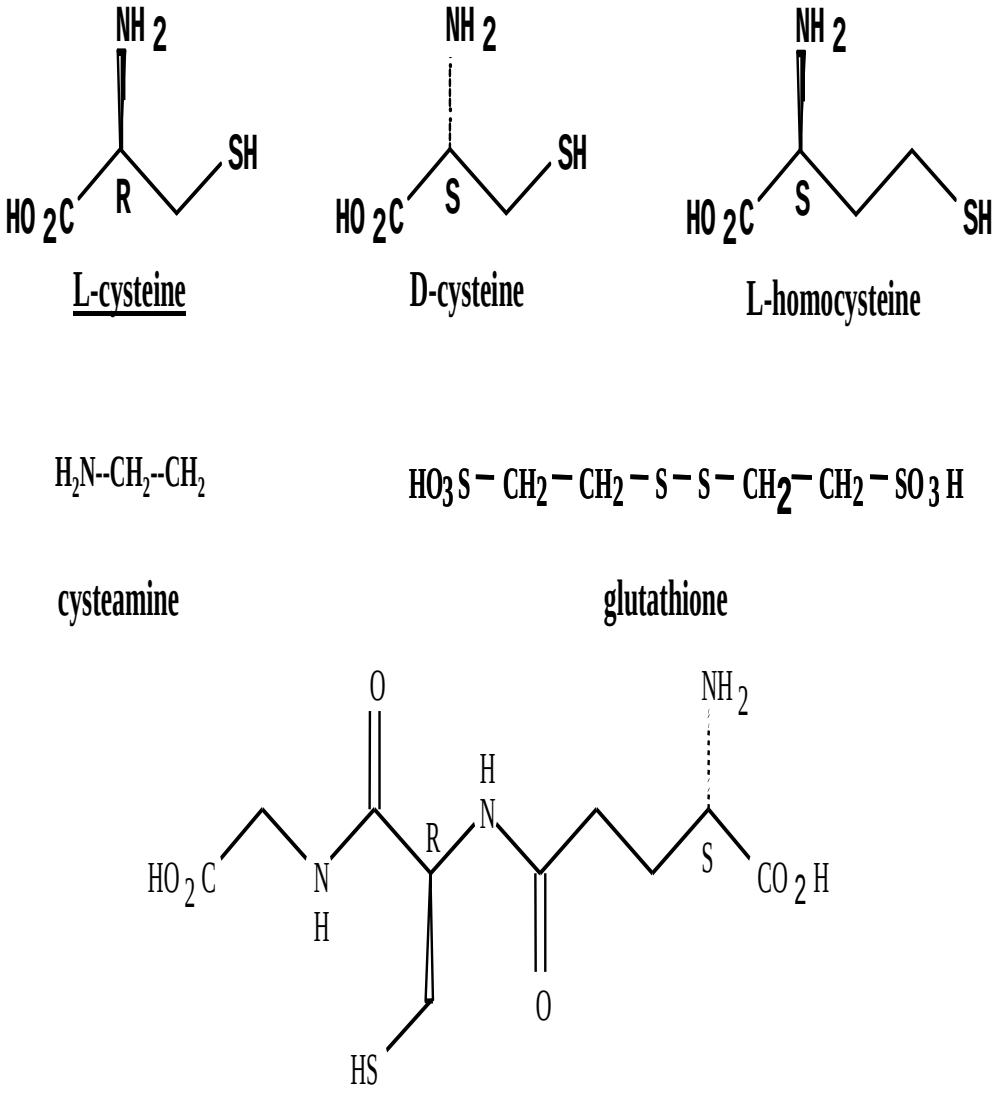

FIGURE 1.14 Structures of thiols and disulfides tested as the electron mediator during the electron transfer between *geobacter sulfurreducens and wolinella succinogenes (*ref. *10)*. The name of compound capable of shuttling electrons is underlined.

ACKNOWLEDGEMENTS

This work was supported by NSF-CAREER grant BES-9732969. Ms. Ratasuk was supported by a grant from the Royal Thai government. The authors gratefully acknowledge Drs. Daniel E. Resasco, John F. Scamehorn and Jose E. Herrera of School of Chemical Engineering, the University of Oklahoma, for their assistances in obtaining the UV-Vis and FT-IR data.

LITERATURE CITED

(1) Cervantes, F. J; Vu-Thi-Thu, L.; Lettinga, G.; Field, J. A. Quinone-respiration improves dechlorination of carbon tetrachloride by anaerobic sludge. *Appl. Environ. Microbiol*. **2004**, *64*, 702.

(2) Nakayasu, K.; Fukushima, M.; Sasaki, K.; Tanaka, S.; Nakamura, H. Comparative studies of the reduction behavior of chromium(VI) by humic substances and their precursors. *Environ. Toxicol. Chem*. 1**999**, *18*, 1085.

(3) Curtis, G. P.; Reinhard, M.. Reductive dehalogenation of hexachloroethane, carbon tetrachloride, and bromoform by anthrahydroquinone disulfonate and humic acid. *Environ. Sci. Tech.* **1994**, *28*, 2393.

(4) Collins, R.; Picardal, F. Enhanced anaerobic transformations of carbon tetrachloride by soil organic matter. *Environ. Toxicol. Chem*. **1999**, *18*, 2703.

(5) Wittbrodt, P.R.; Palmer, C. D. Reduction of Cr(VI) by soil humic acids. *Eur J. Soil Sci*. **1997**, *48*, 151.

(6) Skogerboe, R.K. and Wilson, S.A. Reduction of ionic species by fulvic acid. *Anal. Chem*. **1981**, *53*, 228.

(7) Deiana, S.; Gessa, C.; Manunza, B.; Rausa, R.; Solinas, V. Iron (III) reduction by natural humic acids: A potentiometric and spectroscopic study. *Eur. J. Soil Sci.* **1995**, *46*, 103.

(8) Lovley, D. R.; Coates, J. D.; Blunt-Harris, E. L.; Phillips, E. J. P.; Woodward, J. C. Humic substances as electron acceptors for microbial respiration. *Nature* **1996**, *382*, 445.

(9) Scott, D. T.; McKnight, D. M.; Blunt-Harris, E. L.; Kolesar, S. E.; Lovley, D. R. Quinone moieties act as electron acceptors in the reduction of humic substances by humics-reducing microorganisms. *Environ. Sci. Technol.* **1998**, *32*, 2984.

(10) Klapper, L.; McKnight, D. M.; Fulton, J. R.; Blunt-Harris, E.; Nevin, K. P.; Lovley, D. R.; Hatcher, P. G. Fulvic Acid Oxidation State Detection Using Fluorescence Spectroscopy. *Environ. Sci. Technol.* **2002,** *36*, 3170.

(11) Struyk, Z.; Sposito, G. Redox properties of standard humic acids**.** *Geoderma.* **2001**, *102*, 329

(12) Wilson, S. A.; Weber, J. H. An EPR study of the reduction of vanadium (V) to vanadium (IV) by fulvic acid. *Chem. Geol.* **1979**, *26*, 345.

(13) Nurmi, J. T.; Tratnyek, P.G. Electrochemical properties of natural organic matter (nom), fractions of nom, and model biogeochemical electron shuttles. *Environ. Sci. Technol.* **2002,** *36*, 617.

(14) Nanny, M. A.; Ratasuk, N. Characterization and comparison of hydrophobic neutral and hydrophobic acid dissolved organic carbon isolated from three municipal landfill leachates. *Wat Res*. **2002**, *36*, 1572.

(15) Shakhashiri, B.Z.*Chemical demonstrations: A handbook for teachers of chemistry.* Vol.1. University of Wisconsin Press: Wisconsin**,** 1983.

(16) Leenheer, J.A.; Wilson, M.A.; Malcolm, R.L. Presence and potential significance of aromatic-ketone groups in aquatic humic substances. *Org. Geochem*. **1987**, *11*, 273

(17) Smith, G.V.; Notheisz, F. *Heterogeneous Catalysis in Organic Chemistry*, Academic Press, New York**,** 1999

(18) Rylander, P.N. *Catalytic Hydrogenation over Platinum Metals*. Academic Press, New York, 1967.

(19) Rosenblatt, E. F. *J.* Hydrogenation of quinone with palladium and platinum catalysts. *Am. Chem. Soc*. **1940**, *62*, 1092.

(20) Sohlberg, K.; Pennycook, S. J.; Pantelides, S. T. *J.* Explanation of the Observed Dearth of Three-Coordinated Al on γ-Alumina Surfaces. *Am. Chem. Soc*, **1999**, *121*, 7493.

(21) DeCanio, E. C.; Nero, V. P.; Bruno, J. W. Identification of alcohol adsorption sites on γ-alumina. *J. Catalysis*, **1992**, *135*, 444.

(22) Thomson, R.H. *Natural occurring Quinones*, Academic Press, New York, **1971**

(23) Larson, R.A; Weber, E.J. *Reaction mechanisms in environmental organic chemistry***.** Lewis Publishers, Boca Raton, 1994.

(24) Petrova, S. A.; Kolodyazhnyi, M. V.; Ksenzhek, O. S. Electrochemical properties of some naturally occurring quinones. *J. Electroanal Chem*. **1990**, *277*, 189.

(25) Steelink, C; Tollin G. *Biochim.* Stable free radicals in soil humic acid. *Biophys. Acta.* **1962**, *59*, 25.

(26) Lovley, D. R.; Blunt-Harris, E. L. Role of humic-bound iron as an electron transfer agent in dissimilatory Fe (III) reduction. *Appl. Environ. Microbiol*. **1999**, *65*, 4252.

(27) McCormick, M.; Gerdenich, M.; Kao, L.S.; Adriaens, P. Geochemistry of hydrous ferric oxide reduction by geobacter metallireducens: implications for sustained dechlorination of tetrachloromethane. **2000**. *J. Conference Abstracts.* 5(2), 685.

(28) Sigma-Aldrich: Antioxidants, Protecting Agents, Redox Reactions, MicroSelect. http://www.sigmaaldrich.com/Brands/FlukaRiedelHome/Bioscience/BioChemikaUltra/Antioxidants.html

(29) Nevin, Kelly P.; Lovley, Derek R. Potential for nonenzymatic reduction of Fe (III) via electron shuttling in subsurface sediments. *Environ. Sci. Technol*. **2000**, 34, 2472.

(30) Marcus, B.; Schink, B.; Brune, A. Humic acid reduction by *Propionibacterium freudenreichii* and other fermenting bacteria. *Appl. Environ. Microbiol*, **1998**, 64, 4507.

(31) Dailey, T. A.; Dailey, H. A. Identification of [2Fe-2S] clusters in microbial ferrochelatases. *J. Bacteriol*. **2002**, 184, 2460.

(32) Maillard, M.B. Production of cheese flavour compounds derived from amino acid catabolism by *Propionibacterium freudenreichii***.** Lait. **2002**, 82, 17.

(33) Kaden, J.; Galushko, A. S.; Schink, B. Cysteine-mediated electron transfer in syntrophic acetate oxidation by cocultures of *Geobacter sulfurreducens* and *Wolinella succinogenes*. *Arch. Microbiol*. **2002**, 178, 53.

(34) Lovley, D. R.; Fraga, J. L.; Blunt-Harris, E. L.; Hayes, L. A.; Phillips, E.J. P.; Coates, J.D. Humic substances as a mediator for microbially catalyzed metal reduction. *Acta Hydrochim. Hydrobiol*. **1998**, 26, 152.

(35) Schoenfisch, M.H.; Pemberton, J.E. Air stability of alkanethiol self-assembled monolayers on silver and gold surfaces**.** *J. Am. Chem. Soc*. **1998**, 120, 4502.

(36) Chew, C. F.; Zhang, T. C. Abiotic degradation of nitrates using zero-valent iron and electrokinetic processes**.** *Environ.l Eng. Sci*. **1999**, 16, 389.

(37) Rau, J.; Knackmuss, H. J.; Stolz, A. Effects of different quinoid redox mediators on the anaerobic reduction of azo dyes by bacteria. *Environ. Sci. Technol*. **2002**, *36*, 1497

CHAPTER 2

THE ROLE OF COMPLEXED-IRON AND ORGANOSULFUR FUNCTIONAL GROUPS IN HUMIC SUBSTANCES AS THE NONQUINONE REDOX SITES.

ABSTRACT

Redox sites with nonquinone (NQ) structure were previously identified with other electron transfer centers in humic substances. Electron carrying capacity (ECC) of the NQ redox group ranges between 25-262 μmoleequivalent/g sample, which is approximately 21%-56% of total ECC of the samples. The instability of some NQ sites was observed with soil humic acid and Suwanee river fulvic when they were repeatedly subjected to hydrogenolysis during redox cycling experiments. Since the incidence was observed only with these two samples, it suggests that the NQ sites may include at least two redox functional groups: one that is stable and one that is susceptible to hydrogenolysis. Two candidates for the NQ sites, complexed iron and sulfur functional groups, were examined for their role in electron transport processes. The removal of iron by Chelex-100 resin, which lowers iron content in Aldrich humic acid (AHA) from 129.7 to 2.6 μmol/g-sample did not significantly change the ECC of the sample suggesting that iron is not acting as the NQ site in AHA. The X-ray photoelectron spectroscopic analysis (XPS) of reduced and reoxidized humic substance samples revealed that sulfur functional groups are among the NQ sites that take part in the redox process of humic substances.

The estimated contribution of sulfur redox species to the ECC of the NQ sites is in the range of 18%-120%. One of the sulfur redox site, FeS, has never been previously identified. It was postulated that the complexed-FeS sites only formed in the reduced humic substance samples, via the complexation between the iron (II) and polysulfides functional groups. However, it was also found that some of the FeS sites might also artificially form during the catalytic reduction.

INTRODUCTION

It was demonstrated in Chapter 1 that at least two groups of redox sites can support electron transfer functions for humic substances. These two redox groups were categorized according their resistance to hydrogenolysis, which occurred during the catalytic reduction pH 6.5 using Pd/Al_2O_3 as catalyst. One of the two groups consisted of redox sites that were resistant to the catalytic hydrogenolysis. The other group included quinone sites that were susceptible to this degradation process. The resistant redox sites, classified as nonquinone group (NQ), were responsible for 21%-56% of the electron carrying capacity (ECC) of humic substance samples. The identities of these NQ sites could not be determined by the developed technique described in Chapter 1.

Since the NQ redox sites contribute to a significant portion of the ECC, it is important to identify these redox centers. Complexed-iron and organic sulfur are the most likely possibilities for the NQ redox sites. Both of them are well-known electron mediators. Complexed-iron compounds, such as iron porphyrin, have been shown to enhance the reduction rate of nitroaromatic contaminants in aqueous H_2S by the same

magnitude as quinones such as juglone and lawsone (*1)*. Organosulfur such as thiol is a well-known redox center embedded in many proteins and enzymes (*2*).

Most humic substances contain a certain amount of iron (Table 2.1). Iron, like other metal ions, forms complexes mainly with phenolic or carboxylic functional groups in humic substances (*4*, *5*). Few studies (*6*, *7*) have mentioned complexed-iron as potential redox sites in humic substances. A recent study (*8*) showed that microorganisms could reduce complexed-iron (III) in humic substances to iron (II). However, after the addition of an electron mediator, the reduced iron (II) sites failed to transfer electrons to the acceptor (judging by the fact that no iron (III) formed after the addition of the mediator). Due to this finding, the redox function ability of complexed-iron in humic substances remains arguable.

Similar to complexed-iron, organosulfur is also found in humic substances with oxidation states ranging from -II to +VI, in the form of sulfides, thiols, disulfides, sulfoxides, thiophene, sulfones, sulfonates and sulfate (*9-12*). The amounts of sulfur species in reduced states (sulfides, thiols, disulfides, thiophenes) varies from 10%-50% of the total sulfur content, depending on the source of the humic substances (*11*, *12*). In contrast to iron, the redox activity of reduced sulfur functional groups, thiols and disulfides, in humic substances has already been elucidated. A recent X-ray absorption near-edge structure (XANES) technique study showed that the oxidation of thiols to disulfides in humic substance samples contributed to 6%-100% of the reduction of chromium (VI), depending on the ratio of thiol to chromium (VI) and the types of humic substances used (*13*). Based on these findings, the primary objective of this study is to

TABLE 2.1 Elemental Data and Electron Carrying Capacity of Aldrich Humic Acid (AHA), Peat Humic Acid (PHA), Peat Fulvic Acid (PFA), Elliot Soil Humic Acid (SHA), and Suwanee River Fulvic Acid (SRFA).

Sample	Sulfur content % (wt/wt)	Iron content % (wt/wt)	Fe/S mole ratio	Electron Carrying Capacity (μmolquivalents/g-sample)	
				NQ sites[d]	Sulfur redox sites
AHA	0.95[a]	0.772[c]	0.465	132	78
PHA	0.71[b]	0.052[c]	0.042	174	73
PFA	0.73[b]	0.433[c]	0.340	103	124
SHA	0.44[b]	0.046[c]	0.059	262	117
SRFA	0.44[b]	0.003[c]	0.003	25	5

[a] data from Aldrich

[b] data from International Humic Substances Society (IHSS)

[c] data from ref 49

[d] data from Chapter 1

evaluate the likelihood of complexed-iron and organosulfur functional groups in humic substances acting as the NQ redox sites.

MATERIALS AND METHODS

Samples

Four humic substance samples were purchased from the International Humic Substance Society (IHSS). These samples included Suwanee river fulvic acid (SRFA), Elliot soil humic acid (SHA), peat humic acid (PHA) and fulvic acid (PFA). One sample, Aldrich humic acid (AHA), was purchased from Aldrich.

Iron Removal Process

A glass column containing fresh, clean Chelex-100 resin (styrene divinylbenzene copolymer, Bio-Rad) at a ratio of 5 g of resin per 100 ml of sample was prepared for the iron removal process. The resin was rinsed three times with deionized water. AHA sample (the only sample tested because of its the highest iron content) was dissolved in Nanopure water and the pH was adjusted to 5 with 0.1 M HCl. This solution was slowly run through the column at the rate of 0.5 ml/min. The effluent was collected and rerun through a new column set up as described above. The final effluent was dialyzed (cellulose acetate membrane, MWCO 100, Spectrum; Spectra/Por) and freeze dried. The amount of iron in AHA before and after the treatment was measured by flame atomic

absorption spectrophotometry operated on the air-acetylene mode (SpectroAA-30: Varian). A series of iron (II) standard solutions (Fisher) was used to construct a calibration curve. Triplicates of both the sample and the standard solutions were measured and calculated for iron concentrations.

Redox Cycling Experiment

This test was carried out using the same procedure previously described in Chapter 1 (Materials and methods, Redox Cycling Experiment, Procedure section)

X-ray Photoelectron Spectroscopic (XPS) Analysis

Figure 2.1 illustrated the sample preparation process for the XPS analysis. Samples were mounted on a sample holder by pressing them against adhesive graphite tape inside the anaerobic chamber before being transferred to the XPS vacuum chamber. Spectra were obtained with a Physical Electronics PHI 5800 X-ray photoelectron spectrometer operating under a vacuum of $2x10^{-9}$ Torr. Samples were irradiated with Aluminum Kα X-rays (1486.6 eV) of 350 W and analyzed at an electron take-off angle of 45^{o} measured with respect to the surface plane. Survey and detailed scans were collected using a 800-μm spot size and 23 eV pass energy. The binding energies were corrected by reference to the aliphatic adventitious hydrocarbon C 1s peak at 284.8 eV. The areas under the unsmoothed sulfur S 2p peaks were measured using Shirley background

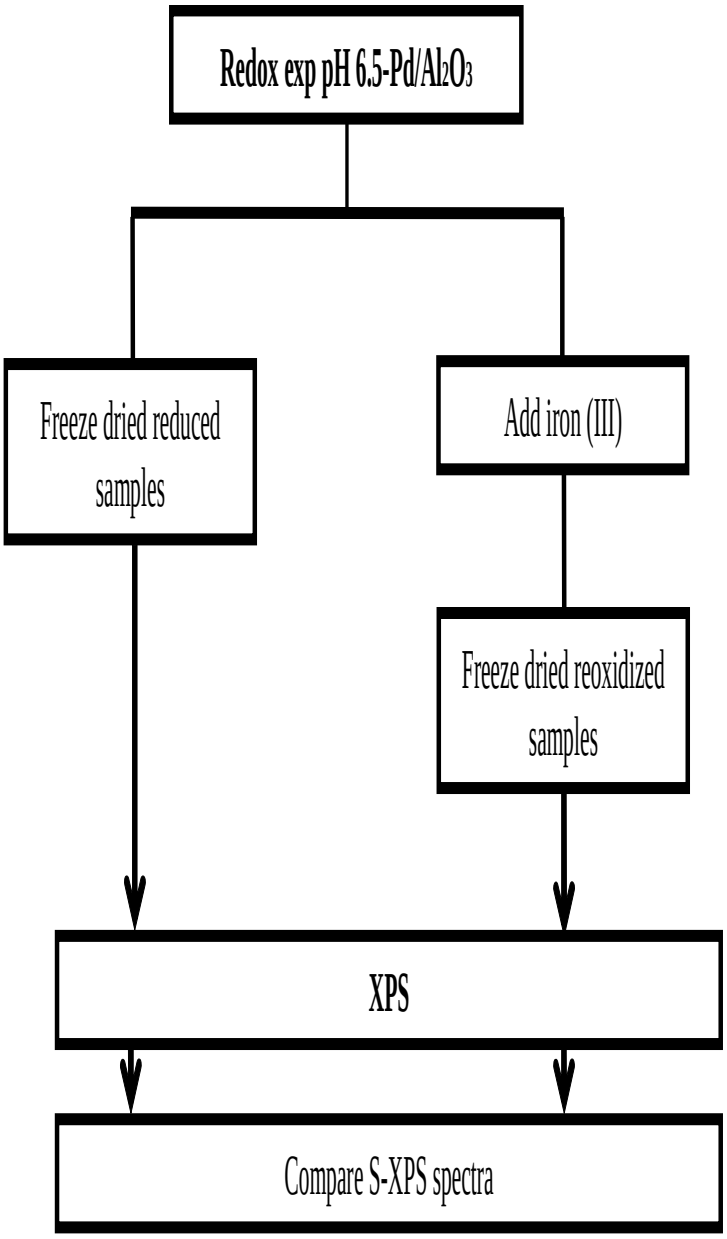

FIGURE 2.1. Experiment layout for XPS analysis of sulfur redox sites

subtraction algorithm (*14*). Spectra that are shown have been smoothed by Gaussian-Lorentzian peak shape. Each XPS spectrum represents the average of three scans.

RESULTS AND DISCUSSION

Characteristics of Nonquinone Redox Sites

During the pH 6.5-Pd/Al_2O_3 catalytic reduction, the hydrogenolysis of quinone moieties occurred. This event disrupted C-O bonds in reduced quinones, which terminated their electron mediating ability. The disruption was noticeably fast. Quinone moieties in eight quinone compounds were removed promptly in the first redox cycle. Although the function of the nonquinone (NQ) redox sites was considered uninterrupted by the hydrogenolytic cleavage, there was evidence that this degradation process might also affect some of the NQ sites' performance. As shown in Figure 2.2, the ECC of both SHA and SRFA, unlike other samples, gradually declined with each test cycle. This evidence implies that some NQ redox sites in SHA and SRFA stopped functioning when they were repeatedly subjected to hydrogenolysis. The swift removal of quinone moieties reported in Chapter 1 disagreed that the unstable NQ sites were not quinone moieties. However, in order to be certain, ubiquinone (Coenzyme Q10) was catalytically reduced by Pd/Al_2O_3 catalyst. This quinone compound was selected because it has a bulky substituent adjacent to its quinone moieties (Figure 2.3 b). Steric effects from small substituents, such as OH and CH_3 functional groups, have been shown to prevent the hydrogenolysis of adjacent quinone moieties of lawsone and plumbagin during the pH8-Pd catalytic reduction (Chapter 1). Results from the ubiquinone test were shown in Figure

2.3 a. As illustrated in this figure, the quinone moieties' signal at 290 nm in the UV-Vis spectrum of ubiquinone disappeared after the Pd/Al_2O_3 catalytic reduction. Thus, it was confirmed that steric effects has no effect on hydrogenolysis of quinone moieties in the Pd/Al_2O_3 catalytic system. It should be noted that the catalytic reduction of ubiquinone was carried out in hexane and without adjusting pH because of its low water solubility. However, these reaction conditions should not promote the hydrogenolysis of ubiquinone. In catalytic reactions, solvents affect the surface reactions by regulating the rate of a compound's sorption on the catalyst's surface (*54*). In the case of hexane (which is not a H^+ donor or acceptor), this nonpolar solvent would slow the ubiquinone's (hydrophobic compound) sorption to the surface of Pd/Al_2O_3, because, due to the acid sites of Al_2O_3, the surface of catalyst is considered more polar than hexane. Due to this argument, it is unlikely that hexane will cause an additive effect to the hydrogenolysis of ubiquinone. Therefore, the observed result with ubiquinone should also occur with aqueous solutions of humic substances.

It was hypothesized that the change in humic substance structure during catalytic reduction could lead to the observed decline in the ECC of SHA and SRFA. Besides quinone moieties, alterations during the catalytic reduction might occur with the other parts of the humic substance samples. If so, this change might appear gradually and slowly affect some of the NQ redox sites of SHA and SRFA. Since none of the humic substance samples other than SHA and SRFA showed any significant changes of ECC over the five redox cycles, the NQ sites in these samples were considered more stable than those of SHA and SRFA. Thus, according to this hypothesis, NQ redox sites may

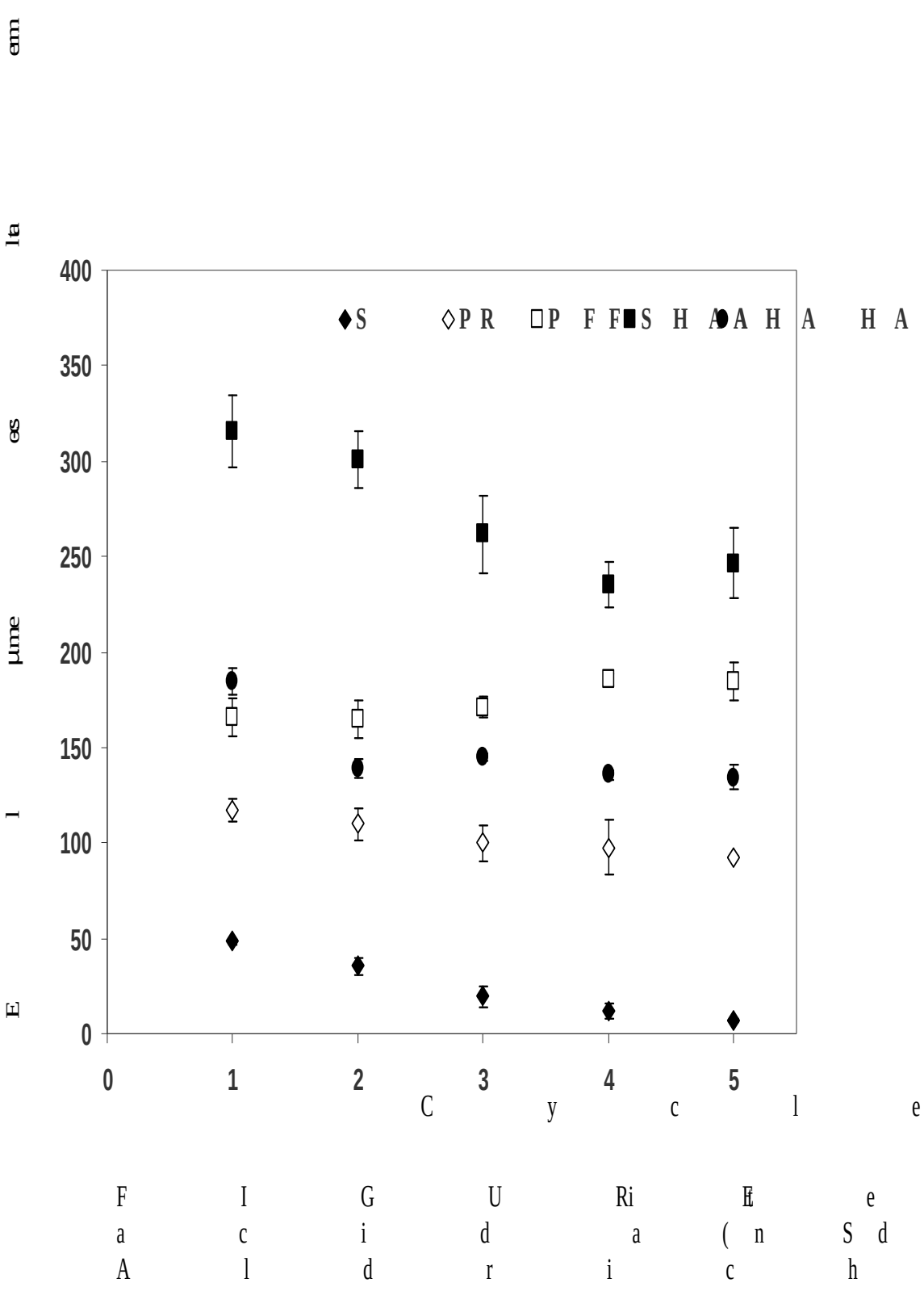
400
350
300
250
200
150
100
50
0
0
1
2
3
4
5
Cycle

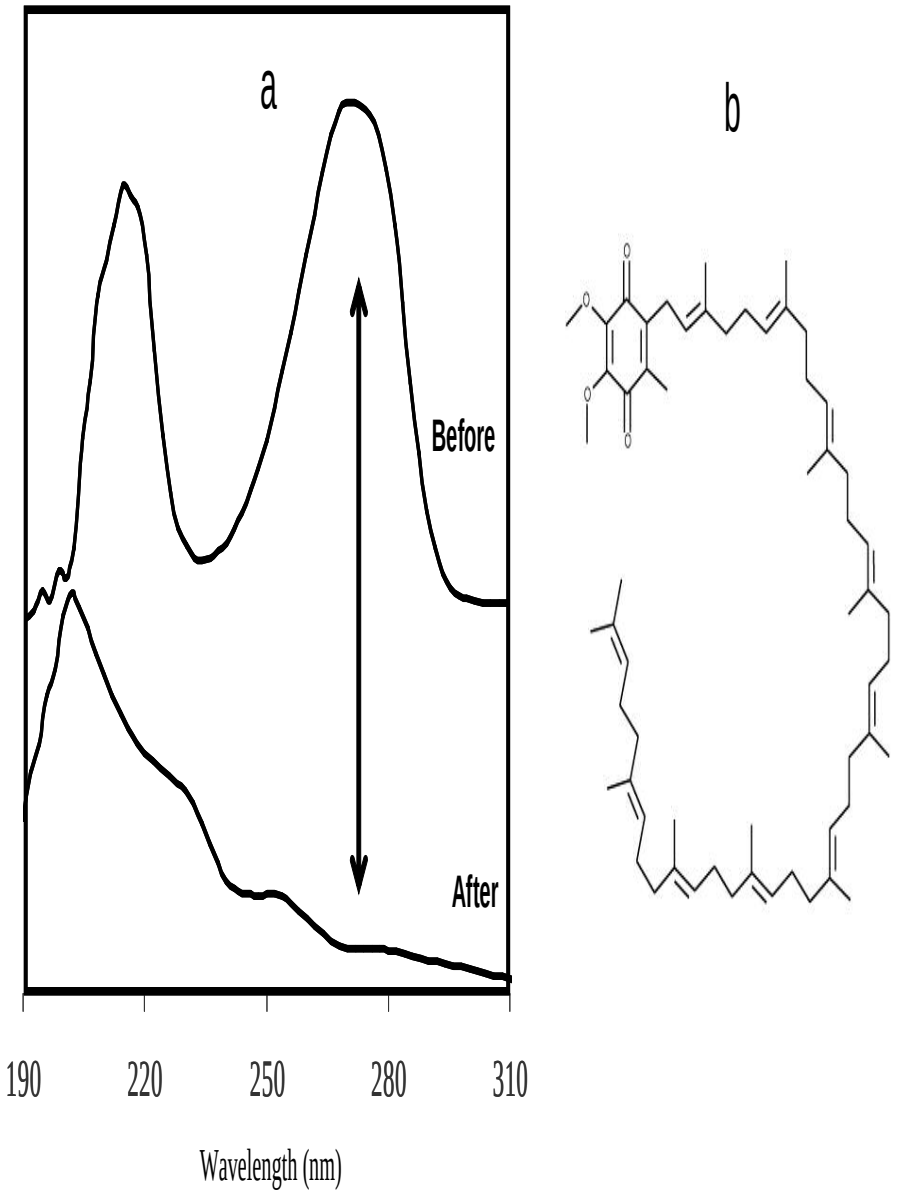

FIGURE 2. 3 a) UV-Vis Spectra and b) chemical structure of coenzyme Q10 in hexane before and after the ph 6.5-Pd/Al_2O_3 reduction. Arrow indicates the signal from quinone moieties.

include at least two redox functional groups: one that is stable and one that is susceptible to hydrogenolysis.

Role of Complexed-Iron

Humic substance samples contain a certain amount of iron (Table 2.1). The redox ability of iron sites in humic substances was tested by comparing the ECC of Aldrich humic acid (AHA) before and after complexed-iron was removed by Chelex-100. AHA was selected because it has the highest iron content among humic substance samples used in this study. Also, this sample was used in previous studies to evaluate the iron redox sites in humic substances (*6, 8*). Iron content in AHA before and after the Chelex-100 treatment was significantly different, 129.7 and 2.6 μmol/g-sample**,** respectively. However, as shown in Figure 2.4, the ECC values of the treated and untreated AHA were almost the same in all five redox cycles. If complexed-iron was among the NQ redox sites, the approximate loss of the ECC after the iron was removed, would be 127 μequivalents/g-sample. If this occurred there would be a dramatic decrease in the ECC of the treated AHA in Figure 2.4. Since no drastic decrease occurred, these results suggest that complexed-iron in AHA is not acting as the NQ redox sites.

A previous study showed that humic-bound iron can be reduced by microorganisms (*8*), so it should be reduced by the Pd/Al_2O_3 catalyst as well. Therefore, the question is: what prevents the reduced complex-iron (II) from transferring electrons to an acceptor? Redox chemistry of the complexed-iron in humic substances is not well understood, but there has been evidence that forming complexes with humic substances

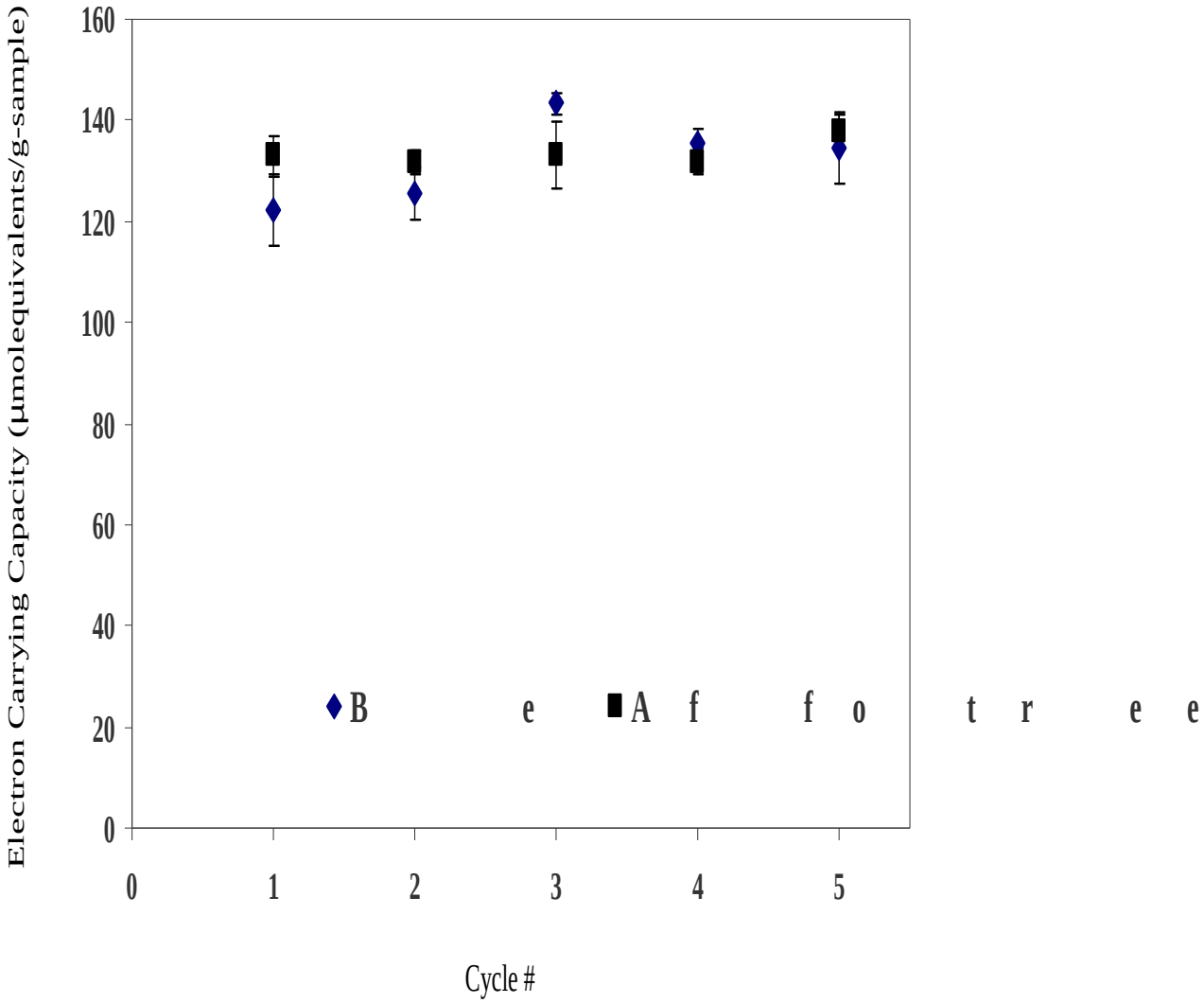

FIGURE 2.4 Electron carrying capacity of Aldrich humic acid before and after the iron removal treatment by Chelex-100.

causes a certain change in the redox property of iron. During the construction of a microelectrode, it was observed that the oxidation potential of ferrocene deceased from 380 mV to 300 mV after it formed a complex with soil humic acid (*16*). Based on this observation, humic-bound iron should be easily oxidized. However, in humic substances, iron as well as other metal ions, forms complexes mainly with phenolic or carboxylic functional groups (*4, 5*). These binding sites might influence the oxidation of complexed-iron (II). Natural iron chelators such as citrinin [(3R-tran)-4,6-dihydro-8-hydroxy-3,4,5-trimethyl-1,6-oxo-3H-2-benzopyran-7-carboxylic acid)], a carboxylic complexing agent produced by *Penicillium* and *Aspergillus spp*., have been shown to prevent the oxidation of iron (II) to iron (III) by a strong oxidizing agent, such as H_2O_2 (*17*). Besides citrinin, several iron chelators such as salicylic acid (*18*) and flavonoids (*19*) are also antioxidants that inhibit the oxidation of iron (II) in iron (II)/ascorbate-induced lipid peroxidation. Most of the iron (II) chelators that are also antioxidants are phenolic compounds with carboxylic groups *ortho* to phenolic functional groups (*17*). It is possible that, if iron binds to humic substances via sites with similar structures, the same effect might occur with the reoxidation of complexed-iron (II).

Role of Sulfur

Similar to iron, humic substance samples contain a certain amount of sulfur (Table 2.1). Sulfur in natural organic matter, such as humic substances, is primarily derived from the reaction between dissolved sulfides and sedimentary organic matter (*20, 21*). The XPS used in this experiment has been employed extensively to study sulfur in

coal (*22)*, iron sulfide metals such as pyrite (*23, 24*), polymer (*25*), and natural organic matter (*20, 21*). XPS differentiates sulfur species by detecting the binding energy of electrons in a sulfur atom. This binding energy varies with the oxidation state of sulfur.

Five humic substance samples, SRFA, SHA, PFA PHA, AHA, were reduced by Pd/Al_2O_3 at pH 6.5 and analyzed by XPS before and after they were reoxidized by iron (III) (Figure 2.1). The XPS spectra of the reduced and iron-oxidized SRFA samples are shown in Figure 2.5. The assignment of peaks in the XPS spectra sulfur is summarized in Table 2.2. These assignments were based on published binding energies reported for sulfur functional groups in minerals, soils, polymers, and coals (*26-37*). Glutathione, a thiol compound, was used as a standard to calibrate the positions of the peaks in the XPS spectra (Figure 2.6). Peak areas and the relative distribution of sulfur functional groups were summarized for each sample in Table 2.3. As shown in this table, sulfur in all samples (except SHA) was primarily in the oxidized form (oxidation state > 0). This fraction increased after iron (III) was added to the sample solutions, which indicates that a certain part of the reduced sulfur species (oxidation state < +I) had been oxidized.

Among the assignments in Table 2.2, it is unlikely that the peak at 162.9 eV is pyrite (FeS_2). This assumption is based on a report that the formation of FeS_2 at pH 5.5-8.0 and 25 °C is slow and takes place over a period of days (*38*). Since the sample solutions (pH 6.5, room temperature) were immediately freeze dried after the reduction and the addition of iron (III), there was insufficient time for the formation of FeS_2. Thus, either polysulfides and /or thiosulfate were providing that signal. A previous XANES study has shown that polysulfides are present in humic substances (*28*).

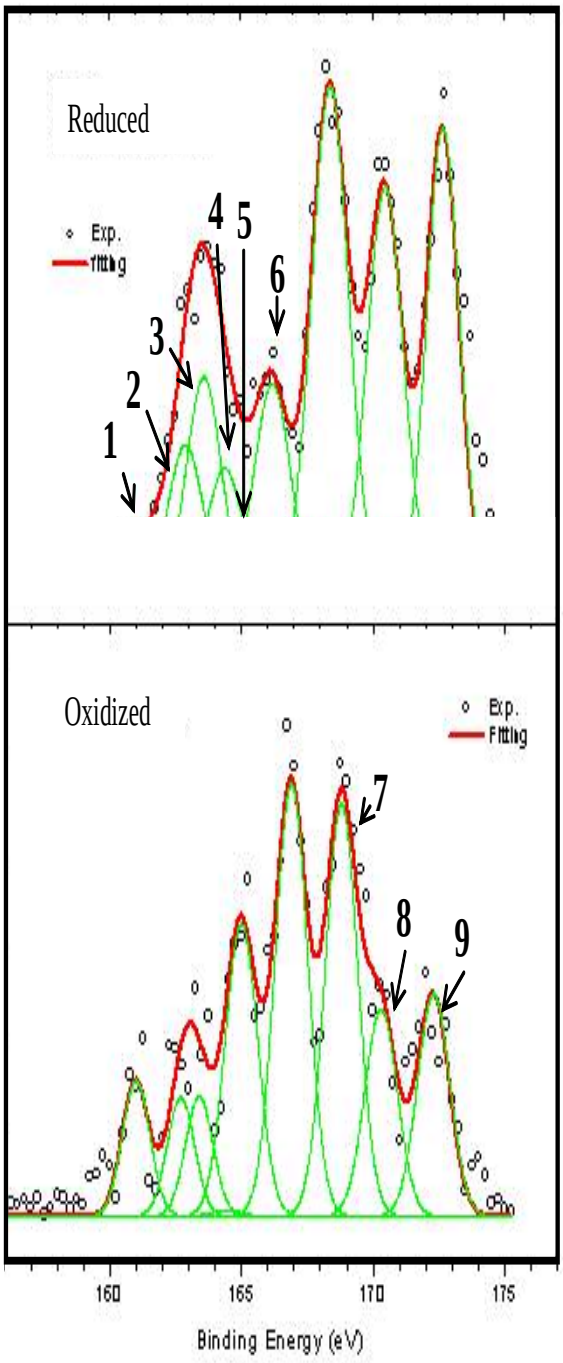

FIGURE 2.5 S (2p) XPS Spectra of reduced and oxidized Suwanee River fulvic acid (SRFA)

TABLE 2.2 Assignments for Sulfur Functional Groups, Structure of Representative Compounds, Oxidation State, and Binding Energy of Each Peak in XPS Spectra.

Peak number	Sulfur compound	Oxidation state	Structure	Binding Energy (eV)[a]
1	FeS	-II		160.1-162.1
2	FeS_2, polydisulfides, outer sulfur atom of thiosulfate	-I		162.2-163.2
3	thiol	-I	R-SH	163.5-163.7
4	disulfides	-I	R-S-S-H	164.4-164.8
5	thiophene, elemental sulfur (S^0)	0		164-165
6	sulfoxide	+II		166
7	sulfonate, inner sulfur atom of thiosulfate	+IV		167.5-168
8	sulfone, sulfite	+V		169-169.4
9	sulfate	+VI	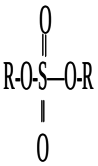	170.9-171.2

[a] Ref. 26-37

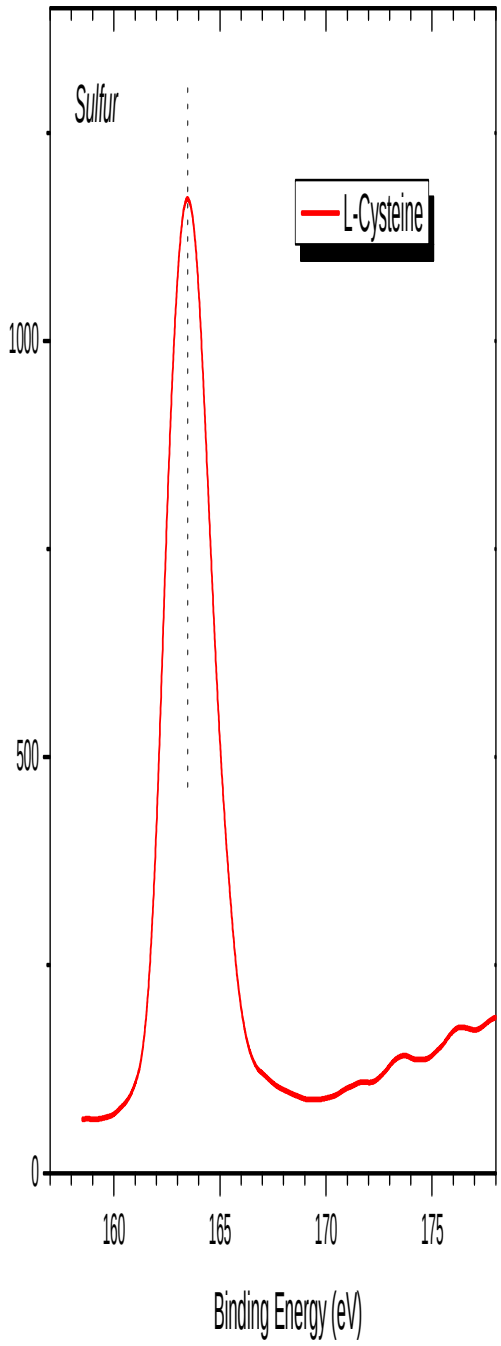

FIGURE 2.6 S (2p) XPS spectrum of L-cysteine, a thiol compound.

TABLE 23. Relative Distribution of Sulfur Species in Reduced and Fe(III)-Oxidized Aldrich Humic Acid (AHA), Peat Humic Acid (PHA), Peat Fulvic Acid (PFA), Elliot Soil Humic Acid (SHA), and Suwannee River Fulvic Acid (SRFA).

Sample	AHA				PHA				PFA				SHA				SRFA			
	reduced		oxidized		reduced		oxidized		reduced		oxidized		reduced		oxidized		reduced		oxidized	
	peak area	%	peak area	%	peak area	%	peak area	%	peak area	%	peak area	%	peak area	%	peak area	%	peak area	%	peak area	%
FeS	14	5	28	4	0	0.45	2	0.45	40	8	10	2	89	32	26	8	8	3	19	7
polysulfides	0	0	53	8	16	6	27	6	25	5	14	3	37	13	11	3	33	11	16	6
thiol	36	13	53	8	39	15	49	11	33	7	31	7	27	10	28	9	38	13	17	7
disulfides	32	12	55	9	27	10	51	11	58	12	54	11	18	6	49	15	23	8	12	5
thiophene	41	15	61	9	34	13	72	16	56	12	55	12	12	4	49	15	21	7	30	12
sulfonamide	35	13	93	14	56	21	42	9	52	11	58	12	15	5	51	16	22	8	38	15
sulfone	35	13	92	14	25	10	47	11	90	19	114	24	8	3	36	11	58	20	49	19
sulfonate	51	18	105	16	36	14	103	23	76	16	73	16	39	14	39	12	43	15	47	19
sulfate	34	12	107	17	29	11	52	12	50	10	61	13	32	12	32	10	46	16	26	10
total	278	100	647	100	262	100	445	100	490	100	470	100	277	100	321	100	292	100	254	100

The most interesting sulfur functional group is FeS. In previous XANES studies of PFA, PHA, SHA and SRFA (*11*, *12*), no FeS peak was detected. XANES is more sensitive to the bonding environment than XPS. It can detect changes in electron distribution resulting from covalent bonding by measuring edge absorbance energies (*12*). Therefore, XANES should have been able to detect FeS if it was present. However, samples examined by XANES were not in the reduced state, so it was postulated that the FeS sites were developed only when the samples were in a reduced state. When the complexed-iron in the samples was reduced to iron (II), some of the complexed-iron might have formed complexes with polysulfides functional groups. A previous XANES study has shown that polysulfides are present in humic substances (*39*).

In the case of AHA, in which FeS formed despite the lack of polysulfides (no 162.9-eV signal), FeS might be catalytically generated from the reaction between complexed-iron (II) and thiols. This is based on a report that a Pd catalyst has been used to prepare FeS cluster for the biosynthesis of a FeS protein (*40*). In the preparation, ferrous acetate and L-cysteine were used as sources of iron and sulfur, respectively. The FeS cluster formation took place in an anaerobic chamber (95%:5%: N_2:H_2: room temperature) in 60 min. after adding Pd catalyst (*40*). Since each humic substance sample was reduced by the same method, it should be noted that the catalytic formation of FeS might be possible in other samples as well.

The appearance of the 162.9-eV signal after adding iron (III) to the reduced AHA solution might be due to the formation of both thiosulfate and polysulfides. In the thiosulfate case, it has been demonstrated that during the reduction of chromium (IV), FeS was oxidized to S^0, sulfite, thiosulfate and sulfate (*41*). Thiosulfate has two sulfur

atoms which have different oxidation states. The oxidation state of the inner sulfur (the one connected to three oxygen atoms) is +VI, the same as sulfonate. The outer sulfur atom (the terminal atom) has an oxidation state of -I, the same as polysufides (*42*). The formation of polysulfides might relate to the decrease in 165-eV signal. This signal was assigned to thiophenic sulfur and S^0. Since it has been reported that thiophenic sulfur is not readily oxidized (*27*), the decrease in 165-eV signal should be due to S^0 depletion. Complexation between iron (III) and *N*-alkylimidazoles has been shown to promote the reactions between the complexed-iron and S^0, which give *N*-alkylimidazoles-iron-polysulfide compounds as products (*43-45*). It is hypothesized that some of the iron binding sites in the humic substances might offer similar reactions. However, since yields of the products have been reported to be dependent on the S^0 concentration (*43*), the formation of polysulfides via the reactions might be limited by the original amount of S^0 in the samples. Besides AHA, none of the humic substance samples showed an increase in the 162.9-eV signal (Table 2.3). According to their lower sulfur content (Table 2.1), the initial amount of S^0 of SRFA, SHA, PHA and PFA might be smaller than that of AHA. Therefore, the polysulfides formation should be minimal in these samples.

The increase in FeS content in PHA and SRFA after adding iron (III) (Table 2.3) was hypothesized as a consequence of complexed-iron (II) shortage. Compared to other samples, the iron to sulfur ratios of PHA and SRFA are significantly lower (Table 2.1). After the addition of iron (III), some of the iron would be reduced by other nonquinone redox functional groups and then served as a supplementary source of iron (II) in the FeS formation in these two samples. In the PHA sample, other significant changes in sulfur composition after the oxidation include the drastic decrease in sulfoxide species (166.5

eV). The oxidation of sulfoxide to sulfone (167.1 eV) has been reported with H_2O_2 using iron (II)-EDTA (*46*) or iron porphyrin (*47*) as a catalyst. However, H_2O_2 was not used in this study and the corresponding increase of sulfone was not observed. At this point, the cause of this change is unknown.

In order to calculate the ECC of the sulfur redox sites, there are two points that were taken into consideration. First, changes in the distribution of many sulfur species after the oxidation by iron (III) indicate that the oxidation of sulfur species involves a complex reaction mechanism and occurs in a multiple-step process. This is due to various oxidation states of sulfur. Second, XPS is a surface survey technique (sensitive to a depth of approximately 5-50 °A (*49*)). Peak areas reported in Table 2.3 represented the distribution of sulfur functional groups only in the top 50 °A of the sample surface. Thus, before estimating the total ECC of sulfur redox sites for the whole sample, the assumption that the distribution of sulfur functional groups is the same at every point, both on the surface and deep inside the sample, has been made. Based on this assumption, the ECC calculation was done in four steps: first, determining changes in the relative distribution of each sulfur species after the iron (III) oxidation (change in % peak area in Table 2.3); second, estimating the corresponding change for the whole sample by multiplying each value from step one with % sulfur content and then expressing the result in terms of moles of sulfur; third, calculating the corresponding number of charges by multiplying results from step 2 with the oxidation state; fourth, combining results from all sulfur function groups and using the number of charge loss as the ECC of the sample. An example for the calculation of the FeS sites of AHA was as follows: *i*) the difference in % peak area of reduced and oxidized AHA is 5-4 = 1; *ii*) the corresponding change in

FeS content (in the whole sample) = ((1/100)x %S) / MW of S = ((1/100) x (0.97/ 100)) / 32.06 = 2 x10^{-6} mol S; *iii*) the corresponding number of charge = 2 x10^{-6} x -2 = - 4 x10^{-6} moles of charge; *iv*) repeat step 1-3 with other functional groups and then combine results. The final value is the ECC attributed to all sulfur functional groups of AHA. The calculated results of all samples are present in Table 2.1.

As illustrated in Figure 2.7, the calculated ECC of sulfur sites represented 18%-120% of the values attributed to NQ redox sites. The number is highest in the PFA sample and lowest in the SRFA sample. However, it must be recognized that these estimates could only represent the upper boundary for the approximation, because some of the FeS sites might be artifacts from the catalytic reduction. The estimation without taking the FeS into consideration provided the estimated total ECC in the range of 20%-90% of the NQ sites' ECC (Figure 2.7). These numbers remain substantial to the total ECC of all NQ sites. Therefore, the XPS results demonstrate that the sulfur redox functional groups are the significant parts of the NQ sites.

One issue that needed to be addressed was whether the formation of FeS was the reason that iron (II) was unable to transfer electrons to an acceptor. In the AHA case, approximately 5% of the sulfur in the top 50 °A of the reduced AHA surface was found as FeS (Table 2.3). Based on the above the assumption and calculation procedure, this would equal to 2.1 μmol-sulfur/g-sample. Thus, for the FeS formation, 2.1 μmol-iron/g-sample would be required. Since the total amount of iron in AHA is 129.7 μmol/g-sample, only 1.6% of iron is needed for the FeS formation. Therefore, the FeS formation is certainly not the cause preventing electron transfer of complexed iron (II).

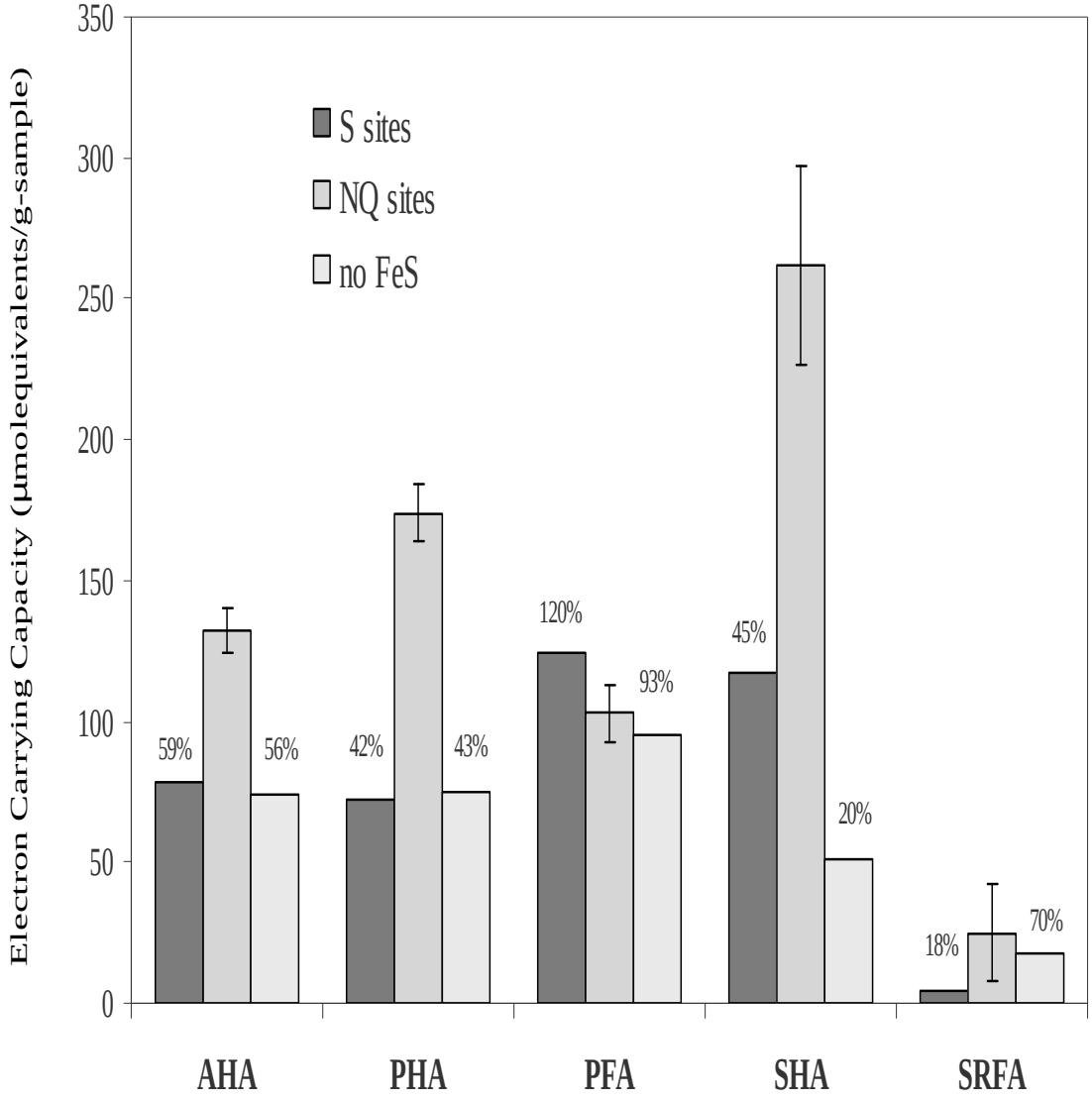

FIGURE 2.7 Comparison between electron carrying capacity of sulfur redox sites and the nonquinone (NQ) redox sites. Suwanee river fulvic acid (SRFA), Elliot soil humic acid (SHA), peat humic acid (PHA) and fulvic acid (PFA), Aldrich humic acid (AHA).

ACKNOWLEDGEMENTS

This work was supported by NSF-CAREER grant BES-9732969. Ms. Ratasuk was supported by a grant from the Royal Thai government. The authors gratefully acknowledge Drs. Daniel E. Resasco and Zhongrui Li for their assistances in obtaining the XPS data, Dr. John F. Scamehorn and Winya Dungkeaw of School of Chemical Engineering, the University of Oklahoma for the AA measurement.

LITERATURE CITED

(1) Schwarzenbach, R. P.; Stierli, R.; Lanz, K.; Zeyer, J. Quinone and iron porphyrin mediated reduction of nitroaromatic compounds in homogeneous aqueous solution. *Environ. Sci. Technol.* **1990**, 24, 1566.

(2) Kinnula, V. L.; Paakko, P.; Soini, Y. Antioxidant enzymes and redox regulating thiol proteins in malignancies of human lung. FEBS Letters, **2004**, 569, 1.

(3) Choe, Y. K.; Nakajima, T.; Hirao, K.; Lindh, R. Theoretical study of the electronic ground state of iron(II) porphine. II. *J. Chem. Phys*. **1999**, 111, 3837

(4) Buschmann, J.,; Sigg, L. Antimony (III) binding to humic substances: Influence of pH and type of humic acid. *Environ. Sci. Technol.* **2004**, 38, 4535.

(5) Pandey, A.; Kumar; P., Shri D.; Misra, V.; Viswanathan, P. N. Formation of soluble complexes of metals with humic acid and its environmental significance. *Chem. Eco*.**1999.** 16, 269.

(6) Benz, M.; Schink, B.; Brune, A. Humic acid reduction by *Propionibacterium freudenreichii* and other fermenting bacteria. *App. Environ. Microbiol*. **1998**, 64, 4507.

(7) Struyk, Z.; Sposito, G. Redox properties of standard humic acids. *Geoderma.* **2001**, 102, 329.

(8) Lovley D R; Blunt-Harris E L Role of humic-bound iron as an electron transfer agent in dissimilatory Fe(III) reduction. *App. Environ. Microbiol*. **1999,** 65, 4252.

(9) Ritz D; Beckwith J. Roles of thiol-redox pathways in bacteria. *Ann. rev. microbial.* **2001**, 5521.

(10) Olivella, M. A.; del Rio, J. C.; Palacios, J.; Vairavamurthy, M.A.; de las Heras, F. X. C. Characterization of humic acid from leonardite coal: an integrated study of PY-GC-MS, XPS and XANES techniques**.** *J. Anal. Appl. Pyrolysis*. **2002**, 63, 59.

(11) Morra, M.J.; Fendorf, Scott E.; Brown, Paul D. Speciation of sulfur in humic and fulvic acids using x-ray absorption near-edge structure (XANES) spectroscopy. *Geochim. Cosmochim. Acta*. **1997,** 61, 683.

(12) Xia, K.; Weesner, F.; Bleam, W. F.; Bloom, P. R.; Skyllberg, U. L.; Helmke, P. A. XANES studies of oxidation states of sulfur in aquatic and soil humic substances. *Soil Sci. Soc.Am. J*. **1998,** 62, 1240.

(13) Szulczewski, M. D; Helmke P. A; Bleam W. F. XANES spectroscopy studies of Cr(VI) reduction by thiols in organosulfur compounds and humic substances. *Environ. Sci. Technol* . **2001**, 35, 1134.

(14) Shirley, D. A. High-resolution X-ray photoemission spectrum of the valence bands of gold. *Phys. Rev*. **1972**, 5, 4709.

(15) Bejblova, M.; Zamostny, P.; Cerveny, L.; Cejka, J. Hydrogenation and hydrogenolysis of acetophenone. *Coll. Chem. Commun*. **2003**, 68, 1969.

(16) Vinodgopal, K.; Subramanian, V.; Carrasquillo, S.; Kamat, P.V. Electrophoretic assembly of naturally occurring humic substances as thin films**.** *Environ. Sci. Technol.* **2003**, 37, 761.

(17) Lozzo, J.E.; Mangrich, A. S.; Rocha, M.E. M.; Martinelli, O. Ma.B.; Carnieri, E. G. S. Effects of citrinin on iron-redox cycle**.** *Cell Biochem. Funct*. **2002**, 20, 19.

(18) Dinis. T. C.; Maderia, V. M.; Almeida, L. M. Action of phenolic derivatives (acetaminophen, salicylate, and 5-aminosalicylate) as inhibitors of membrane lipid peroxidation and as peroxyl radical scavengers. *Arch. Biochem. Biophys.* **1994**, 315, 161.

(19) Mitchell, J. H.; Gardner, P. T.; McPhail, D. B.; Morrice, P. C.; Collins, A. R.; Duthie, G. G. Antioxidant efficacy of phytoestrogens in chemical and biological model systems. *Arch. Biochem. Biophys.* **1998**, 360, 142.

(20) Ferdelman, T.G.; Church, T. M.; Luther, G.W., III. Sulfur enrichment of humic substances in a Delaware salt marsh sediment core. *Geochim. Cosmochim. Acta*. **1991**, 55, 979.

(21) Urban, N. R.; Ernst, K.; Bernasconi, S. Addition of sulfur to organic matter during early diagenesis of lake sediments. **.** *Geochim. Cosmochim. Acta* .**1999**, 63, 837.

(22) Dutta, S. N.; Dowerah, D.; Frost, D.C. Study of sulfur in Assam coals by x-ray photoelectron spectroscopy**.** *Fuel*. **1983**, 62, 840.

(23) Leiro, J. A.; Mattila, S. S.; Laajalehto, K. XPS study of the sulphur 2p spectra of pyrite. *Surf. Sci*. **2003**, 547, 157.

(24) Descostes, M.; Mercier, F.; Thromat, N.; Beaucaire, C.; Gautier-Soyer, M. Use of XPS in the determination of chemical environment and oxidation state of iron and sulfur samples: constitution of a data basis in binding energies for Fe and S reference compounds and applications to the evidence of surface species of an oxidized pyrite in a carbonate medium. *Appl. Surf. Sci*. **2000**, 165, 288.

(25) Xia, Nan; Hu, Yunhua; Grainger, David W.; Castner, David G. Functionalized poly(ethylene glycol)-grafted polysiloxane monolayers for control of protein binding. *Langmuir*. **2002**, 18, 3255.

(26) Schoenfisch, M.H.; Pemberton, J.E. Air stability of alkanethiol self-assembled monolayers on silver and gold surfaces**.** *J. Am. Chem. Soc*. **1998**, 120, 4502.

(27) Grzybek, T.; Pietrzak, R.; Wachowska, H. The comparison of oxygen and sulfur species formed by coal oxidation with O_2/Na_2CO_3 or peroxyacetic acid solution. XPS studies. *Energy Fuels*. **2004**, 18, 804.

(28) Smart, R. S. C.; Skinner, W. M.; Gerson, A. R. XPS of sulfide mineral surfaces: metal-deficient, polysulfides, defects and elemental sulphur. *Surf. Interface Anal*. **1999**, 28, 101.

(29) Peisert, H.; Chasse, T.; Streubel, P.; Meisel, A.; Szargan, R. Relaxation energies in XPS and XAES of solid sulfur compounds. *J. Electron Spectrosc. Relat. Phenom*. **1994**, 68, 321.

(30) Wang, X.; Hu, W.; Ramasubramaniam, R.; Bernstein, G. H.; Snider, G.; Lieberman, M. Formation, Characterization, and sub-50-nm patterning of organosilane monolayers with embedded disulfide bonds: An engineered self-assembled monolayer resist for electron-beam lithography. *Langmuir*. **2003**, 19, 9748.

(31) Bearinger, J. P.; Terrettaz, S.; Michel, R.; Tirelli, N.; Vogel, H.; Textor, M.; Hubbell, J. A. Chemisorbed poly(propylene sulphide)-based copolymers resist biomolecular interactions. *Nature Materials*. **2003**, 2, 259.

(32) Jugnet, Y.; Tourillon, G.; Tran Minh Duc. Evidence of intrinsic extended π-bonding band and metalliclike behavior in undoped and doped electropoly-merized poly(3-methylthiophene) films. *Phys. Rev. Lett*. **1986**, 56, 1862.

(33) Cavalleri, O.; Gonella, G.; Terreni, S.; Vignolo, M.; Pelori, P.; Floreano, L.; Morgante, A.; Canepa, M.; Rolandi, R. High resolution XPS of the S 2p core level

region of the L-cysteine/gold interface**.** *J. Phys.: Condens. Matter*. **2004,** 16, S2477.

(34) Skinner, W. M.; Nesbitt, H. W.; Pratt, A.R. XPS identification of bulk hole defects and itinerant Fe 3d electrons in natural troilite (FeS). *Geochim. Cosmochim. Acta*. **2004**, 68, 2259.

(35) Sugama, T.; Webster, R.; Reams, W.; Gawlik, K. High-performance polymer coatings for carbon steel heat exchanger tubes in geothermal environments. *J. Mat. Sci*. **2000**, 35, 2145.

(36) Wang, L.; Chen, P**.** Mechanism study of iron-based catalysts in co-liquefaction of coal with waste plastics. *Fuel*. **2002**, 81, 811.

(37) Ni, H.; Anderson, R. K.; Givens, E. N. Surface characterization and liquefaction of iron- and molybdenum-impregnated subbituminous coal. *Energy Fuels*. **1994,** 8, 1316.

(38) Luther, G.W., III. Pyrite synthesis via polysulfide compounds**.** *Geochim. Cosmochim. Acta*.1991, 55, 2839.

(39) Vairavamurthy, Murthy A.; Maletic, Dusan; Wang, Shenghe; Manowitz, Bernard; Eglinton, Timothy; Lyons, Timothy. Characterization of sulfur-containing functional groups in sedimentary humic substances by X-ray absorption near-edge structure spectroscopy. *Energy Fuels,* **1997**, 11, 546.

(40) Sutak, R.; Dolezal, P.; Fiumera, H. L.; Hrdy, I.; Dancis, A.; Delgadillo-Correa, M.; Johnson, P. J.; Mueller, M.; Tachezy, J. Mitochondrial-type assembly of FeS centers in the hydrogenosomes of the amitochondriate eukaryote Trichomonas vaginalis. *PNAS*. **2004**, 101, 10368.

(41) Mullet, M.; Boursiquot, S.; Ehrhardt, J. J. Removal of hexavalent chromium from solutions by mackinawite, tetragonal FeS. *Colloids and Surfaces, A: Physicochem.Eng.Aspects*. **2004**, 244, 77.

(42) Vairavamurthy, A.; Manowitz, B.; Luther, G. W., III; Jeon, Y. Oxidation state of sulfur in thiosulfate and implications for anaerobic energy metabolism. *Geochim. Cosmochim. Acta* (1993), 57(7), 1619.

(43) Rauchfuss, T. B.; Dev, S.; Wilson, S. R. N-methylimidazole-promoted reactions of iron and nickel carbonyls with chalcogens: interconversions of iron polysulfide complexes and the structure of $[FeSe_8(CO)_2]^{2-}$. *Inorg. Chem*. **1992**, 31, 153.

(44) Dev, S.; Ramli, E.; Rauchfuss, T.B.; Wilson, S.R. Synthesis and structure of [M(*N*-methylimidazole)$_6$]S_8 (M = manganese, iron, nickel, magnesium). Polysulfide salts prepared by the reaction N-methylimidazole + metal powder + sulfur. *Inorg. Chem.* **1991**, 30, 2514.

(45) Rauchfuss, T.B. Research on Soluble Metal Sulfides: From polysulfido complexes to functional models for the hydrogenases. *Inorg. Chem*. **2004**, 43, 14.

(46) Cantrell K.J.; Yabusaki, S. B.; Engelhard, M. H.; Mitroshkov, A. V.; Thornton, E.C. Oxidation of H_2S by iron oxides in unsaturated conditions. *Environ. Sci. Technol*. **2003**, 37, 2192.

(47) Nakao, L.S.; Iwai, L. K.; Kalil, J.; Augusto, O. Radical production from free and peptide-bound methionine sulfoxide oxidation by peroxynitrite and hydrogen peroxide/iron(II). *FEBS*. **2003**, 547, 87.

(48) Marques, A.; Marin, M.; Ruasse, M. F. Hydrogen peroxide oxidation of mustard-model sulfides catalyzed by iron and manganese tetraarylporphyrins: Oxygen transfer to sulfides versus H_2O_2 dismutation and catalyst breakdown. J. Org. Chem. **2001**, 66, 7588.

(49) Nurmi, J. T.; Tratnyek, P.G. Electrochemical properties of natural organic matter (NOM), fractions of nom, and model biogeochemical electron shuttles**.** *Environ. Sci. Technol.* **2002**, 36, 617.

CHAPTER 3

ORGANIC CARBON IN DEGRADED MUNICIPAL SOLID WASTE FROM A LANDFILL: COMPOSITION, SOURCES AND INTERACTIONS WITH HYDROPHOBIC COMPOUNDS

ABSTRACT

The overall nature of organic carbon (OC) composition of degraded municipal solid waste (MSW) is relatively unknown due to limited information regarding the decomposition of MSW noncellulosic constituents. A unique highly aliphatic property of dissolved organic carbon in leachate produced from MSW in landfills suggests that OC of MSW itself should be different from soils and other materials. Since OC in MSW is gradually transformed during decomposition, it is expected that several properties including sorption capacity of MSW would be changed over time. The insight into these issues has been limited due to lack of understanding on the OC property of MSW in landfills. To study the OC of refuse in landfills, MSW was excavated from a 16-23 yrs old dumping area in the Norman Landfill at 12-16 ft, 20-24 ft, and 32-26 ft below the surface. Fourteen samples representing the two smallest fractions (80-200 mesh and >200 mesh) of the MSW insoluble component were characterized for OC composition by cross-polarization, magic-angle spinning ^{13}C nuclear magnetic resonance (CP-MAS ^{13}C NMR) spectroscopy, tetramethylammonium hydroxide (TMAH) thermochemolysis gas chromatography/mass spectrometry (GC/MS), pyrolysis GC/MS and organic solvent

extraction. From ^{13}C NMR spectra, over 75% of OC in MSW samples is attributed to cellulose, aliphatic and aromatic carbons. Relative degradation indices, O-alkyl/alkyl (OA/A) and cellulose/lignin (C/L) ratios, revealed that although all samples were in the landfill for almost the same period, those from the 12-16 ft depth were the least degraded. Between the two selected fractions, the larger one (80-200 mesh) was usually less degraded than its smaller counterpart. A decrease in cellulose content with corresponding increases in aliphatic and aromatic carbons were consistently found in MSW samples with lower OA/A ratio. Due to signals of cellulose in ^{13}C NMR spectra, both amorphous and crystalline cellulose in these samples were substantially degraded. TMAH thermochemolysis, pyrolysis GC/MS and organic solvent extraction revealed that aliphatic carbon was mainly derived from lipids, alkanes, and resin acids. The origins of these constituents include plant biomass and hazardous compounds with a minimal input from bacteria. Aromatic carbon primarily originates from lignin but additional input from PAHs was also found in some samples. Comparison of TMAH yields of pyrene between samples at each depth showed a higher amount of sorbed pyrene in the sample with a lower OA/A ratio. An irreversible sorption of PAHs was found in the most degraded sample. These results suggested that both sorption affinity and sorption mechanism for hydrophobic contaminants of degraded MSW samples might have been modified during the decomposition in the landfill.

INTRODUCTION

Decomposition of municipal solid waste (MSW) in landfills involves numerous

chemical and biological processes. Most of the current understanding on this issue is focused on the cellulosic component of MSW because it is a potential source of leachate and methane gas, which are the two primary concerns in MSW landfill operation (*1*, *2*). Relative to cellulose, an insight into the compositional changes of other MSW components during long term degradation in landfill is rather limited. Since MSW is well-known for its extraordinary degree of heterogeneity, this shortcoming leaves the overall nature of degraded MSW poorly understood.

Hazardous waste can be found in many old landfills, either from illegal dumping or the disposing of household hazardous materials. Sorption of the contaminants to MSW is among key processes that limit transport and bioavailability of hazardous compounds in landfills (*3*). As in other environments, OC of MSW plays a key role in the sorption process. During long term decomposition in landfills, not only the amount of MSW is decreased, but compositional change has also occurred because of the varying degradability of its components. Inevitably, the compositional transformation would have a direct effect on sorption capacity of refuse. A recent study showed that the affinity of toluene and *o*-xylene for plastics, paper products and rabbit food were increased after the samples had been degraded in a methanogenic landfill reactor (*3*). Newsprint samples degraded in a laboratory and in a landfill also showed a higher toluene sorption capacity than fresh newsprint. The K_{oc} value of the most degraded newsprint sample was almost 5 times higher than that of the fresh one (*4*). It was explained that the decrease in polarity of newsprint samples due to the decomposition of cellulose and the simultaneous increase in hydrophobicity due to the accumulation of refractory components, mostly lignin, and resin acids, enhanced the samples' sorption capacity. Results from these early works

might not be suitable to apply directly to the situation in landfills. Samples in those studies represent only certain elements of MSW. Thus, they do not depict an overall picture for degraded MSW. In addition, the environment in landfills is far more complex than the conditions set up in the laboratory.

Previous studies involving the characterization of landfill leachate reported that the decomposition of MSW produced leachate in which the hydrophobic component primarily consisted of aliphatic constituents (*5, 6*). This piece of information suggests the possibility that the degraded MSW, which is the source of the leachate, might also have a distinctive OC characteristic. In this study we examined the two smallest particle size samples selected from seven sets of the insoluble component of 16-20 yrs old MSW excavated from the Norman landfill. The principal objectives of the study were; *i*) to characterize OC structure of degraded MSW samples as a function of landfill depth and size of the samples, *ii*) to identify sources of OC in the MSW samples, and *iii*) to examine the possible correlation between the MSW samples' affinity for hydrophobic contaminants and the extent of the samples' degradation. Based on the chemical characteristic of DOC in leachate, the hypothesis of this research is that the preferential decomposition of cellulosic materials in MSW results in an increasing influence of hydrophobic components primarily aliphatic carbon compounds.

MATERIALS AND METHODS

Sampling Site

MSW samples in the study were excavated from the Norman Landfill. This landfill has been the research site for the U.S. Geological Survey since 1995. The landfill accepted waste from the City of Norman during 1922-1985. The sampling region located at the cell where waste was deposited from 1970-1985. In this area, waste was placed 2 ft above groundwater level and covered daily with sand. After the landfill was closed in 1985, compacted clay was used as a final cap and vegetation was subsequently introduced (*7*). The sampling cell covers an area of 204,600 ft^2 and rises almost 40 ft above land surface. Neither liners nor a leachate collection system was installed in the area. Currently, leachate has reached groundwater and the leachate plume extends at least 225 m from the edge of the landfill. Solid waste in the landfill was predominantly residential and commercial solid waste but there were reports of suspected hazardous waste disposal (*7*). Annual precipitation at the site is approximately 860 mm (*8*). Biochemical and geochemical study conducted at this sampling site reported that methanogenic condition is still prevalent in the landfill (*9*).

Sampling Method and Sample Preparation

Geoprobe direct push machine equipped with macro-core piston rod sampler (geoprobe®system) was used to retrieve three MSW core samples (1, 2, 3) at every four ft interval from the top through the base of the landfill. Each core sample was within 50 ft of the others. Three sections of each core, 12-16 ft, 20-24 ft, and 32-36 ft from the top of the landfill, were selected for analysis (referred as top (T), middle (M) and bottom (B) sections, respectively) Only the top section was available for the third core sample,

because the excavation was stopped at approximately 20 ft when the Geoprobe machine hit a hard object and could not go deeper. To avoid interferences from a final cover material and to ensure the anaerobic environment of MSW samples, the 0-12-ft section was not selected for the study. The soluble component in each selected core sections was removed by mixing samples with Nanopure water (1:10 v/v) and agitating for 24 hours at room temperature. After centrifuging (4000 rpm) for 30 min, the supernatant was decanted and the extraction was repeated. Insoluble component (referred as MSW) was freeze dried and separated according to particle size using 20, 40, 80, and 200 mesh sieves. The two smallest sizes were selected for further analysis. One was the fraction retaining on a 200-mesh sieve (labeled as 200). The other was the residue passing a 200-mesh sieve (labeled as R). These two fractions made up more than 50% of total refuse dry weight. Their appearance was not different from soils and their parent materials could no longer be recognized. All of these selected samples were treated with 10% hydrofluoric acid twice to remove clay mineral and paramagnetic ions following the protocol described by Schmidt *et al.* (*10*). After the treatment, all samples were analyzed by CP-MAS ^{13}C NMR, TMAH-thermochemolysis and pyrolysis GC/MS. Four samples were subsequently selected for solvent extraction. Each sample was labeled by number of core (1, 2, 3), location (T, M, B) and particle size (200, R).

Total Organic Carbon (TOC)

TOC of freeze dried MSW samples was measured by the platinum combustion catalytic oxidation method using a Shimadzu TOC 5050 Total Organic Carbon Analyzer

equipped with a solid sample module SSM-5000A and Non-Dispersive Infrared (NDIR) detector. TOC was calculated by subtracting an inorganic carbon (IC) content from a total carbon (TC) content (*i.e.*, TOC = TC-IC). TC of the pre-weight MSW sample was measured by the catalytically aided combustion oxidation at 900°C. In the IC measurement, the pre-weight MSW sample was acidified with 0.2 M phosphoric acid and combusted at 250°C. The measuring range for TC is 0.1-30 mg carbon; IC is 0.1-20 mg carbon. Glucose and sodium carbonate (Sigma) were used to construct standard curves for the TC and IC, respectively.

CP-MAS ^{13}C Nuclear Magnetic Resonance Analysis

CP-MAS ^{13}C NMR spectra of all selected MSW samples were obtained using Chemegnetics CMX-II solid-state NMR spectrometer operating at 75.694 MHz and using a chemagnetics 5 mm double resonance magic-angle spinning probe. A quasi-adiabatic sequence (*11*) using two-pulse phase modulation (TPPM) decoupling (*12*) at 75 kHz was employed. The ^{13}C CP contact pulse of 1 ms length was divided into 11 steps of equal length with ascending radio frequency field strength, while the ^{1}H contact pulse had constant radio frequency field strength. The sample spinning frequency was 6.0 kHz, maintained to within a range of ± 5Hz or less with a chemagnetics speed controller. Spectra were obtained from 12,910-56,700 scans.

TMAH Thermochemolysis

An accurate amount of 3-10 mg of MSW sample was placed in a thick-walled 10 mL ampoule with 200 µL of tetramethylammonium hydroxide (TMAH) (25% TMAH in methanol) (Aldrich). After methanol was evaporated under vacuum, the ampoule was subsequently flame-sealed. The sample was baked at 250 ºC for 30 min. After cooling in the freezer, the ampoule was opened and was thoroughly washed twice with CH_2Cl_2. This solution was dried under N_2 and then reconstituted in 100 µL of CH_2Cl_2 containing 40 ng of n-eicosane/µL. Methylation products were analyzed using a Hewlett Packard 6980 gas chromatograph interfaced with a HP 5973N mass selective detector. An MDN-5S (Sigma-Aldrich) fused silica capillary column (30 m x 0.25 mm *i.d.* x 0.25 μm film thickness) was used for the separation. The GC oven was temperature-programmed from 60 to 150 °C at a rate of 15 °C/min and then from 150 to 240 °C at 4 °C/min., after that the temperature was held constant for 10 min. The injector and interface were kept at 250 and 280°C, respectively. Peaks were identified by comparing with the Wiley/NBS library.

Organic Solvent Extraction

Four MSW samples (1TR, 1MR, 1B200, 2TR) were extracted by adding 15 mL of DCM/MeOH (2:1v/v) and the extraction was performed following the procedure described by Guntries *et al.* (*13*). Briefly, the mixture was sonicated for 3 hrs and allowed to sit for 24 hrs prior to decanting the solvent supernatant. This procedure was repeated twice and the extracts were combined together. Two mL of the extract was added into a 10 mL glass ampoule and solvents were dried under vacuum. A 200 µL of

tetramethylammonium hydroxide (TMAH) (25% TMAH in methanol) (Aldrich) was added to initiate the methylation. Then the same procedure as previously described in the TMAH-thermochemolysis section was applied for the TMAH-thermochemolysis analysis, with the use of naphthalene (50 ng/µL (Aldrich)) instead of *n*-eicosane as an internal standard.

Pyrolysis GC/MS

Freeze-dried MSW samples were analyzed by pyrolysis-GC-MS using a double-shot pyrolyzer PY-2020iD (Frontier Lab), and a Shimadzu gas chromatograph/mass spectrometer GCMS QP 5000 fitted with the GCMS solution 2.2 data system. Approximately 0.5 mg of MSW sample was placed in a platinum sample cup and dropped by a double shot sampler into the pyrolysis chamber which was subsequently heated at 5 °C/ms to 610 °C and held for 10 s. Volatiles were swept into a 30-m fused silica capillary column coated with chemically bound XTI-5 (0.25 mm *i.d.*, a film thickness 0.25 µm) (VWR, Bridgeport, NJ).The GC oven was programmed from an initial temperature of 40 to 280 °C at a heating rate of 8 °C/min and held at 280 °C for 30 min

RESULTS AND DISCUSSION

Residential Time of MSW Samples in The landfill

Residential time of MSW samples in the landfill were estimated according to three evidence: first, the 1978 aerial photograph of the sampling site showing the empty dumping area at the time (*7*); second two pieces of newspaper published in 1983 found in the middle layer (20-24 ft) of core 2; and third, the closure of the landfill in 1985 and the sample excavation in 2001. These time intervals put the residential period in the range of 16-23 yrs for MSW in the bottom section (32-36 ft) and 16-18 yrs for those in both middle and top (12-16 ft) sections.

Organic Carbon Composition of MSW Samples

OC content of the two smallest fractions (80-200 mesh (200) and > 200 mesh (R)) of these MSW was around 1-6 % (wt) (Table 3.1), the same range reported for soils and sediment samples (*10, 13-16*). However, OC in MSW samples exhibited a distinctive fingerprint. As shown in Figure 3.1 (peak assignments are given in Table 3.2), ^{13}C NMR spectra of MSW samples shows a strikingly sharp and well-resolved signal in the carbohydrate region (60-110 ppm), which is atypical for soil (*10, 14-16*) or sediment samples (*13*). On the other hand, this characteristic of MSW samples is similar to the OC profile in ^{13}C NMR spectra of degraded MSW composts (*17, 18*). Besides carbohydrates, other primary components of MSW samples include aliphatic and aromatic carbons. The relative distributions of these three major components totally make up 75-80% of OC content in each MSW sample (Table 3.1). Less than 25 % of OC is comprised of phenolic, carboxyl and carbonyl carbons (Table 3.1) .The distribution of each principal OC shows no preference along the depth profile, but there is a consistent change at all

TABLE 3.1 Relative Distribution of Organic Carbon in MSW Samples Based on ^{13}C-NMR Integration Results and Relative Decomposition Indices. T: Top Section (12-16 ft); M: Middle Section (20-24 ft); B: Bottom Section (32-36 ft); R: Particle Size > 200 mesh; 200: Particle Size 80-200 mesh.

Organic carbon functional groups	Core 1						Core 2						Core 3	
	TR	MR	BR	T200	M200	B200	TR	MR	BR	T200	M200	B200	TR	T200
organic carbon[a] (%)	3.6	5.4	2.2	1.2	3.0	0.9	4.7	1.6	1.6	2.4	0.6	1.0	4.3	2.4
alkyl (0-50 ppm) (%)	33.8	25.8	34.9	14.7	32.7	21.9	30.6	35.7	32.3	27.7	34.0	31.5	32.3	27.0
methoxy (50-60 ppm) (%)	6.7	6.8	8.7	6.9	6.6	9.7	7.3	8.4	6.7	6.8	8.0	6.6	7.1	6.3
cellulose alcohol (60-100 ppm)	17.9	21.0	22.0	32.1	18.9	34.6	30.6	23.6	21.3	34.5	27.0	24.4	30.3	33.7
anomeric (100-110 ppm) (%)	3.2	3.4	4.6	5.5	3.5	6.8	6.1	4.5	3.6	7.4	5.0	4.4	5.9	6.7
aromatic (110-145 ppm) (%)	23.4	28.7	16.5	27.9	25.0	14.1	12.2	13.7	21.0	11.7	13.0	19.9	12.2	12.8
phenolic (145-165 ppm)(%)	9.0	9.6	7.8	9.6	8.2	8.8	7.3	7.2	9.2	6.8	7.0	8.5	6.7	7.4
carboxylic (165-185 ppm)(%)	5.9	4.8	5.5	3.4	5.1	4.0	5.8	6.9	5.5	5.1	6.0	4.6	5.5	6.1
OA/A[b]	0.8	1.2	1.0	2.8	0.9	2.3	1.4	1.0	1.0	1.8	1.2	1.1	1.3	1.7
C/L[c]	0.5	0.5	0.5	0.8	0.5	0.7	1.1	0.6	0.6	0.8	0.5	0.6	0.8	1.1
G:AD/AL[d]	1.1	1.3	1.3	1.1	0.6	1.5	1.1	1.2	0.8	1.6	1.3	1.1	0.7	2.0
S:AD/AL[e]	1.8	1.1	1.8	1.3	1.8	1.7	0.6	1.8	1.0	6.4	2.4	1.2	6.2	10.3
TMAH yield of lignin (mg/g OC)	0.19	0.24	0.24	0.17	0.12	0.19	0.40	0.30	0.27	0.22	0.28	0.16	0.29	0.07

[a] before hydrofluoric treatments. [b] O-alkyl/alkyl ratio. The region for the O-alkyl is 50-110 ppm. [c] Cellulose/lignin ratio equals to anomeric/methoxy. [d] Guaiacyl acid/aldehyde ratio equals to the ratio of 3,4-dimethoxybenzoic acid methyl ester and 3,4-dimethoxybenzaldehyde. [e] Syringyl acid/aldehyde ratio equals to the ratio of 3,4,5-trimethoxybenzoic acid methyl ester and 3,4,5-dimethoxybenzaldehyde.

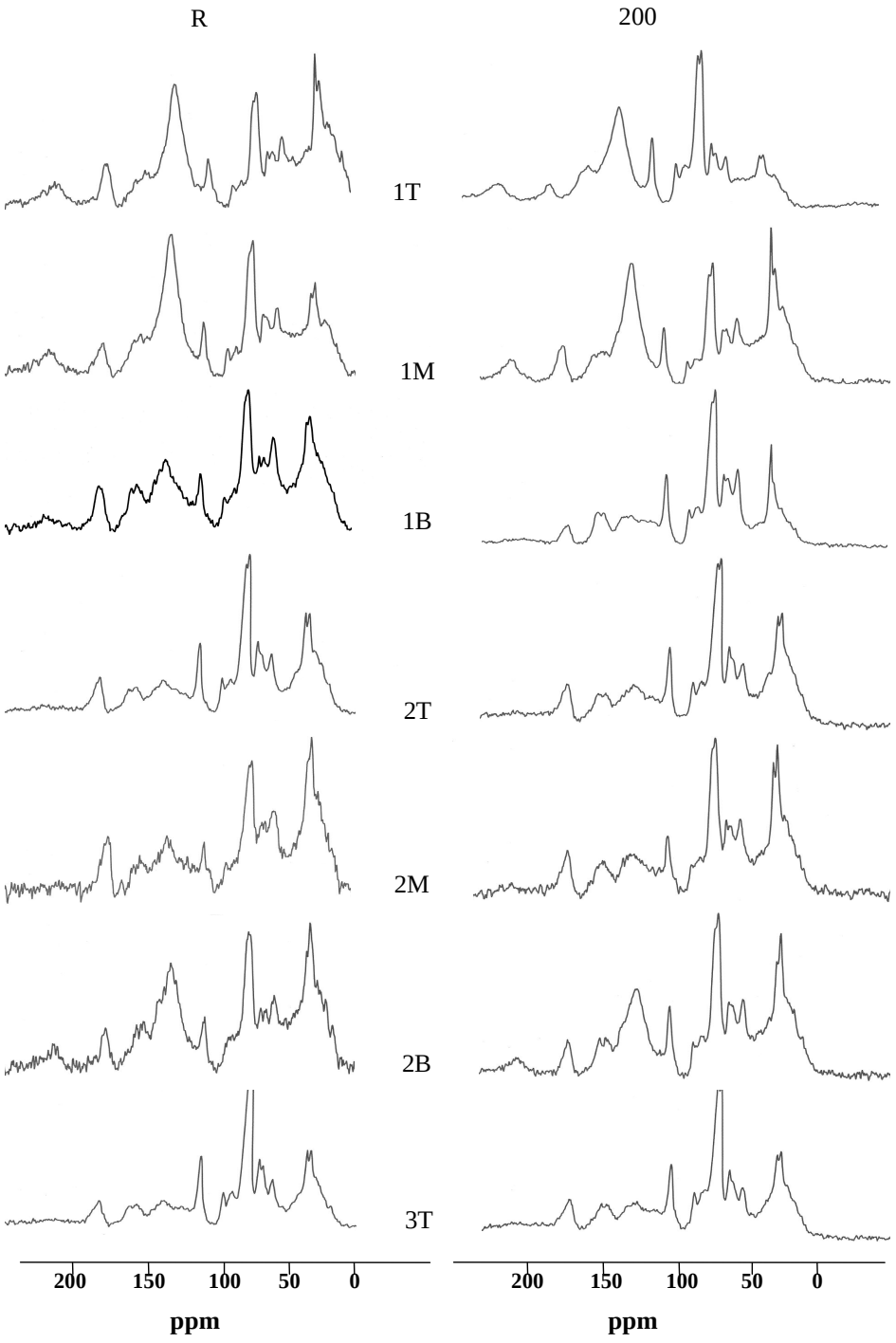

FIGURE 3.1 CP-MAS ^{13}C NMR spectra of MSW samples: R, 200 refer to particle size (>200 and 80-200 mesh); T, M, B refer to sampling depths (top (12-16 ft), middle (20-24 ft), bottom (32-36 ft); 1, 2, 3 refer to number of core samples.

TABLE 3.2 Tentative Chemical Shift Assignments for ^{13}C NMR Spectra of Municipal Solid Waste (ref. *4,17,59*)

Chemical shift (ppm)	Assignments
15	methyl carbons in terminal position
22	branched-methyl carbons in isopropyl groups
25	methylene carbons in cyclic structures
29	straight-chains polymethylene
32	C1 in isoprenoid chains, C3 in *n*-alkyl and ω3 in acyl chains
38	methylene (*trans*)
48	quaternary C
56	methoxy C and C in amino acids
62	C6 cellulose in an amorphous region
64	C6 cellulose in a crystalline region
72-74	C2, C3 and C5 cellulose and hemicellulose
82	C4 cellulose in an amorphous region
89	C4 cellulose in a crystalline region
100-110	C1 cellulose (anomeric carbon)
110-145	aromatic C
145-165	phenolic C
165-185	carboxylic C

depths between two different particle size samples selected from the same location. Aliphatic carbonis relatively abundant in the small particle size sample (R) while carbohydrate is concentrated in the larger fraction (200).

Extents of the Degradation

In order to estimate the extent of refuse decomposition, the ratio of carbohydrate to aliphatic carbons (OA/A) was calculated from the corresponding carbon distributions in ^{13}C NMR spectra. The OA/A ratio has been previously used to monitor the progress of NMR spectra. The OA/A ratio has been previously used to monitor the progress of MSW composting process (*19*) and measured the extent of refuse degradation in a simulated landfill (*3*). The lower the ratio, the greater extent of the decomposition. Except for 1T200 and 1B200, the OA/A ratios of MSW samples (Table 3.1) are all below ratios reported for fresh MSW (1.8-2.8) and fall in the range calculated for MSW composts that were processed up to 55 weeks with an alternated windrow system (0.7-1.8) (*18, 19*). Due to these numbers, most samples represent parts of refuse that were substantially degraded in the landfill. In order to supplement this data, cellulose/lignin (L/C) ratios were also approximated using the ratio of anomeric carbon of cellulose (105 ppm) to methoxy carbons of lignin (56 ppm) (interference from amino acids' signal which also resonates at 50-60 ppm (*17, 20*) was estimated to be minimal due to the scarcity of pyrolysis products, such as pyridine, pyrrole and indole that link to proteins (*21, 22*)). Results based on C/L ratio are in a good agreement with the conclusions from OA/A ratios. The C/L ratio of MSW samples ranged between 0.48-1.09 (Table 3.1). Values between 3 and 4 have been

reported for fresh MSW and lower numbers have been calculated for decomposed MSW (*1, 2, 23*).

When comparing the decomposition indices as a function of particle size, the ratios indicated that all small samples (R), except 1MR, were degraded more than their larger counterparts (200) (Figure 3.2). When the comparison was done as a function of depth, the results suggested that samples from the top section (except 1TR) were the least degraded. Due to the estimated residential period, these top-section samples are less than 2 yrs younger than those in the middle section. The results also revealed that samples from middle and bottom layers were broken down to a similar extent (Figure 3.3). The better preservation stage of top-section samples, such as 1T200, 2T200, and 3T200, could be visualized in the 72-74-ppm region of MSW ^{13}C NMR spectra. This peak, which represents signals from C2, C3 and C5 of the cellulose and hemicellulose in these samples, appears with a sharp and noticeable doublet that vanishes in more degraded samples (see the comparison between 1T200 (least degraded) and 1TR (most degraded) in Figure 3.4). The doublet pattern was previously observed in fresh MSW composts and a fresh newsprint sample but disappeared after the intensified decomposition of the samples (*4, 17*). Change in the doublet pattern has been mentioned as indicative of structural modification of hemicelluloses (*24*). The remnant of this feature in 1T200, 2T200, and 3T200, therefore, depicts a better preserved stage of hemicellulose in these less degraded samples. Meanwhile, evidence for the advanced breakdown stage of samples from the middle and bottom sections could also be observed. In the middle and bottom-section samples, signals from cellulose C6, both in crystalline and amorphous regions are not as prominent in relation to their neighboring methoxy carbon as in 1T200,

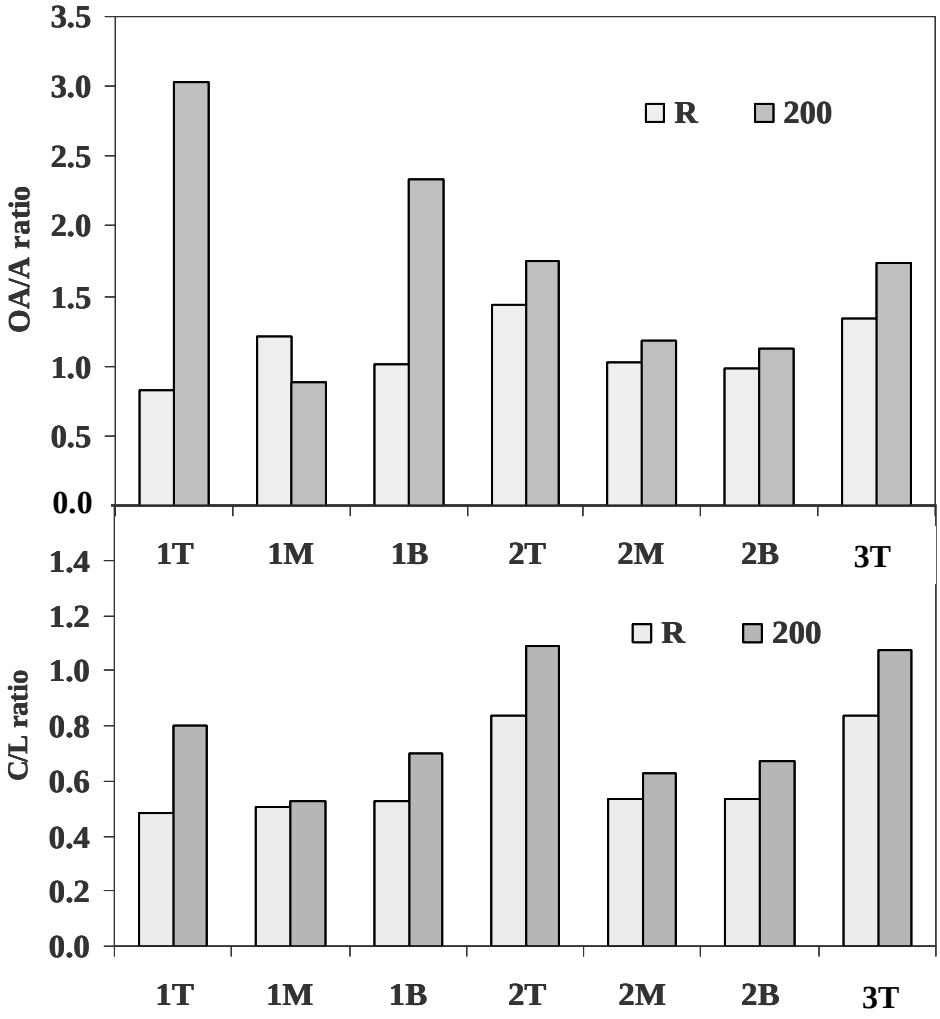

FIGURE 3.2 Comparison between relative degradation indices (OA/A, *O*-akyl/alkyl ratio; C/L ratio, cellulose/lignin ratio) of different particle sizes samples (R, >200 mesh; 200, 80-200 mesh).

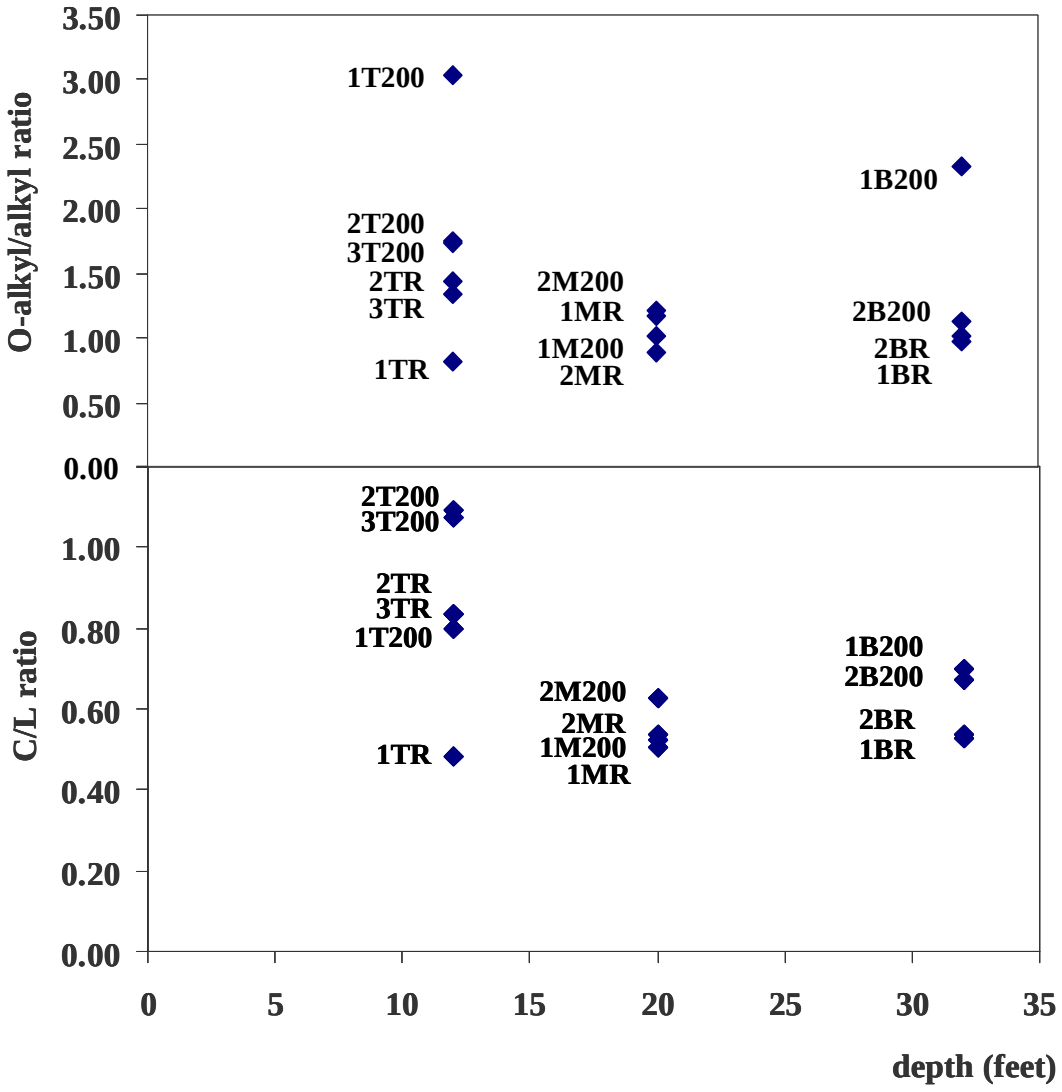

FIGURE 3.3 Comparison between relative degradation indices (OA/A, *O*-akyl/alkyl ratio; C/L ratio, cellulose/lignin ratio) of samples from different depths.

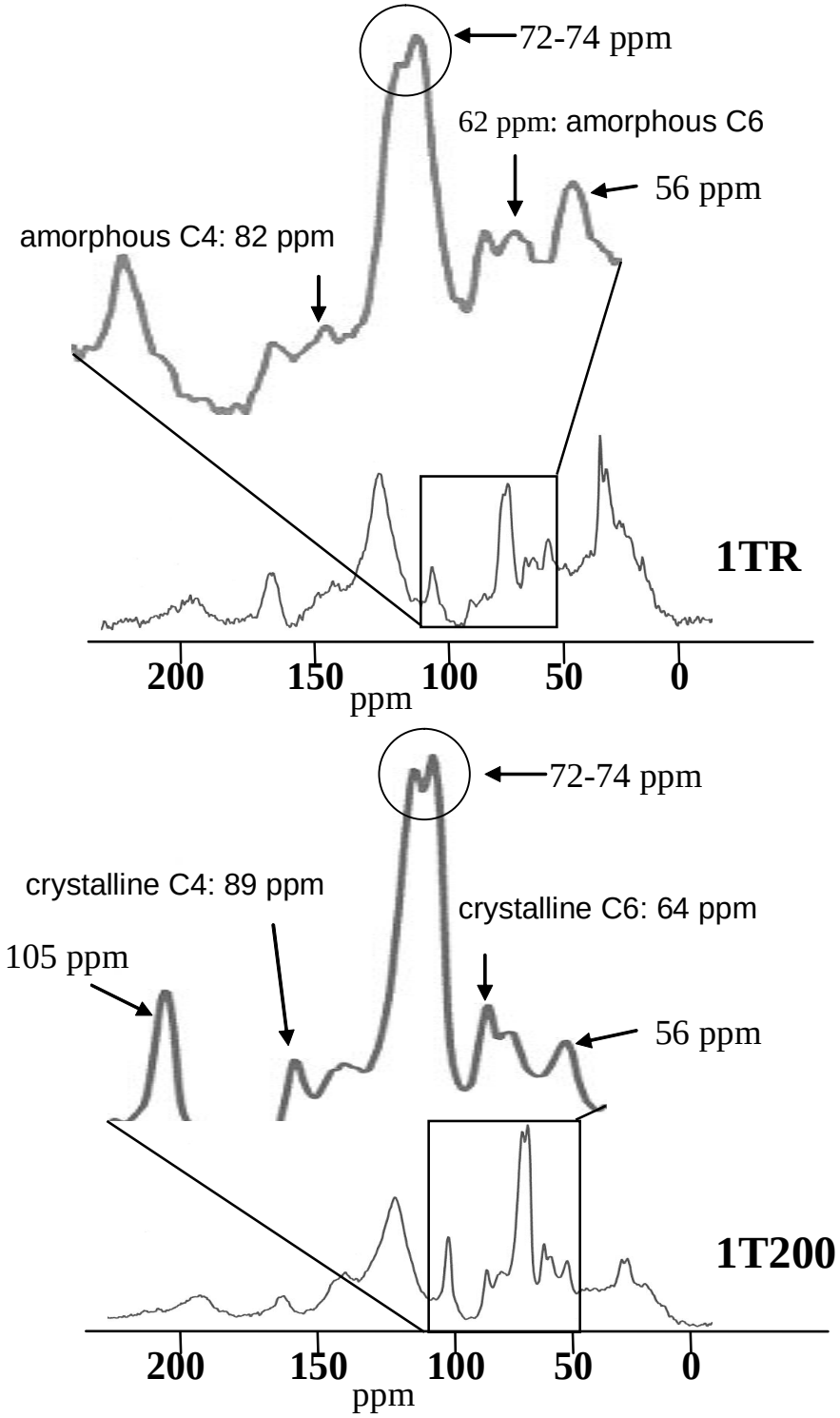

FIGURE 3.4 Comparison between ^{13}C signals of cellulose in samples 1TR and 1T200.

2T200 and 3T200. This accounts for the significant disintegration of cellulose in both forms. A similar situation is also observed with signals from cellulose C4.

Sources of Organic Carbon

Cellulose

One possible source of cellulose in MSW samples could be fibrous materials which are similar in appearance to plant fibers. Under microscopic examination using Scanning Electron Microscope (SEM), a number of these materials (Figure 3.5a) was found in each sample. From the SEM micrograph of the fiber in sample 2T200 (Figure 3.5b) a rough surface bearing an amorphous structure (*25*) is clearly visible. A close up of the fiber in more degraded samples such as 2B200 (Figure 3.5c) shows the wavy surface structure similar to that of low-crystalline cellulose (*26*)**.** These features are consistent with cellulose as interpreted from ^{13}C signals

Natural wood fibers contain both cellulose and lignin. Lignin occurs as a protective layer which is known to significantly delay the degradation of cellulose in an anaerobic environment such as landfills. Detailed lignin analysis using TMAH-thermochemolysis showed that most lignin-derived products were common among MSW samples (Figure 3.6 and Table 3.3). Ratios of acid-substituted lignin monomers to aldehyde-substituted lignin monomers (AD/AL) for both guaiacyl and syringyl units in most MSW samples are in the same range as the numbers reported for fresh woods (0.5-1

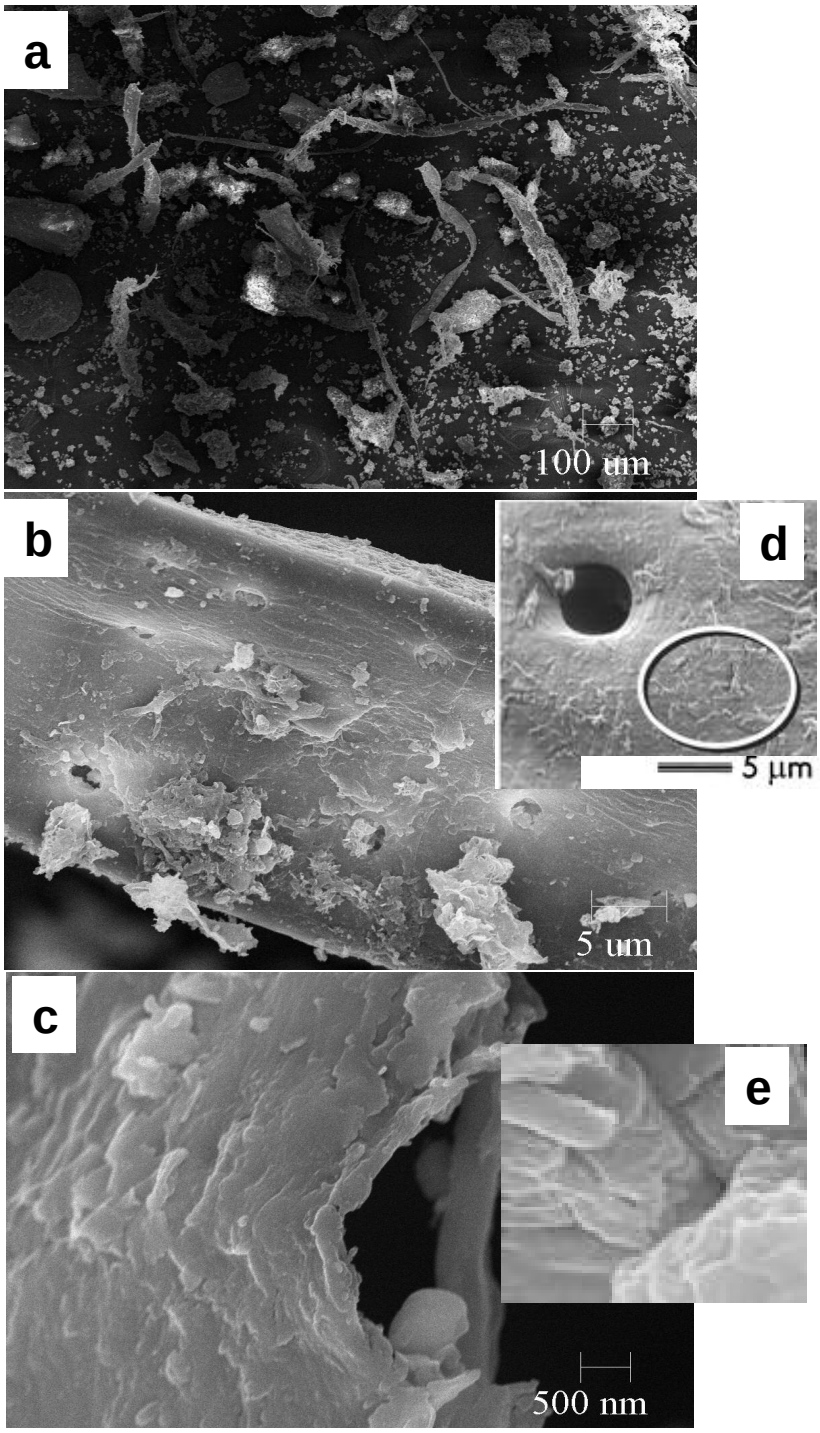

FIGURE 3.5 SEM micrographs of a) 2TR, b) 2T200, c) 2B200, d) wood fiber after MnO_2 oxidation showing an amorphous surface (ref.*25*), and e) surface of a low crystalline cellulose sample (ref.*26*)

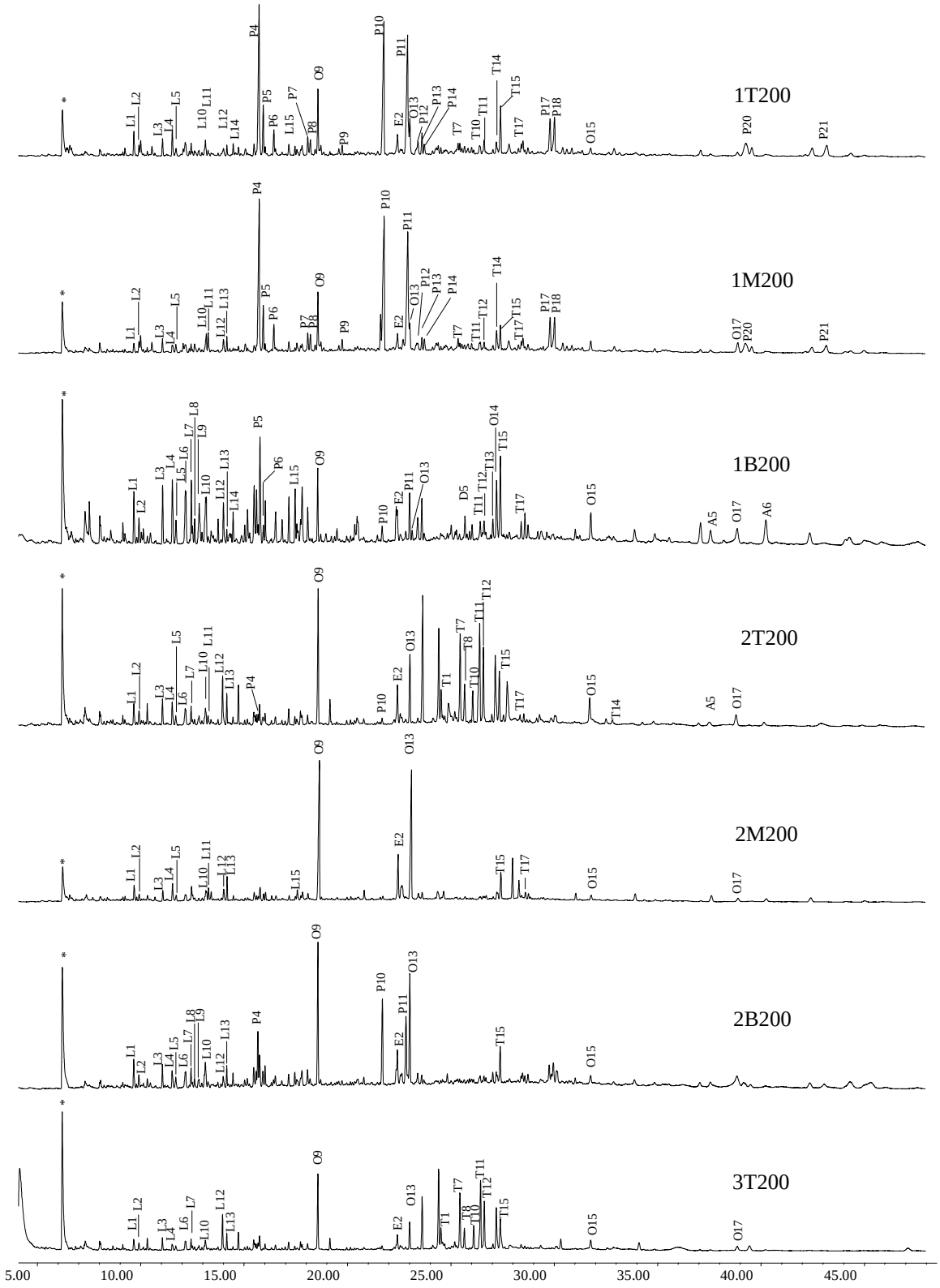

FIGURE 3.6 TIC of TMAH thermochemolysis products of MSW samples. Peak labels are identified in Table 3.

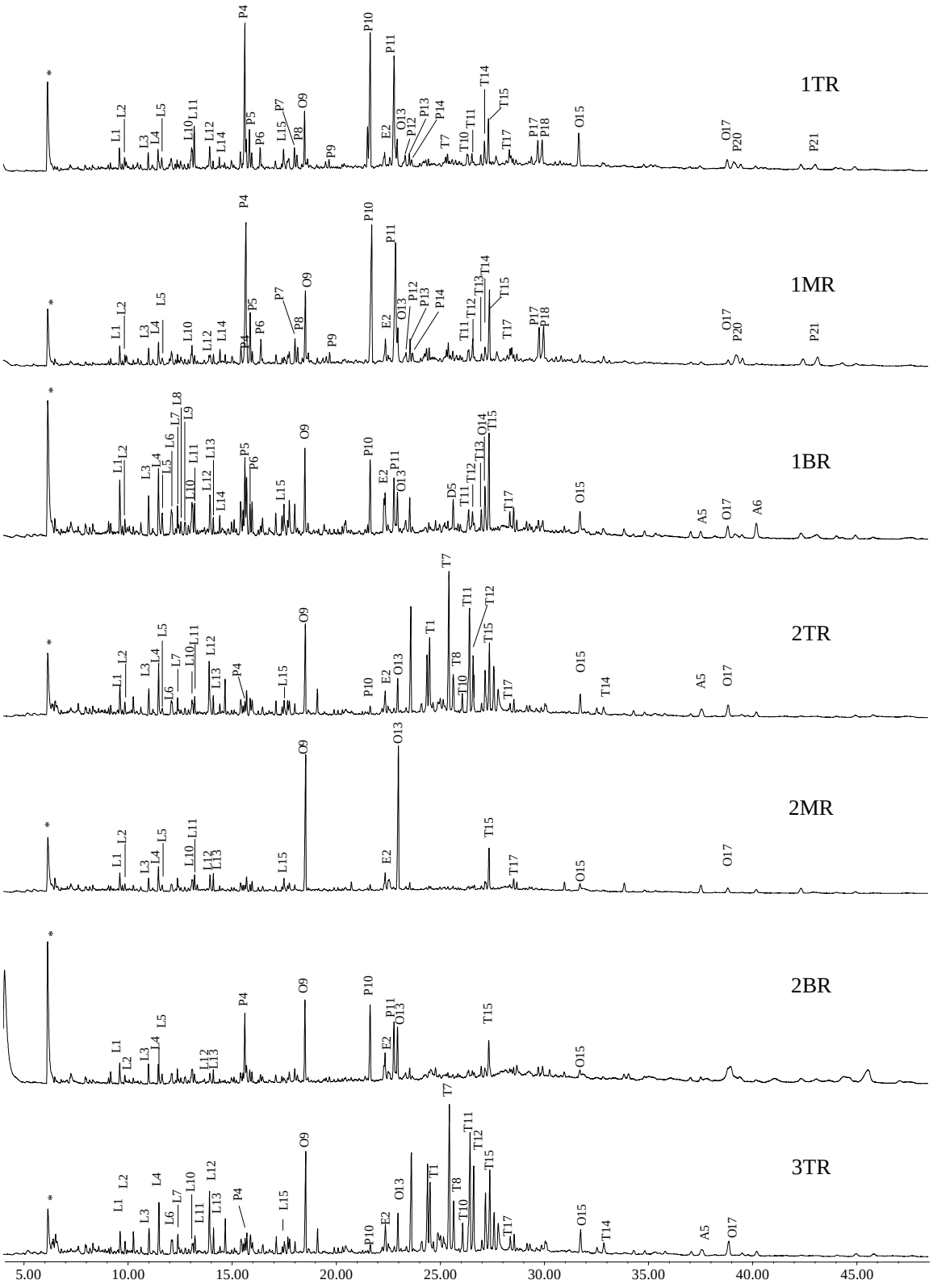

FIGURE 3.6 (Continued)

TABLE 3.3 Organic Compounds in the MSW samples as Identified by TMAH Thermochemolysis, Solvent extractions, and Pyrolysis GC/MS

Compounds derived from lignin structures[a]	
benzene, 4-ethenyl-1,2-, dimethoxy-	L1
2-propenoic acid, 3-phenyl-	L2
benzoic acid, 4-hydroxy-3-methoxy-	L3
benzaldehyde, 3,4-dimethoxy-	L4
benzene, 1,2-dimethoxy-4-(1-propenyl)-	L5
ethanone, 1-(3,4-dimethoxyphenyl)-	L6
benzoic acid, 3,4-dimethoxy-,methyl ester	L7
benzaldehyde, 3,4,5-trimethoxy-	L8
benzenepropanoic acid, 3,4-dimethoxy-	L9
2-propenoic acid , 3-(4-hydroxy-3-methoxyphenyl)-, methyl ester	L10
benzene, 1,2,3-trimethoxy-5-(2-propenyl)-	L11
benzene, 1,2,4-trimethoxy-5-1-propenyl-(*E*)	L12
benzene, 1,2,4-trimethoxy-5-1-propenyl-(*Z*)	L13
2-propenoic acid, 3-(4-methylphenyl)-, methyl ester	L14
benzoic acid, 3,4,5-trimethoxy, methyl ester	L15
Benzenepropanoic acid, 3,4-dimethoxy-methyl ester	L16
2-propenoic acid, 3-(3,4-dimethoxyphenyl)-, methyl ester	L17
Resin acids[b]	
methyl δ8-isopimarate	T1
9-phenanthrenecarboxylic acid, 1,2,3,4,4a,9,10,10a-octahydro-6-methoxy-1,1,4a-trimethyl-7-(1-ethylethyl)-	T2
retene	T3
methyl dihydro-δ8-isopimarate	T4
14-isopropyl-13-methoxy-podocarpa-8,11,13-triene	T5
pimaric acid	T6
dihydroisopimaric acid	T7
sandaracopimaric acid	T8
Resin acids[b]	
tetrahydropimaric acid	T9
dihydroisodextropimaric acid, methyl ester	T10
dihydrosandaracopimaric acid	T11
isopimaric acid, methyl ester	T12
13β-ethyl-13-methyl-podocarpan-15-oic acid, methyl ester	T13
13α-ethyl-13-methyl-podocarp-7-en-15-oic acid, methyl ester	T14
dehydroabietic acid	T15
1-phenanthrenecarboxylic acid, 1,2,3,4,4a,6,7,8,10,10a-dodecahydro-1,4a-dimethyl-7-(1-methylethyl)-, methyl ester	T16
abietic acid, methyl ester	T17
14-isopropyl-13-methoxy-podocarpa-8,11,13-trien-3-one	T18
7-oxodehydroabietic acid, methyl ester	T19
(±)-O-methylpisiferic acid	T20
Fatty acid: Monocarboxylic acids[b]	
decanoic acid, methyl ester	O1
dodecanoic acid, methyl ester	O2
tridecanoic acid, 12-methyl, methyl ester	O3
tetradecanoic acid, methyl ester	O4
tetradecanoic acid, 9-methyl, methyl ester	O5
dodecanoic acid, 12-hydroxy, methyl ester	O6
pentadecanoic acid, methyl ester	O7
pentadecanoic acid,14-methyl, methyl ester	O8
hexadecanoic acid, methyl ester	O9
hexadecanoic acid, 14-methyl, methyl ester	O10
heptadecanoic acid, methyl ester	O11
hexadecanoic-3,7,11,15-tetramethyl, methyl ester	O12
octadecanoic acid, methyl ester	O13

TABLE 3.3 (Continued)

Fatty acid: Monocarboxylic acids[b]	
dodecanoic acid, methyl ester	O2
tridecanoic acid, 12-methyl, methyl ester	O3
tetradecanoic acid, methyl ester	O4
tetradecanoic acid, 9-methyl, methyl ester	O5
dodecanoic acid, 12-hydroxy, methyl ester	O6
pentadecanoic acid, methyl ester	O7
pentadecanoic acid,14-methyl, methyl ester	O8
hexadecanoic acid, methyl ester	O9
hexadecanoic acid, 14-methyl, methyl ester	O10
heptadecanoic acid, methyl ester	O11
hexadecanoic-3,7,11,15-tetramethyl, methyl ester	O12
octadecanoic acid, methyl ester	O13
hexadecanoic acid, 16-hydroxy, methyl ester	
eicosanoic acid, methyl ester	O14
docosanoic acid, methyl ester	O15
tricosanoic acid, methyl ester	O16
tetracosanoic acid, methyl ester	O17
Fatty acids: Dicarboxylic acids[b]	
hexanedioic acid, dimethyl ester	D1
octanedioic acid , dimethyl ester	D2
nonanedioic acid, dimethyl ester	D3
decanedioic acid , dimethyl ester	D4
hexadecanedioic acid, dimethyl ester	D5
tetradecanedioic acid, dimethyl ester	D6
octadecanedioic acid, dimethyl ester	D7
eicosanedioic acid, dimethyl ester	D8
docosanedioic acid, dimethyl ester	D9

Unsaturated fatty acids[b]	
9-hexadecenoic acid, methyl ester	E1
9-octadecenoic acid, methyl ester	E2
9,12-Octadecadienoic acid	E3
PAHs and heterocyclic PAHs[bc]	
acenaphthylene	P1
fluorene	P2
dimethylthiophene	P3
phenanthrene	P4
anthracene	P5
9H-carbazole	P6
biphenylene	P7
1-methylanthracene	P8
2-phenylnaphthalene	P9
fluoranthene	P10
pyrene	P11
benzo[b]naphtho[2,3-d]furan	P12
benzo[b]naphtho[2,3-d]furan	P12
2-methylphenanthrene	P13
3,4,5,6-tetramethylphenanthrene	P14
1-methylpyrene	P15
benzo[c]phenanthrene	P16
benz[a]anthracene	P17
triphenylene	P18
1-methylchrysene	P19
indeno[1,2,3-cd]pyrene	P20
benzo[k]fluoranthene	P21
benz[e]acephenanthrylene	P22

TABLE 3.3 (Continued)

PAHs and heterocyclic PAHs[bc]	
2-methylphenanthrene	P13
3,4,5,6-tetramethylphenanthrene	P14
1-methylpyrene	P15
benzo[c]phenanthrene	P16
benz[a]anthracene	P17
triphenylene	P18
1-methylchrysene	P19
indeno[1,2,3-cd]pyrene	P20
benzo[k]fluoranthene	P21
benz[e]acephenanthrylene	P22
benzo[e]pyrene	P23
benz(a)pyrene	P24
perylene	P25
benzo[b]triphenylene	P26
benzo[ghi]perylene	P27

Alkenes and alkanes[c]	
1-decene and decane	\ C10
1-undecene and undecane	\ C11
1-dodecene and dodecane	\ C12
1-tridecene and tridecane	\ C13
1-tetradeceneand tetradecane	\ C14
1-pentadecene and pentadecane	\ C15
1-hexadecene and hexadecane	\ C16

Alkenes and alkanes[c]	
1-heptadecene and heptadecane	\ C17
1-octadecene and octadecane	\ C18
1-nonadecene and nonadecane	\ C19
1-eicosene and eicosane	\ C20
heneicosane	C21
docosane	C22
tricosane	C23
tetracosane	C24
pentacosane	C25
hexacosane	C26
heptacosane	C27
octacosane	C28
nonacosane	C29
triacontane	C30
hentriacontane	C31

Other compounds[abc]	
4-ethynyl-1,2-dimethoxybenzene	U1
dimethyl phthalate	U2
phytol	U3
2-ethenyl-1,3,4,5-tetramethoxybenzene	U4

[a] indentified by TMAH thermchemolysis; [b] identified by solvent extractions; [c] identified by pyrolysis GC/MS

for both soft and hard woods (*27*)), indicating a minimal change of lignin over 16-23 yrs in the landfill.

Aromatic Carbon

Based on ^{13}C NMR analysis, the intensity of aromatic carbon varies significantly among MSW samples. The signal from aromatic carbon is particularly high in samples 1TR, 1T200, 1MR, 1M200, 2BR, and 2B200. Previous studies showed that lignin is the primary source of aromatic carbon in MSW composts (*17*) and newsprint samples (*4*). However, it is unlikely that all aromatic carbon in samples 1TR, 1T200, 1MR, 1M200, 2BR, and 2B200 were entirely originated from lignin. This is because, compared to other samples, the intensity of signals from phenolic and methoxy carbons, which are also major components of lignin, did not increase. The other possible source of aromatic carbon is polystyrene. This plastic also provides aromatic carbon signal in ^{13}C NMR spectra of shredded MSW composts (*17*). Polystyrene also produces other signals plastic also provides aromatic carbon signal in ^{13}C NMR spectra of shredded MSW composts (*17*). Polystyrene also produces other signals including a moderately intense one at 43 ppm (*17*). This signal was not observed in ^{13}C spectra of MSW samples which have high aromatic carbon content (Figure 3.1). Thus, the intense aromatic signal was not generated by polystyrene.

As further revealed by the organic solvent extraction procedure, some samples with high aromatic carbon content such as 1TR and 1MR contained a large number of multiple-rings PAHs, mostly with molecular weight 202 amu or higher. In comparison,

samples with a less intense aromatic peak such as 1B200 and 2TR showed fewer numbers and minor amounts of these contaminants (Figure 3.7) A lower scale PAHs contamination was also confirmed in other samples (except 1T200 and 1M200). Subsequent ^{13}C NMR analysis of 1TR and 1MR after being extracted by organic solvents showed that the intensity of the aromatic signal was lowered by approximately 40% after the extraction process (Figure 3.8); TMAH-thermochemolysis and pyrolysis GC/MS of samples after the extraction showed mostly lignin-related products).

The distribution of high molecular weight PAHs with a small amount of alkyl PAHs is consistent with a pyrogenic source (*22, 28, 29*). Fluoranthrene/(fluoranthrene plus pyrene) (Fl/202) ratio (5.8 and 5.9 for 1TR and 1MR, respectively) and the indeno[1,2,3-*cd*]pyrene/(indeno[1,2,3-*cd*]pyrene plus benzo[*ghi*]perylene)(IP/276) ratio (0.58 and 0.62, respectively) greater than 0.5 indicates a major input from wood or coal combustion (*28*). The identification of N-heterocyclic aromatic hydrocarbons (azaarenes) and other hetero-PAHs, such as dibenzothiophene and benzo[*b*]naphtho[2,3-*d*]thiophene, in the water soluble fraction and an atomic sulfur during pyrolysis GC/MS analysis subsequently suggests coal combustion as the possible primary source of PAHs in MSW samples (*30*).

Aliphatic Carbon

The aliphatic component of MSW samples identified by TMAH thermochemolysis, pyrolysis GC/MS and solvent extractions includes long-chain fatty acids, *n*-alkanes and resin acids. The presence of these compounds in MSW samples is

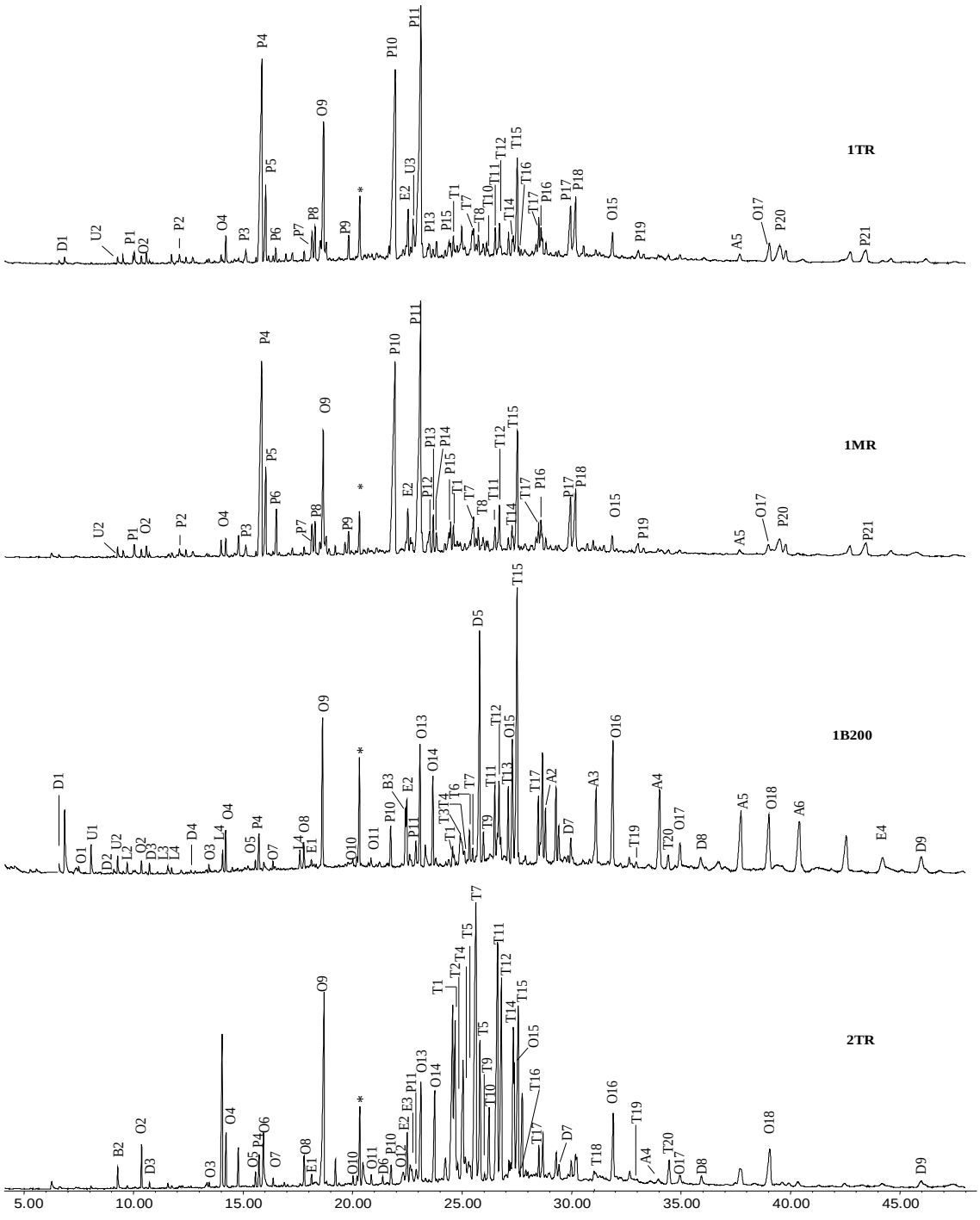

FIGURE 3.7 TIC of solvent extracts of MSW samples. Peak lables are identified in Table 3.3.

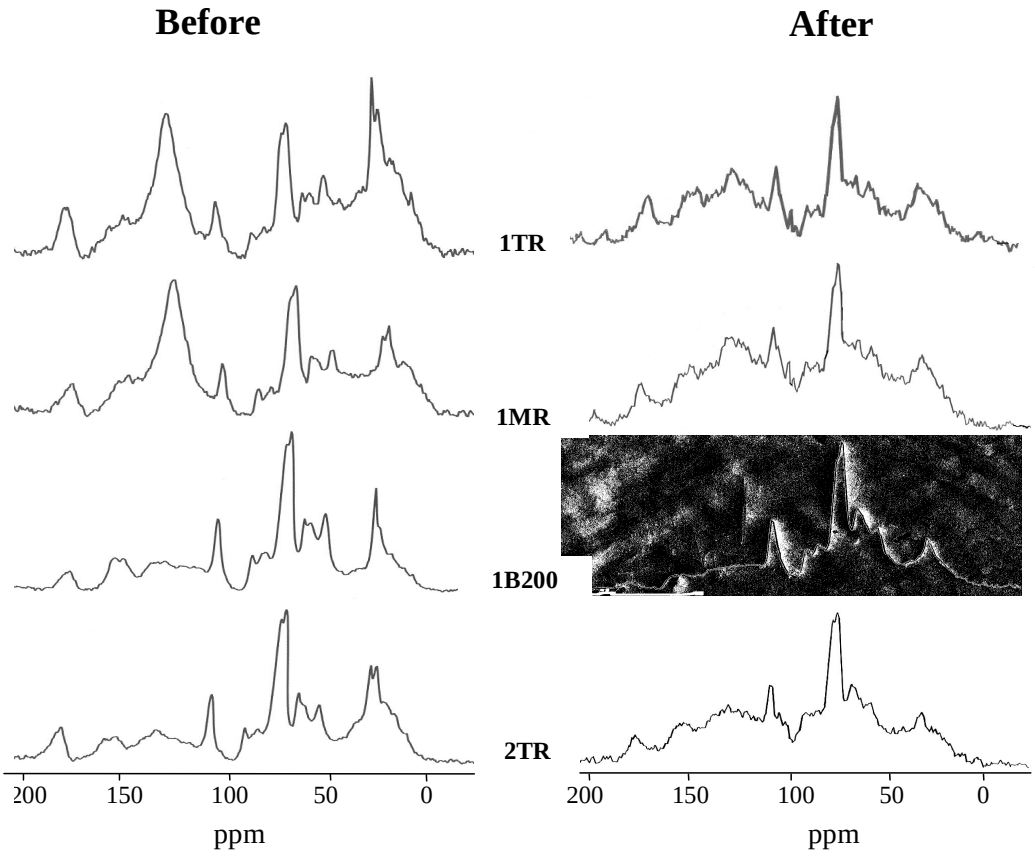

FIGURE 3.8 ^{13}C NMR of MSW samples before and after solvent extraction.

consistent with the assignments of ^{13}C signals in an alkyl region in Table 3.2 (Figure 3.9) Fatty acids in MSW samples are present in both mono and diacid forms (identified by TMAH-thermochemolysis and solvent extraction techniques as fatty acid methyl esters (FAME)). The distribution of FAME ranges between C10-C24 with maxima at C16 and C18, and with the predominance of even-numbered FAME. Straight chain fatty acids with chain lengths less than 20 carbons are common in plants and animal lipids and bacteria, whereas monocarboxylic acids with longer chain are typically limited to plant waxes (*31-33*). The influence from microbial input is ruled out in this case since multimethyl-branched fatty acids with methyl groups on even carbon atoms, typical markers for bacterial fatty acids, are not detected. Although some monomethyl-branched fatty acids (methyltetradecanoate, 9-methyl (O4), hexadecanoic acid, 14-methyl (O10): Figure 3.7) might indicate bacteria contribution (*33, 34*), these are minor constituents in the MSW samples. These branched fatty acids could originate from plant residues in the landfill. Hexadecanoic acid, 14-methyl (O10: Figure 3.7) for example, has been found in seed oil of species *Pinaceae* (*35*). The only multimethyl-branched fatty acid found in MSW samples is hexadecanoic acid, 3,7,11,15-tetramethyl (O12: Figure 3.7). This phytanic acid is one of biotransformation products of phytol, the ester-linked side-chain of chlorophyll-*a* (*36*). Phytol (U3) itself was also identified in the solvent extract of 1TR.

Fatty acids with long carbon skeleton (C14-C22) in refuse have been reported to originate from lipids of higher plant biomass deposited in landfills (*37*). Plant waxes, cutin and suberin, are two plant lipids often regarded as the major contributors. However, only evidence of suberin was found in MSW samples. One C16-ω-hydroxy acid (O14) and two dicarboxylic acids (O17 and O18: Figure 3.7) identified in 1B200 and 2TR are

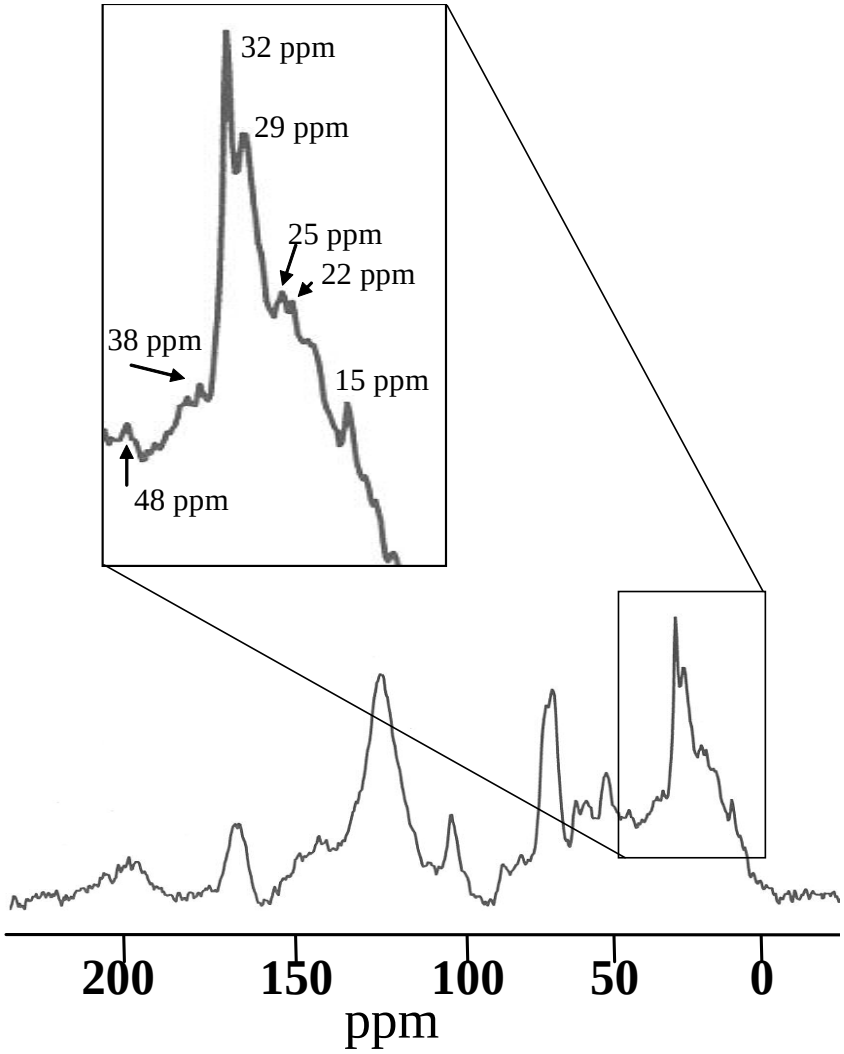

FIGURE 3.9 ^{13}C NMR signals in the alkyl region of sample 1TR.

plausible links to suberin. Dihydroxy C16 and C18 FAME, two key components of cutin (*38, 39*), were not identified.

The distribution pattern of *n*-alkane in Figure 3.10 indicates an input from multiple sources. Although there is evidence of suberin, the distribution of alkanes without the odd-carbon predominance indicates additional sources other than plant biomass. Plant lipids contain odd-carbon alkanes from *n*-C23 to *n*-C33, with a maximum at *n*-C27 or *n*-C29 (*28, 40*). As revealed in the pyrograms of samples 1B200, 1BR, and 2TR in Figure 3.10, *n*-alkanes appeared in a sequence up to C31 without an odd-even carbon preference. In addition, a series of *n*-alkenes/*n*-alkanes up to C20 dominated the first half of the pyrograms. This distribution pattern was common to all MSW samples. The absence of pristine and phytane as well as a hump indicating an unresolved complex mixture (UCM) of primarily short chain length hydrocarbons and isoprenoids in the pyrograms, indicates that *n*-alkenes/*n*-alkane are not a contamination from crude oil (*29*). Small amounts of alkyl PAHs found in MSW samples also rule out sources such as gasoline or diesel fuel (*22, 28*). With coal combustion being the potential source of PAHs, it is possible that alkenes and significant fraction of alkanes may also originate from this source. Elevated amount of C29 alkane in 1B200 and 2TR is the reminder of the influence from plant alkanes. Other samples with a high OA/A ratio (all samples from the top section (except 1TR)) also showed this noticeable C29 alkane.

Resin acids, another component of aliphatic carbon in MSW samples were identified in every MSW sample, but their high concentrations were found mainly in the top section of core 2 and 3 (Figure 3.6). As many as 15 species of resin acid were extracted from sample 2TR (Figure 3.7), one of five samples abundant in these

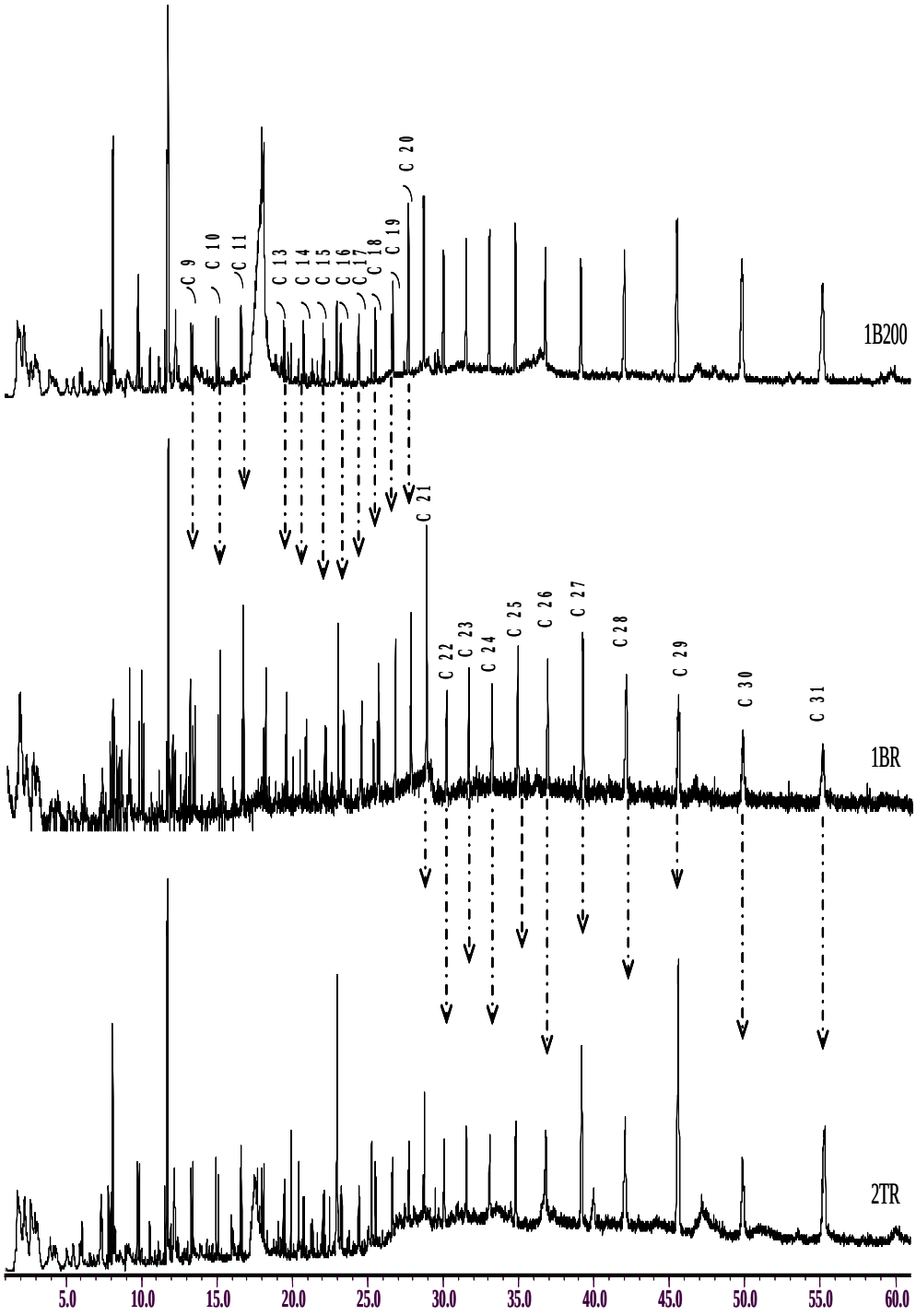
C 9
C 10
C 11
C 13
C 14
C 15
C 16
C 17
C 18
C 19
C 20
C 21
C 22
C 23
C 24
C 25
C 26
C 27
C 28
C 29
C 30
C 31
1B200
1BR
2TR
5.0
10.0
15.0
20.0
25.0
30.0
35.0
40.0
45.0
50.0
55.0
60.0

terpenoids. Some of these resin acids (T15, T17) have been found in the leachate plume several ft down gradient from the landfill (*5*, *6*). A few studies reported the contamination of resin acids in MSW landfills (*41-43*), but none of them mentioned origins of these acids. Resin acids are aerobically degradable, but they are very persistent in anaerobic environment, primarily because they are highly toxic to anaerobic bacteria, especially to methanogens (*44*, *45*).

Resin acids in MSW samples were not released directly from coniferous woods in the landfill. First supporting evidence comes from the relative ^{13}C distribution of methoxy carbon. Comparing to sample 1B200, four other samples with high concentration of resin acids (2TR, 2T200, 3TR, 3T200) are less abundant in this characteristic carbon of lignin, but they are loaded with more resin acids. Second, levopimaric acid, one of primary resin acid species in pines (*46*), was absent in all samples. Third, other terpenoids such as feruginol or suriol, also common in coniferous wood, were not detected. These two species should not be easily degraded in the landfill since they are so persistent that geologists have used them as makers for fossil conifers (*47*). Resin acids have been used in several manufacturing processes including resins, adhesive, printing ink, but their major use has been an internal sizing agent in paper manufacturing (*46*). However, paper wastes in the landfill are unlikely sources of resin acids in MSW samples. Nineteen resin acids were identified in MSW samples (Figure 3.7), whereas only nine species were found in newsprints samples collected from the same locations (*4*), and only six of them were repeatedly found in MSW samples.

Two of resin acids in MSW samples (T3, T9) were anaerobic microbial alteration products (*48*). However, retene (T3) can be produced during the combustion of pine

woods (*49*) and coal (*50*) as well. The most likely source of resin acids in the Norman landfill was tall oil pitch. Tall oil pitch is a nonvolatile part of tall oil separated in crude tall oil fractionation processes. It is highly variable in composition with contains nearly 50% resin acids, almost equal amounts of esters (mainly oleic and linoleic acids), and unsaponifiable neutral compounds such as stigmastan-3-ol and stigmast-5-en-3-ol (*51*). Both oleic acid (E12), and stigmast-5-en-3-ol were among compounds identified in the organic solvent extract and in the pyrogram of sample 2TR, one of samples with high amounts of resin acids. Tall oil pitch has been used as a bonding agent or a plasticizer in asphalt industry (*46*). From 1970 to its closure in 1985, the Norman landfill was operated by a local asphalt company. Disposal of any materials contacted with tall oil pitch could lead to the contamination of resin acids in MSW samples.

Changes in OC Pattern during MSW Decomposition

The consistent pattern of OC in 14 MSW samples from three different depths and locations in the landfill indicates that cellulose, aliphatic and aromatic carbons are the top three most abundant OC in degraded MSW samples. The third species, aromatic carbon, generally originate from lignin, but its abundance is subjected to high variability due to contamination by hydrophobic compounds, such as PAHs. The distributions of these primary OC are a function of the size of the samples rather than depth at which MSW was buried. In most cases, a MSW sample with a small particle size was more degraded than its larger counterpart. It contains a smaller amount of cellulose with a greater extent of aliphatic and aromatic carbons. Based on this finding, the cellulosic component of

MSW will be depleted upon degradation, whereas the relative amount of aliphatic carbon will become enriched. Therefore, unless it was contaminated with compounds like PAHs, degraded MSW samples should become increasingly hydrophobic because of the growing influence of their aliphatic component. Similar change was observed with the newsprints' degradation, but the source of the hydrophobicity of the degraded newsprints primarily came from aromatic carbon of lignin (*4*). The manner to which OC is shifted during the course of degradation is consistent with the property of dissolved organic carbon (DOC) in leachate. Previous studies at this landfill showed that DOC in leachate contaminated groundwater collected from monitoring wells around the landfill, contained a significant amount of aliphatic carbon components (*5, 6*). Thus, as aliphatic carbon continues to be a dominant OC of degraded MSW, it is conceivable that DOC in leachate may become increasingly aliphatic.

Factors Affecting the Decomposition of MSW samples

Difference in the extent of degradation among MSW samples, which had been left in the landfill for the same period clearly demonstrates that time is not the crucial parameter for refuse degradation. There are other factors more important. In the case of samples from the top section, it is hypothesized that the variation in refuse's moisture content could be one of those factors that make these samples less degraded than samples in two lower parts. Due to high ground water level which varies seasonally from land surface to about 4 m. below ground level (*7*), and the lack of a liner system within the landfill, groundwater could reach refuse in the lower part of the dumping area. As a

result, the refuse's moisture content could increase. Moisture content is one of key parameters controlling the degradation of MSW (*52-54*). Thus, with higher moisture content, refuse in the lower section of the landfill might be degraded faster than those in the upper part.

It was also noticed that most samples from the top section (except 1TR) contain a high amount of resin acids (Figure 3.11). Resin acids are toxic to anaerobic bacteria, particularly methanogen (*44, 45*), which is still predominant in the landfill (*9*). Due to this adverse impact of resin acids, it is plausible that the accumulation of resin acids, mainly in the top section samples, could be the other factor impeding the decomposition of these MSW. Substances toxic to bacteria can enter landfills in many ways and are not limited to hazardous waste. Disinfection and antibiotic products are prime examples. At least 20 of 76 organic compounds identified in leachate contaminated groundwater collected at the Norman landfill were antibiotics (*55*).

The Affinity for Hydrophobic Compounds

There are some indications that the shift in type of primary OC had changed the affinity for hydrophobic compound of MSW samples. The decrease in sorbent polarity due to decomposition of cellulose and simultaneous increase in hydrophobicity due to the increasing influence of aliphatic carbon might be the reason. First evidence is the subsiding influence of plant alkanes in samples from middle and bottom sections. C29 alkane, a biomarker of plant alkanes (Figure 3.12), is noticeable only in samples from top section (the least degraded samples, except 1TR). In samples with low OA/A ratios (from

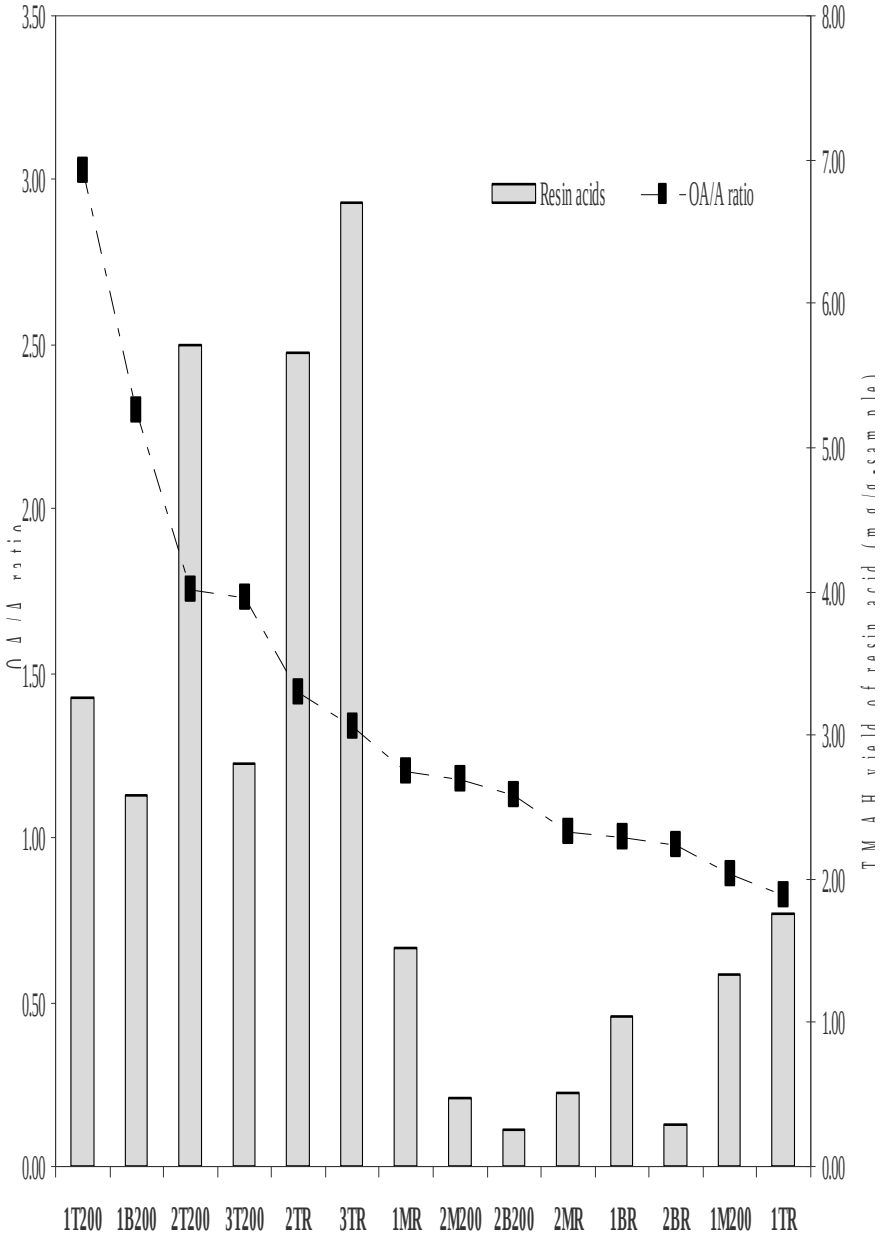

FIGURE 3.11 Correlations between OA/A ratio and yields of resin acids released from TMAH thermochemolysis of MSW samples.

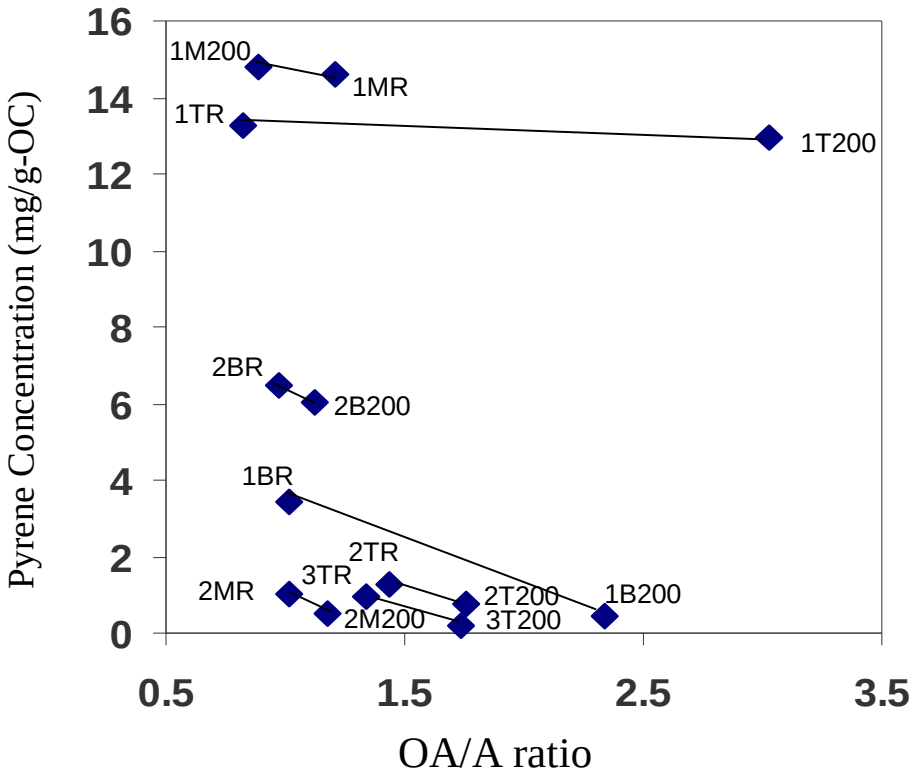

FIGURE 3.12 Correlation between OA/A ratio and yield (mg/g-OC) of pyrene released by TMAH thermochemolysis of MSW samples.

middle and bottom sections), the buildup of alkanes from contamination overwhelmed the signal of C29 plant alkane. The second indication is observed within a pair of samples of different particle sizes. Elevated OC-normalized-TMAH yield of pyrene is evident in a sample with a lower OA/A ratio (Figure 3.12). High concentration of pyrene in 1T, 1M and 2B couples suggests that they might have been present with initial deposits. Therefore, the observed result could reflect the accumulation of pyrene which is recalcitrant to microbial degradation. In the case of other samples, however, the contamination might occur later and the difference in pyrene concentration could be due to the variation in sorption affinity of MSW samples. Although MSW samples were not tested for their actual sorption capacity, the coherent change between OA/A ratios and the amounts of sorbed pyrene in all pairs of samples suggests that the affinity for hydrophobic compounds of MSW samples might increase with the degree of sample decomposition.

The increase in the aliphatic component upon decomposition might not only modify the sorption affinity of MSW samples but also could affect the sorption mechanism. Some of the natural organic matter enriched with aliphatic functional groups exhibit an irreversible sorption with hydrophobic compounds such as PAHS (*56-58*).

Based on the TMAH thermochemolysis of sample 1TR before and after solvent extraction, nearly 10 % of the original amount of phenanthrene, fluoranthene and pyrene (in the range of 1,389-1,499 μg/g-sample) was not extractable. Sequestration of PAHs in this sample could occur via noncovalent binding. This mechanism has occurred in microbial-active sediment incubated with pyrene for only 60 days (*13*). Due to much longer residential time of MSW in the landfill (16-23 yrs), it is possible that this process

could occur with MSW samples. It is interesting that evidence for non extractable PAHs was not observed with 1MR, which contains higher amount of PAHs (2,131-2,328 μg/g-sample). The major difference between 1TR and 1MR is their extent of degradation. Among MSW samples, sample 1TR was the most degraded sample and contained the highest aliphatic carbon component (Table 3.1). The possibility of irreversible sorption of hydrophobic compound to degraded MSW will have a significant implication to the remediation of contaminated landfills. When occurs, it would lower biodegradability of pollutants and make them more difficult to be removed by physical or chemical remediation methods.

ACKNOWLEDGEMENTS

We thank Mr. Scott Christensen and Mr. Dale Ferree from the U.S. Geological Survey (Oklahoma City) for collecting the core samples, and Dr. Margaret Eastman from Oklahoma State University for assistance with the ^{13}C NMR analysis. This research was funded by the National science foundation (BES-9732969 and BES-001700). Ms. Ratasuk was funded by the Royal Thai Government.

LITERATURE CITED

(1) Bookter, T. J.; Ham, R. K. *J.* Stabilization of solid waste in landfills. *Envir. Engrg*. ASCE. **1982**, 108, 1089.

(2) Barlaz, M. A.; Ham, R. K.; Schaefer, D. M. *J.* Mass-balance analysis of anaerobically decomposed refuse. *Environ. Engrg*. **1989**, 115, 1088.

(3) Wu, B.; Taylor, C. M.; Knappe, D. R.U.; Nanny, M.A.; Barlaz, M. A. Factors controlling alkylbenzene sorption to municipal solid waste. *Environ. Sci. Tech.* **2001**, 35, 4569.

(4) Chen, L.; Nanny, M.A.; Knappe, D. R. U.; Wagner, T. B.; Ratasuk, N. Chemical characterization and sorption capacity measurements of degraded newsprint from a landfill. *Environ. Sci. Tech.* **2001**, 38, 3542.

(5) Nanny, M. A.; Ratasuk, N. Characterization and comparison of hydrophobic neutral and hydrophobic acid dissolved organic carbon isolated from three municipal landfill leachates. *Water Res*. **2002**, 36, 1572.

(6) Leenheer, J.A.; Nanny, M.A.; McIntyre, C. Terpenoids as major precursors of dissolved organic matter in landfill leachates, surface water, and groundwater. *Environ. Sci. Tech.* **2003**, 37, 2323.

(7) Schlottmann, J. L. *Water Chemistry near the Closed Norman Landfill, Cleveland County, Oklahoma, 1995*; Water-Resources Investigations Report 00-4238; U.S. Department of the Interior, U.S. Geological Survey: Reston, VA, 1995.

(8) Christenson, S.; Scholl, M. A.; Schlottmann, J. L.; Becker, C. J. *Geochemical and Microbiological Processes in Ground Water and Surface Water Affected by Municipal Landfill Leachate*, Toxic Substances Hydrology Programs Proceedings of the Technical Meeting, Charleston, SC, 1999; U.S. Geological Survey: Reston, VA, 1999; Vol. 3. Section E, pp 501.

(9) Cozzarelli, I. M.; Suflita, J. M.; Ulrich, G. A.; Harris, S. H.; Scholl, M. A.; Schlottmann, J. L.; Christenson, S. Geochemical and microbiological methods for evaluating anaerobic processes in an aquifer contaminated by landfill leachate. *Environ. Sci. Tech.* **2001**, 34, 18, 4025.

(10) Schmidt, M.W.I.; Knicker, H.; Hatcher, P.G.; Kogel-Knabner, I. Improvement of 13C CPMAS NMR spectra of bulk soils, particle size fractions and organic material by treatment with 10% hydrofluoric acid. *Eur. J. Soil Sci.* **1997**, 48, 319.

(11) Bennett, A. E.; Rienstra, C. M.; Auger, M.; Lakshmi, K. V.; Griffin, R. G. Heteronuclear decoupling in rotating solids. *J. Chem. Phys*. **1995**, *103*, 6951.

(12) Socrates, G. *Infrared and Raman Characteristic Group Frequencies:Tables and Charts*, 3rd ed.; John Wiley & Sons: New York, 2001; p 347.

(13) Guthrie, E. A.; Bortiatynski, J. M.; Van Heemst, J. D. H.; Richman, J. E.; Hardy, K. S.; Kovach, E. M.; Hatcher, P. G. Determination of [^{13}C]pyrene sequestration in sediment microcosms using flash pyrolysis-GC-MS and ^{13}C NMR. *Environ. Sci. Tech*. **1999**, 33, 119.

(14) Chen, Jenn-Shing; Chiu, Chih-Yu. Characterization of soil organic matter in different particle-size fractions in humid sub-alpine soils by CP/MAS 13C NMR. *Geoderma.* **2003**, 117, 129.

(15) Ahmad, R.; Kookana, R. S.; Alston, A.M.; Skjemstad, J.O. The nature of soil organic matter affects sorption of pesticides. 1. Relationships with carbon chemistry as determined by 13C CPMAS NMR spectroscopy. *Environ. Sci. Tech.* **2001**, 35, 878.

(16) Schmidt, M. W. I.; Kogel-Knabner, I. Organic matter in particle-size fractions from A and B horizons of a Haplic Alisol. *Eur. J. Soil Sci.* **2002**, 53, 383.

(17) Pichler, M.; Knicker, H.; Koegel-Knabner, I. Changes in the chemical structure of municipal solid waste during composting as studied by solid-state dipolar dephasing and PRSE 13C NMR and Solid-State 15N NMR Spectroscopy. *Environ. Sci. Tech.* **2000,** 34, 4034.

(18) Chefetz, B.; Adani, F.; Genevini, P.; Tambone, F.; Hadar, Y.; Chen, Y. Humic-acid transformation during composting of municipal solid waste. *J. Environ. Qual*. **1998**, 27, 794.

(19) Pichler, M.; Knicker, H.; Kogel-Knabner, I. Solid-state (13)C NMR spectroscopic, chemolytic and biological assessment of pretreated municipal solid waste. *J. Ind. Microbiol.* **2001**, 26, 83.

(20) Barber, Larry B.; Leenheer, Jerry A.; Noyes, Ted I.; Stiles, Eric A. Nature and transformation of dissolved organic matter in treatment wetlands. *Environ. Sci. Tech.* **2001,** 35, 4805.

(21) Leenheer, J. A.; Croue, J. P. Characterizing aquatic dissolved organic matter. *Environ. Sci. Tech.* **2003**, 37, 18A.

(22) Deshmukh, A. P.; Chefetz, B.; Hatcher, P. G. Characterization of organic matter in pristine and contaminated coastal marine sediments using solid-state 13C NMR, pyrolytic and thermochemolytic methods: A case study in the San Diego harbor area. *Chemosphere*. **2001**, 45, 1007.

(23) Eleazer, W. E.; Odle, W. S.; Wang, Y.-S.; Barlaz, M. A. Biodegradability of municipal solid waste components in laboratory-scale landfills. *Environ. Sci. Technol.* **1997**, *31*, 911.

(24) Hua, X.; Capretti, G.; Focher, B.; Marzetti, A.; Kokta, B. V.;Kaliaguine, S. Characterization of aspen explosion pulp by CPMAS carbon-13NMR. *Appl. Spectrosc.* **1993**, *47*, 1693.

(25) Kurek B; Gaudard F. Oxidation of spruce wood sawdust by MnO(2) plus oxalate: a biochemical investigation. *J. Agri. Food Chem*. **2000**, 48, 3058.

(26) Stromme, Maria; Mihranyan, Albert; Ek, Ragnar; Niklasson, Gunnar A. Fractal dimension of cellulose powders analyzed by multilayer bet adsorption of water and nitrogen. *J. Phys. Chem*. B. **2003**, 107, 14378.

(27) del Rio, J. C.; McKinney, D. E.; Knicker, H.; Nanny, M. A.; Minard, R. D.; Hatcher, P. G. Structural characterization of bio- and geo-macromolecules by off-line thermochemolysis with tetramethylammonium hydroxide. *J. Chromatography A.* **1998**, 823, 433.

(28) Yunker, M. B.; Backus, S. M.; Graf Pannatier, E.; Jeffries, D. S.; Macdonald, R. W. Sources and significance of alkane and PAH hydrocarbons in Canadian arctic rivers. *Estuarine, Coastal and Shelf Science*. **2002**, 55, 1.

(29) Zakaria, M. P.; Takada, H.; Tsutsumi, S.; Ohno, K.; Yamada, J.; Kouno, E.; Kumata, H. Distribution of polycyclic aromatic hydrocarbons (PAHs) in rivers and estuaries in Malaysia: A widespread input of petrogenic PAHs. *Environ. Sci. Tech.* **2002**, 36, 1907.

(30) Chuang, J.C.; Wise, S.A.; Cao, S.; Mumford, J.L. Chemical characterization of mutagenic fractions of particles from indoor coal combustion: a study of lung cancer in Xuan Wei, China**.** *Environ. Sci. Tech*. **1992**, 26, 999.

(31) Estanislau do Amaral, M. C.; Ribeiro da Silva, A.J.; Salatino, A. Alkanes of surface waxes from eight species of aquatic angiosperms. *Aqua. Bot*. **1990**, 36(3), 281.

(32) Yunker, M. B.; Macdonald, R. W.; Whitehouse, B. G. Phase associations and lipid distributions in the seasonally ice-covered arctic estuary of the Mackenzie shelf. *Org. Geochem*. **1994**, 22(3-5), 651.

(33) Aloisi, G.; Bouloubassi, I.; Heijs, S. K.; Pancost, R.D.; Pierre, C.; Sinninghe D., Jaap S.; Gottschal, J. C.; Forney, L. J.; Rouchy, J. M. CH_4-consuming microorganisms and the formation of carbonate crusts at cold seeps. *Earth Planet. Sci*. **2002**, 203, 195.

(34) Zhang, C. L.; Li, Y.; Wall, J. D.; Larsen, L.; Sassen, R.; Huang, Y.; Wang, Y.; Peacock, A.; White, D. C.; Horita, J.; Cole, D. R. Lipid and carbon isotopic evidence of methane-oxidizing and sulfate-reducing bacteria in association with gas hydrates from the Gulf of Mexico. *Geology*. **2002**, 30, 239.

(35) Wolff, R. L.; Christie, W. W.; Coakley, D. The unusual occurrence of 14-methylhexadecanoic acid in Pinaceae seed oils among plants. *Lipids*. **1997**, 32, 973.

(36) Rontani, J. F.; Volkman, J. K. Phytol degradation products as biogeochemical tracers in aquatic environments. *Org. Geochem*. **2003**, 34, 1.

(37) Liu, Q. T.; Chen, R.; McCarry, B. E.; Diamond, M.L.; Bahavar, B. Characterization of polar organic compounds in the organic film on indoor and outdoor glass windows. *Environ. Sci. Tech.* **2003**, 37.

(38) del Rio, J.C.; Hatcher, P. G. *Org.* Analysis of aliphatic biopolymers using thermochemolysis with tetramethylammonium hydroxide (TMAH) and gas chromatography-mass spectrometry. *Org. Geochem*. **1998**, 29, 1441.

(39) Graca, J.; Pereira, H. Suberin structure in potato periderm: Glycerol, long-chain monomers, and glyceryl and feruloyl dimers. *J. Agri. Food Chem*. **2000**, 48, 5476.

(40) Faure, P.; Landais, P.; Schlepp, L.; Michels, R. Evidence for Diffuse Contamination of River Sediments by Road Asphalt Particles. *Environ. Sci. Tech*. **2000**, 34, 1174.

(41) Schwarzbauer, J.; Heim, S.; Brinker, S.; Littke, R. Occurrence and alteration of organic contaminants in seepage and leakage water from a waste deposit landfill. *Water Res*. **2002**, 36, 2275.

(42) Reinhard, M.; Barker, J. F.; Goodman, N. L. Occurrence and distribution of organic chemicals in two landfill leachate plumes. *Environ. Sci. Tech.* **1984**, 18, 953.

(43) Ahel, M.; Tepic, N. Distribution of polycyclic aromatic hydrocarbons in a municipal solid waste landfill and underlying soil. *Bull. Environ. Contam. Toxicol*. **2004,** 73, 437.

(44) Murray, W. D.; Richardson, M. Development of biological and process technologies for the reduction and degradation of pulp mill wastes that pose a threat to human health. *Crit. Rev. Environ. Sci. Technol.* **1993**, *23*, 157.

(45) Patoine, A.; Manuel, M. F.; Hawari, J. A.; Guiot, S. R. Toxicity reduction and removal of dehydroabietic and abietic acids in a continuous anaerobic reactor.*Water Res.***1997**, *31*, 825.

(46) McSweeney, E. E.; Arlt, H.G. Jr.; Russell, J. *Tall Oils and Its Uses-II*; Pulp Chemical Association: New York, 1987.

(47) Otto, A.; Simoneit, B. R. T. Biomarkers of Holocene buried conifer logs from Bella Coola and north Vancouver, British Columbia, Canada. *Org. Geochem*. **2002**, 33, 1241.

(48) Liss, S. N., Bicho, P.A.; Saddler, J.N. Microbiology and biodegradation of resin acids in pulp mill effluents: A minireview. *Can. J. Microbiol*. **1997**, 43, 599.

(49) Schauer, J. J.; Kleeman, M. J.; Cass, G. R.; Simoneit, B. R. T. Measurement of emissions from air pollution sources. 3. C1-C29 Organic compounds from fireplace combustion of wood. *Environ. Sci. Technol.* **2001**, 35, 1716.

(50) Oros, D. R.; Simoneit, B. R. T. Identification and emission rates of molecular tracers in coal smoke particulate matter. *Fuel*. **2000**, 79, 515.

(51) Holmbom, B.; Era, V. Composition of tall oil pitch. *J. Am. Oil Che. Soc.* **1978**, 55, 342.

(52) Komilis, D. P.; Ham, R. K.; Stegmann, R. The effect of landfill design and operation practices on waste degradation behavior: a review. *Waste Manage. Res*. **1999**, 17, 20.

(53) Gawande, Nitin A.; Reinhart, Debra R.; Thomas, Philip A.; McCreanor, Philip T.; Townsend, Timothy G. Municipal solid waste in situ moisture content measurement using an electrical resistance sensor. *Waste Manage*. **2003**, 23, 667.

(54) Chugh, S.; Clarke, W.; Pullammanappallil, P.; Rudolph, V. Effect of recirculated leachate volume on MSW degradation. *Waste Manage. Res*. **1998**, 16, 564.

(55) Barnes, K. K.; Christenson, S.C.; Kolpin, D. W.; Focazio, M. J.; Furlong, E. T.; Zaugg, S. D.; Meyer, M.T.; Barber, L. B. Pharmaceuticals and other organic waste water contaminants within a leachate plume downgradient of a municipal landfill. *Ground Water Monitoring and Remediation*. **2004**, 24, 119.

(56) Chefetz, B.; Deshmukh, A. P.; Hatcher, P. G.; Guthrie, E. A. Pyrene sorption by natural organic matter. *Environ. Sci. Technol.* **2000**, *34*, 2925.

(57) Rice, J.A. Humin. *Soil Sci.* **2001**, 166, 848.

(58) Salloum, M. J.; Chefetz, B.; Hatcher, P. G. Phenanthrene sorption by aliphatic-rich natural organic matter. *Environ. Sci. Technol*. **2002**, *36*, 1953.

(59) Almendros, G.; Tinoco, P.; Gonzalez-Vila, F. J.; Ludemann, H. D.; Sanz, J.; Velasco, F. 13C-NMR of forest soil lipids. *Soil Sci.* **2001**, 166, 186.

CHAPTER 4

CONCLUSIONS AND RECOMMENDATIONS

CONCLUSIONS

The ultimate goal of this study was to determine and characterize redox functional groups that could be responsible for the reversible electron mediating capacity of humic substances. A novel analytical technique based on palladium and H_2 catalytic system was developed to determine the types of the actual redox functional groups of several humic materials. Other analytical techniques, such as X-ray photoelectron spectroscopy analysis, solid state ^{13}C NMR, were also employed to clarify details concerning some redox functional groups and to verify the formation of redox sites in some humic substance samples. From the results observed during these studies, several conclusions can be made:

1. Electron mediating capacity varies among humic substances, ranging from 0-538 μequivalents/g-sample for the humic substances examined.
2. Redox sites of humic substances are less likely associated with aliphatic carbon functional groups because samples such as landfill leachate humic substances, which are highly aliphatic, lack redox sites.
3. For humic substances that are electron mediators, their redox sites can be divided into two groups: *i*) quinone redox sites and *ii*) redox functional groups with nonquinone structures.

4. There are at least two forms of quinone redox sites. One is quinone moieties with an electron withdrawing substituent. The other includes quinone moieties without any substituent and/or quinone moieties with an adjacent electron donating functional group. Quinone moieties in the first group are more prevalent in humic substances which contain high carboxylic carbon content.
5. For humic substances that are electron mediators, sulfur functional groups are important nonquinone redox sites, contributing from 18%-120% of the NQ redox sites' ECC and 4%-62% of the total ECC of the humic substances determined.
6. Because OC in MSW will become enriched with aliphatic carbon components as refuse degradation processes continue in landfills, dissolved organic carbon of leachate, which is one of refuse degradation products, would most likely remain highly aliphatic. Therefore, humic substances, which represent approximately 50-60 % of the dissolved organic carbon (ref.5, Chapter 3), would also continue to be highly aliphatic. Under this circumstance, there is unlikely possibility that redox functional groups of landfill leachate humic substances will be enriched in the future.

RECOMMENDATIONS

Several promising results have been found during this study. However, like any new findings, additional research is necessary to sharpen the insights into redox

functional groups of humic substances and to account for some data limitations. Recommendations for future studies are presented as follows:

1. Evaluation of the accessibility of each redox functional groups to various types of bacteria. The comparison between data from microbial reduction and from catalytic reduction methods in Chapter 1 suggests that each group of bacteria might be able to transfer electrons through different redox sites of humic substances. *Geobacter metallireducens*, for instance, probably uses quinone sites rather than sulfur redox functional groups during electron transfer processes.
2. Reexamination of the actual contribution of sulfur redox functional group. As described in Chapter 3, some of the FeS sites are artifacts generated by the catalytic reaction between thiol and complexed-iron. A new approach that would be an excellent substitute for the catalytic reduction is to use anaerobic microbes to reduce humic substances. This approach not only eliminates artificial FeS sites, but also verifies the formation of this sulfur functional group in an anaerobic condition. Also, in order to verify the formation of FeS sites, iron XPS analysis would be a suitable supplementary technique to further confirm the presence of these redox sites in reduced humic substance samples. Furthermore, to accurately determine the contribution of sulfur redox sites, a new electron acceptor is required. The use of iron (III) as an electron accepter complicated the estimation of electron carrying capacity, particularly of the FeS sites.

3. There is an interesting issue regarding the formation of redox sites. It has been known that redox functional groups such as quinone sites are formed via oxidative transformation of phenol moieties (ref. 21, Chapter 3). The facts that landfill leachate humic substances are formed under a highly reducing environment and turn out to be short of redox sites rather imply that some of redox functional groups of humic substances might be developed in an aerobic environment. Comparison of the redox property of leachate humic substances produced during aerobic and anaerobic degradation of MSW might shed a light on this issue.
4. Finally, since redox sites with a nonquinone structure are more resistant to hydrogenolysis than quinone moieties, these redox sites might be able to function in more varied environments than do the quinone redox centers. For example, in a remediation process using zero valent iron, one of three reductive transformation pathways of pollutants included catalyzed hydrogenolysis by the H_2 that is formed by the reduction of H_2O during anaerobic corrosion of the iron (ref. 36, Chapter 1). In such condition, if humic substances are involved, quinone redox sites would be disabling. Only nonquinone sites supposedly remain operable. This issue is interesting because it suggested that the electron carrying capacity of the same humic substance might vary from one environmental condition to another.